THESIS

MONITORING THE EFFECTIVENESS OF RIVER REALIGNMENT ON THE UPPER COLORADO RIVER, ROCKY MOUNTAIN NATIONAL PARK

Submitted by

Matthew Sparacino

Department of Geosciences

In partial fulfillment of the requirements

For the Degree of Master of Science

Colorado State University

Fort Collins, Colorado

Spring 2017

Master's Committee:

Advisor: Sara Rathburn

Tim Covino
Peter Nelson
Mike Ronayne

ABSTRACT

MONITORING THE EFFECTIVENESS OF RIVER REALIGNMENT ON THE UPPER COLORADO RIVER, ROCKY MOUNTAIN NATIONAL PARK

A 2003 debris flow introduced 36,000 m^3 of sediment into a high-elevation wetland on the Upper Colorado River in Rocky Mountain National Park. In September 2015, Park staff built an earthen diversion dam and realigned a 190 m reach of the Colorado River into its historic thalweg through the center of Lulu City wetland. Initial dimensions of the constructed channel were 1.6 m wide and 0.4 m deep with an average bed slope of 1.9%. Pre- and post-restoration measurements are compared to assess the hydro-geomorphic response to the channel realignment within the adjacent wetland. The constructed diversion berm redistributed at least 48% of river discharge from a pre-realignment, west-side channel, to a central channel, which decreased surface-water groundwater exchange as well as the size of near-stream hyporheic zones and altered sediment transport capacity. A sodium chloride tracer was injected during base-flow and electrical resistivity was used to monitor changes in near-channel hyporheic exchange across the realigned channel for approximately 24 hours following the injection. Pre-and post-realignment electrical resistivity analyses indicate a loss of hyporheic exchange in the northern wetland, likely a result of decreased river complexity. Tracer mass balances derived from concurrent surface conductivity measurements indicate increases in solute retention throughout Lulu City wetland, possibly due to increased overbank flow. These results imply that solute retention can increase without an equal increase in hyporheic exchange. Furthermore, local incision greater than 0.5 m, widening of 0.2 to 1 m, and upstream knickpoint migration within the realigned channel during 2016 runoff indicate increases in erosion and local sediment transport. The growth of gravel bars upstream of the diversion berm indicate increased sediment deposition at the head of Lulu City wetland. Results from one year of post-realignment monitoring suggest that the channel realignment has had small-scale effects on hyporheic exchange, solute retention, and sediment

transport capacity, with potentially negative consequences for the ecosystem services provided by river-wetland systems. Long-term monitoring and increased instrumentation are required to predict how these changes may be amplified in a larger restoration attempt.

ACKNOWLEDGEMENTS

I sincerely thank Jackie Randell for her invaluable electrical resistivity field assistance and on the spot trouble shooting - this research could not have happened without you. I thank Kamini Singha for supplying the electrical resistivity equipment, as well as her expert geophysics knowledge. I thank Dave Dust for providing advice from an engineer's perspective, for field help, and for his endless supply of wit. I thank my summer field assistants, Tyler Rich and Ford Fowler, for putting up with long days with heavy packs and fast walking. I thank Garrett Brown, Annette Patton, Andrew Pfeiffer and Ivan Prushnok for field help during the busy, cold, and sometimes rainy, 2015 and 2016 salt tracer tests. Thanks to DerekSchook for field help in 2016, and especially for being willing to excavate 4 feet of snow and literally jump in to find the Colorado River. I thank the fluvial geomorphology lab at CSU for academic and research support, and for thought-provoking conversation. I thank Mike Ronayne, Austin Abendschein and Jay Merrill for field help during the 2015 salt tracer test. Thanks to Jeremy Sueltenfuss for insightful ecological conversations about Lulu City wetland. I thank Ryan Brown, Allie Rhea, Nikki Seymour, Corrine Horner, Laura Marques, Kayla Neuharth, Matt Succo, Nick Santiago, Leland Dorchester, Graham Peterson, Tavon Boamon, and Josh Nugent for field help during the 2016 electrical resistivity surveys. I thank Bethany Avera for field help in 2016 and for her loving support over the past year. I thank Bill Sanford for loaning pumping equipment for both the 2015 and 2016 salt tracer tests. I thank Tim Covino for loaning conductivity probes, and for feedback on tracer tests. Thank you to Rocky Mountain National Park employees Tara Vassella and Ken Rybkiewicz for providing invaluable livestock teams to haul equipment into the backcountry, particularly llamas Mister, Specs and Luxor. I thank Paul McLaughlin and Scott Esser for facilitating research in such a beautiful place. I thank the funding agencies who supported this work, including Rocky Mountain National Park, the Colorado Water Institute, American Water Resources Association - Colorado, the American Alpine Club, CSU Warner College of Natural Resources, and the CSU Department of Geosciences. Finally, I thank Sara Rathburn

for enabling two years of fantastic research, for providing unwavering field, school, and life support, for her contagious enthusiasm, and for always keeping lunch breaks on schedule.

TABLE OF CONTENTS

LIST OF TABLES

LIST OF FIGURES

1. INTRODUCTION

River and wetland restoration has become increasingly popular in the United States in response to ecosystem degradation. Total wetland area in the continental United States has decreased by more than half during the past 200 years as a result of human activity (Dahl, 1990, 2000). River and wetland restoration has recently adopted an holistic and process-based approach, with broadened goals to incorporate ecological, geomorphological and aesthetic components (Palmer et al., 2005). Prior to this shift, river restoration historically prioritized the enhancement of river form over function (Wohl et al., 2015). Improving fish habitat or water quality through small-scale bed modifications was a popular means of addressing the negative ecological impacts forced by centuries of navigation-focused river management (Wohl et al., 2015). The benefits of this form-based restoration were often short-lived, and researchers began to see the value of considering the watershed scale when addressing site-specific restoration (Gowan and Fausch, 1996). The recent transition is supported by a growing body of literature emphasizing the importance of three types of river connectivity: upstream-downstream, river-riverbed, and river-floodplain interactions when working towards sustainable process-based river restoration (Findlay, 1995; Kondolf et al., 2006; Wohl et al., 2015; Covino, 2016).

Natural wetlands, which are transitional zones characterized by high water tables and saturated soils during part of the growing season (Windell et al., 1986), are intricately linked to rivers through all three forms of connectivity. Consistent and extensive overbank flooding is essential to the health of wetland ecosystems (Junk et al., 1989). When functioning properly, wetlands provide valuable ecosystem services through water filtration, oxygen cycling, fine sediment storage, flood peak attenuation, nutrient cycling, and support for diverse ecological communities (Triska et al., 1989; Zedler and Kercher, 2005; Toran et al., 2012; Hester and Gooseff, 2013). The benefit gained from these processes can be improved by increasing the timing and extent of surface water-groundwater exchange, often by promoting slower

flow paths and greater floodplain inundation through added river complexity (Findlay, 1995; Wohl et al., 2015). High-elevation wetlands, including those in the American Rockies, provide the same essential ecosystem services as low-elevation wetlands, but are especially vulnerable to degradation through human activity and land use changes (Windell et al., 1986). Many of these high-elevation wetlands form in glacial valleys and are delicately sustained by beaver ponds, despite low temperatures and short growing seasons, and have complex hydrologic interactions linked to near-channel surface water-groundwater exchange (Windell et al., 1986; Ringelman, 1992). The complexity introduced by active and relic beaver dams consistently increases the frequency and duration of the important overbank flows that can drive surface water-groundwater exchange (Westbrook et al., 2006). Historical beaver activity along the Upper Colorado River, in Rocky Mountain National Park, facilitated frequent floodplain inundation that would otherwise have required flows with recurrence intervals greater than 200 years (Westbrook et al., 2006).

The natural hydro-geomorphic processes acting within a high-elevation wetland on the Upper Colorado River have been impaired by sediment aggradation sourced from a 2003 debris flow (RMNP, 2013). This event, plus nearly a century of earlier debris flows (Grimsley et al., 2016), has since created inconsistent water tables throughout Lulu City wetland and sediment supplies that are unsuitable for the tall willow (*Salix drummondiana* and *S. monticola*) and beaver communities that historically existed there (Cooper, 2007). Rocky Mountain National Park staff believe that sedimentation at the head of the Lulu City wetland, a critical resource within the Park, has redistributed surface water flow, altered channel slopes and modified surface water-groundwater interactions between the channel and riparian zone (RMNP, 2013). In the fall of 2015, Rocky Mountain National Park staff rerouted a 190 m section of the Colorado River into its historic channel. This realignment, as it is referred to throughout this thesis, was the first step in a larger plan aimed at restoring the system to a less disturbed, pre-debris flow state.

The goal of this research is to combine an interdisciplinary set of methods - shallow geophysics, surface water tracer injections, and sediment transport characterizations - to evaluate the effectiveness of channel realignment in restoring lost ecosystem services within Lulu City wetland. This research does not explicitly address the restoration goals proposed and implemented by Rocky Mountain National Park staff. Earlier research within the Upper Colorado River valley has monitored certain aspects of the system-wide response to the debris flow, as well as characterized the history of disturbance in the area (Rubin et al., 2012; Rathburn et al., 2013; Mangano, 2014; Grimsley et al., 2016). A decade of baseline monitoring data makes this system an ideal one in which to evaluate changes imposed by the channel realignment. I use a series of pre-and post-realignment measurements to assess the degree of change imposed by the channel realignment. Three objectives address specific factors that influence ecosystem services provided by the Lulu City river-wetland system:

Objective$_1$: Determine the effect of channel realignment on the redistribution of flow through the Lulu City wetland.

Objective$_2$: Determine the effect of channel realignment on hyporheic exchange and solute retention within Lulu City wetland.

Objective$_3$: Determine the effect of channel realignment on the capacity of the Upper Colorado River to transport sediment into and through Lulu City wetland.

In addition to adding to the rich body of research on the Upper Colorado River, this research is unique in two ways; i) it builds upon a relatively new application for electrical resistivity imaging used to monitor the hydrologic response to channel restoration in remote and environmentally sensitive areas; and, ii) it helps fill a knowledge gap in the literature, where quantitative evaluations of restoration outcomes are lacking (Bernhardt and Palmer, 2011).

2. BACKGROUND

2.1 Study area

The Lulu City wetland is located on the Upper Colorado River in the northwest corner of Rocky Mountain National Park (Figure 1). It has an upstream drainage area of 29 km^2 and receives on average 66 cm of precipitation per year, the majority of which falls as snow between October and May (NRCS, 2016). Peak flows on the Upper Colorado River usually occur in early to mid-June. Lulu City wetland is surrounded by the Never Summer Mountains to the west, Thunder Mountain and La Poudre pass to the north, and Specimen Mountain to the east. The wetland elevation is 2,840 masl and the highest point in the watershed, Mt. Richthofen, is 3,944 masl.

The Upper Kawuneeche valley, within which the Lulu City wetland lies, was created during Pleistocene glaciation, when alpine glaciers extended from the Continental Divide through Grand Lake, Colorado, to the south (Meierding, 1980). Valley sediment deposits in the upper 4 meters of the Lulu City wetland are spatially heterogeneous, and are composed primarily of sand (coarse to fine), silty clays, and peat layers (Rubin et al., 2012). Total deposit depths have not been measured within the wetland, but down-valley seismic surveys have estimated depths to bedrock between 15 and 122 m below the present-day surface (Braddock and Cole, 1990). The underlying geology on the hillslopes upstream of Lulu City wetland is primarily Tertiary rhyolite tuff (Braddock and Cole, 1990), which has been weathered, *in situ*, by hydrothermal alteration (Grimsley et al., 2016). The remainder of the Upper Colorado basin above Lulu City wetland consists of Tertiary basalt and smaller igneous intrusions, as well as Proterozoic gneiss (Braddock and Cole, 1990).

The history of land use in the Upper Kawuneeche River valley extends to the last glacial maximum. Following glacial retreat 11,000 years ago, the valley saw intermittent habitation by paleo-peoples and more permanent Ute habitation between 1400 and 1879 (Andrews, 2011). Gold and silver mining drove the Utes out of the valley and supported a

short-lived mining camp at Lulu City between 1879 and 1884, which reached a maximum population of $\sim$ 500 people (Andrews, 2011). Intermittent mining continued in the Upper Kawuneeche valley through the establishment of Rocky Mountain National Park in 1915. Beaver populations, which decreased as a result of human land use, recovered following the establishment of the Park. As late as 1947, 600 beaver were estimated to have lived in the Kawuneeche valley between the Lulu City wetland and the Park boundary 19 km to the south (Packard, 1947). These beaver thrived on tall willows that grew abundantly throughout the wetlands (Packard, 1947). In recent years, tall willows have declined in Rocky Mountain National Park riparian areas as a result of biotic stressors, including increased ungulate grazing and infection from *Cytospora chrysosperma* (Kaczynski, 2007). Abandoned beaver ponds in the modern Lulu City wetland suggest an active beaver community in the past, but modifications to natural water and sediment regimes imposed by Grand Ditch have further stressed them and other plant and animal communities in the valley.

Grand Ditch is a 27 km, trans-mountain water diversion structure built into the bedrock on the east side of the Never Summer Mountains between 1890 and 1936 to ensure a consistent and sufficient water supply for growing Front Range agricultural needs (Andrews, 2011). Annually, Grand Ditch diverts out of the Colorado River drainage up to 50% of snow runoff from the Never Summer Mountains, with significant downstream ecological and geomorphic effects (Clayton and Westbrook, 2008; Rathburn et al., 2013). In May 2003 a debris flow initiated from Grand Ditch (Figure 2) and introduced 36,000 m^3 of sediment into the Upper Colorado River valley (Rathburn et al., 2013). Up to 1 m of sands and gravels were deposited in Lulu City wetland during snowmelt in 2003 (Rathburn et al., 2013). The majority of debris accumulated in a fan at the confluences with Lulu Creek (Figure 1), where it continues to weather in place, and is transported downstream each year during snowmelt. While the amount and spatial extent of sediment released and deposited by this debris flow was not outside the historical range of variability for this area, the unnatural disturbance regime induced by Ditch-related diversions is linked to debris flows large

enough to cause persistent sedimentation within the Colorado River valley (Grimsley et al., 2016). In low-flow years, when debris flows may be less frequent, ditch diversions effectively erase natural peak flows.

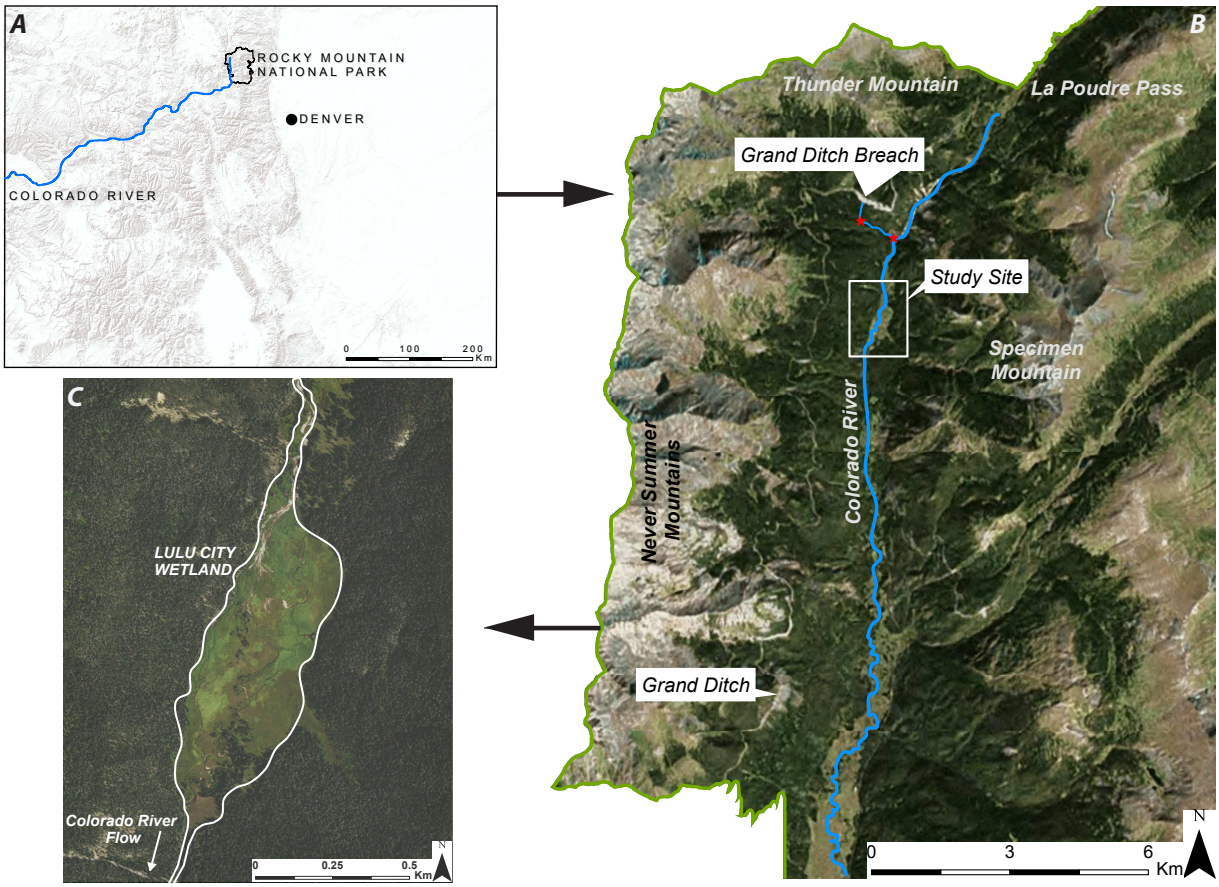

Figure 1: Panel A: Map of Colorado with selected landmarks. Panel B: Satellite image of the northwest corner of Rocky Mountain National Park, including relevant geographic features and the field study site; stars mark the location of sediment accumulation in debris fans. Red stars indicate the location of sediment deposition in debris fans. Panel C: study site, including a detail outline of Lulu City wetland.

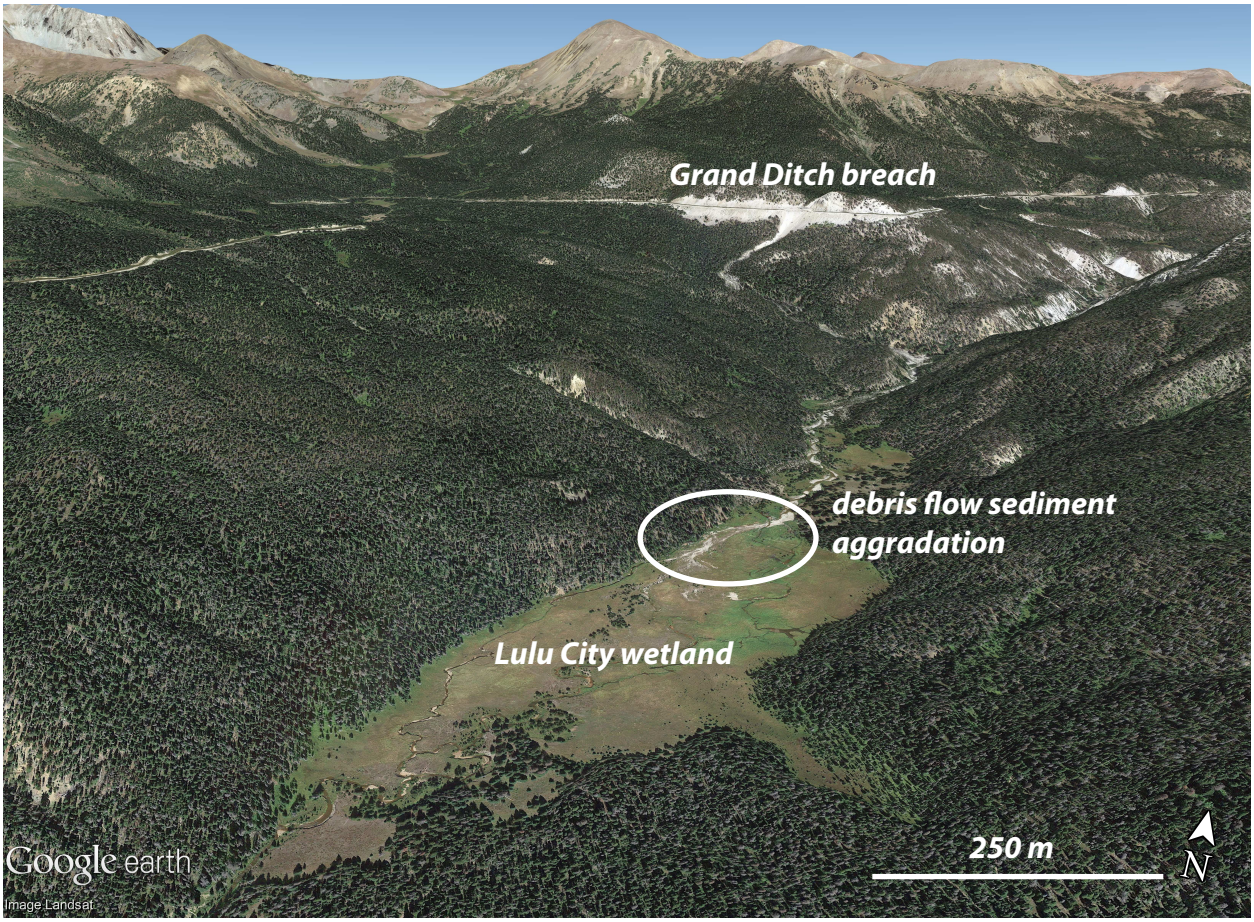

Figure 2: Oblique aerial view of the field study site, including Lulu City wetland and Grand Ditch, Rocky Mountain National Park. The initiation site of the 2003 debris flow is evident in the exposed hillside along "Grand Ditch breach." Imagery date: 7 September 2016.

2.2 Objective 1: Flow redistribution

In late September, 2015, Rocky Mountain National Park staff completed work to divert and realign a 190 m section of the Colorado River as it flows into Lulu City wetland (Figure 3). In order to fulfill requirements of the civil lawsuit settlement reached over the Grand Ditch breach and debris flow, Rocky Mountain National Park staff aimed to restore the natural hydrologic processes, ecological function, and wilderness character to the Lulu City wetland primarily by re-rerouting the Colorado River through its historical channel (RMNP, 2013). The bed slope of the realigned channel originally ranged between 0.2% upstream to 3% downstream, with an average reach slope of 1.9%, which is steeper than the 1% slope of the western channel for which it was meant to replace. The initial channel was dug by hand to an

average width of 1.6 m and average depth of 0.4 m. The channel was cut into an area heavily vegetated by sedges (*Carex utriculata* and *Carex aquatilis*) and tall grass (*Calamagrostis canadensis*), and the channel depth was largely controlled by the depth required to remove the sedge root wads. An earthen diversion berm was also constructed adjacent to the right bank of the realigned channel with initial dimensions of 1 m high, 2 m wide, and 27 m long, and composed of roughly 27 m^3 of sand and gravel excavated from the realigned channel and topped with logs. Prior to realignment, over 50% of discharge entering the wetland flowed through a western channel, while less than 50% of discharge entering the wetland flowed through a center channel. The earthen diversion berm appears to have been built to facilitate the transition of Colorado River flow from the western channel into the realigned portion and through the center of the Lulu City wetland. This objective will assess the effects of the berm and associated channel (referred to collectively as "channel realignement") and quantify the redistribution of discharge between wetland channels, hypothesis 1 (H_1) is as follows:

H_1: The 2015 channel realignment will decrease discharge through the western channel and increase discharge through the realigned reach and into the central wetland channel.

(A) (B)

Figure 3: Realigned channel and diversion berm at the head of Lulu City wetland, Rocky Mountain National Park. Panel A: Colored polygons indicate the path of the realigned channel (red hatch) and the approximate areal extent of the diversion berm (solid black); time lapse camera locations are also indicated by camera icons. Panel B: View to the south, from the diversion berm on the right bank of the realigned channel. Flow direction is into the page.

2.3 Objective 2: Hyporheic exchange and solute retention

"Hyporheic exchange" is a term often used to describe a wide range of surface water-groundwater interactions. As hyporheic exchange has become a more familiar concept in river restoration, interpretations of the term have become varied and numerous. An early definition proposed by White (1993) describes the hyporheic zone simply as a saturated subsurface region that either has stream water or has been affected by stream water advection, but even White concedes that defining this zone is often easier than delineating it in natural systems. Stanford and Ward (1988) found the extent and scale of the hyporheic zone to vary across gravel bed rivers, but they believe that its study should be included in any holistic consideration of river-floodplain systems. Gooseff (2010) expands upon the White (1993) definition by describing three realms in which hyporheic exchange is often considered: biological, geochemical and hydrologic, and he stresses the importance of including a timescale with every hyporheic definition. This research limits consideration of hyporheic exchange to that which occurs on short (<24 hour) timescales, but hyporheic exchange has widely been

used to describe surface water-groundwater exchanges on timescales of minutes to months. Given the short timescale considered here, this research is likely to characterize a cm^2- to m^2-scale portion of the larger hyporheic zone surrounding the Upper Colorado River through Lulu City wetland. This interpretation is consistent with the White (1993) definition, but also fits within the Gooseff (2010) geochemical interpretation by referring to a subsurface zone where two chemically distinct parcels of water mix together. Solute retention refers to the removal of solutes from the water column through physical processes, such as storage in floodplain sediments. Clear definitions are essential in the science of river restoration, where varying forms of hyporheic exchange have implications for project implementation and policy decisions.

The channel realignment will likely alter solute retention, due to changes in overbank flooding, and hyporheic exchange, due to changes in channel geometry. Numerical modeling conducted by Harvey and Bencala (1993) found that small-scale changes in bed topography are effective at prolonging water-sediment contact times, and at increasing hyporheic exchange fluxes. Additional modeling of river sinuosity found hyporheic exchange to increase with increasing hydrologic fluxes related to elongating meander necks (Boano et al., 2006). Fanelli and Lautz (2008) found that local changes in slope, which are often associated with transitions to pools, may control where groundwater returns to streams. Increasing hydraulic head often induces hyporheic exchange (Menichino and Hester, 2014), but where groundwater inputs are significant, groundwater head may readjust to reach equilibrium with higher stream head, thus limiting the effect of stream stage on hyporheic exchange (Storey, 2003). In systems with a large supply of fine sediment, infilling of coarse bed material may act to limit hyporheic exchange through the bed by creating a smooth, impermeable surface (Boulton et al., 1998). The effect of the 2015 channel realignment, which introduced many of the controlling factors described above, is evaluated based on hypothesis 2 (H_2):

H_2: The 2015 channel realignment will decrease hyporheic exchange and solute retention in the Colorado River channel and surrounding Lulu City wetland as a result of reduced channel complexity.

2.4 Objective 3: Sediment transport

During annual snowmelt, coarse-grained sediment is mobilized from the upstream debris fans and transported to the head of Lulu City wetland, where it is deposited in such a way that disperses flow and limits the main channel sediment transport capacity. Due to *in situ* weathering of coarse-grained, hydrothermally altered rhyolite tuff in the upstream debris fans, there exists a large supply of fine-grained sediment that may be transported into Lulu City wetland (Rathburn et al., 2013). Ideally, fine sediment will be transported through the Colorado River channel or deposited in the adjacent floodplain so as not to limit hyporheic exchange. Junk et al. (1989) suggest that floodplain fertility depends on fine sediment deposited during regular, long-duration flood pulses. Following the debris flow and prior to Colorado River channel realignment, natural flooding within the wetland was spatially variable and inconsistent. Pollutants and heavy metals that are typically transported with fine sediment are not a concern in this headwater stream, where the upstream drainage area is largely free of development. Instead, the fine sediment itself poses a threat to water quality and reduced drinking water storage capacity in downstream supplies.

Sediment transport assessments within this thesis are largely qualitative, and will primarily be used to inform a more comprehensive and quantitative sediment transport characterization of the Lulu wetland system planned for a later date. Sediment rating curves developed for cross sections on the Upper Colorado River upstream from Lulu City wetland indicate that sediment moving as bedload is positively correlated to high flows (Rathburn et al., 2013), while suspended sediment falls out of suspension in the low velocity flow associated with overbank flooding. The hypothesis addressing sediment transport is:

H_3: The 2015 channel realignment will increase the sediment transport capacity of the Colorado River through Lulu City wetland.

3. METHODS

Field and analytical methods will be presented in this section, following the order in which the associated objectives were introduced. Discharge measurements were used to create hydrographs to characterize the redistribution of flow throughout Lulu City wetland following channel realignment (Objective 1: Flow redistribution). A salt tracer injection was paired with continuous surface conductivity measurements and subsurface electrical resistivity to assess changes in surface water-groundwater interactions (Objective 2: Hyporheic exchange and solute retention). Sediment transport sampling, bed grain size analyses, and repeat bed elevation surveys were used to characterize sediment transport through the wetland (Objective 3: Sediment transport). Methods were replicated in 2016 following 2015 protocols, with 2016 deviations explained where they occur.

Study site and electrical resistivity transect names and notation will be consistent throughout. In-stream measurements on the Colorado River channel were recorded at gaging stations established at six study sites throughout the wetland. Gaging stations at each study site included a staff plate, 4-cm diameter PVC pipe to house a water level logger, and stable right and left bank cross section end points. Gaging stations were specifically installed to record multi-year stage, discharge and channel cross-section data. Study sites and associated data are color coded and include: **Upstream (US)**, **Realigned Reach (RR)**, **Wetland East (WE)**, **Wetland West (WW)**, **Wetland Center (WC)**, and **Lower Sentinel (LS)** (see Figure 4 and Figure 5). A distinction will be made between references to specific study sites and associated channels along the Colorado River within Lulu City wetland; specific study sites will be capitalized (e.g. the Wetland Center study site) while references to the associated channel reach will not be capitalized (e.g. the center channel). Electrical resistivity transects are named XS0, XS1 and XS2, from north to south. XSLW is the north-south trending transect on the west side of Lulu City wetland (Figure 4).

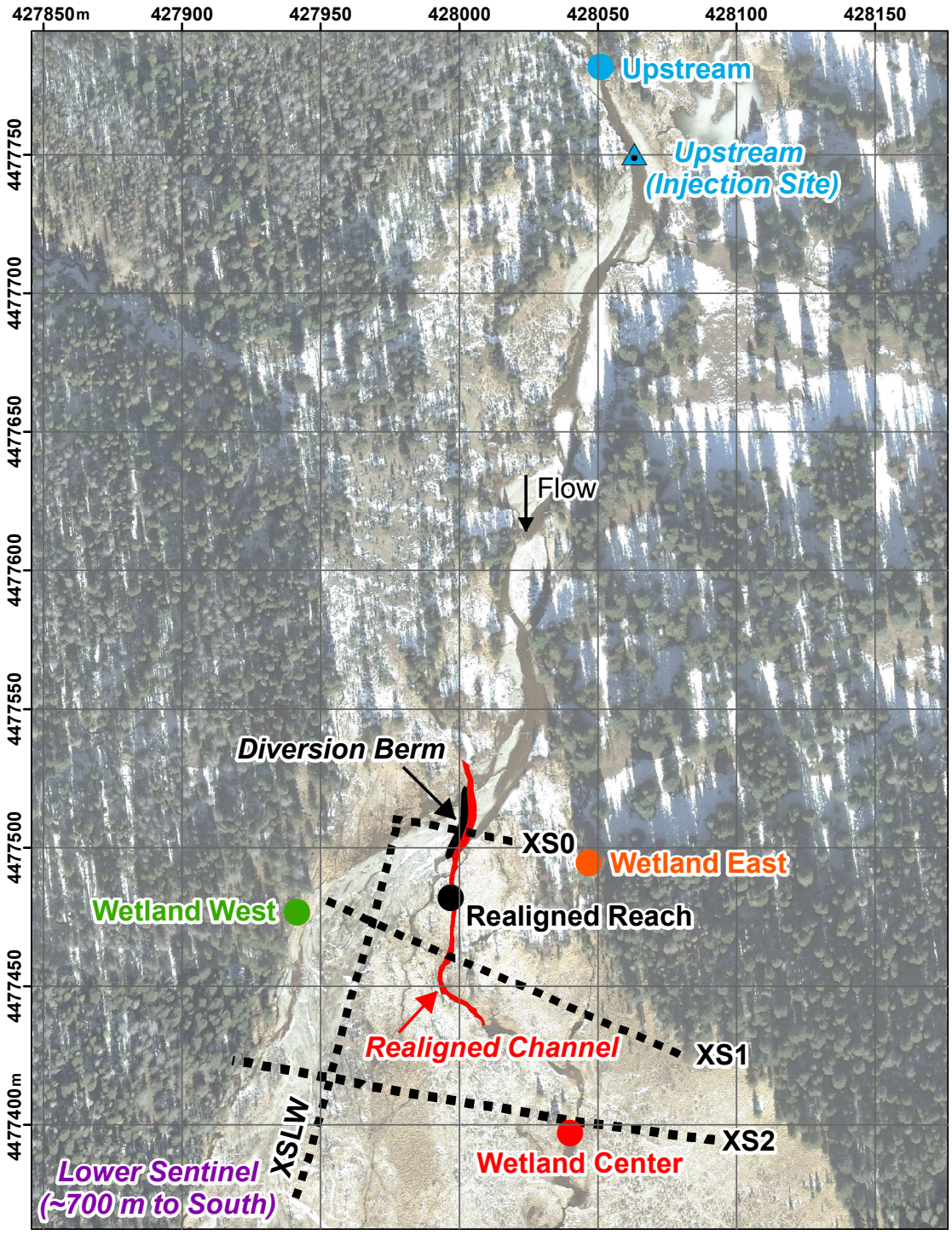

Figure 4: The Upper Colorado River and northern extent of Lulu City wetland, Rocky Mountain National Park. Circles indicate study site gaging locations. Dotted lines indicate electrical resistivity transects. The realigned channel and associated diversion berm are also indicated. Not pictured is the Lower Sentinel gage location on the Colorado River, 700 m to the South. Upstream (injection site) indicates the location of the Upstream surface conductivity meter.

Figure 5: Downstream views of study site gage locations on the Colorado River and within Lulu City wetland, Rocky Mountain National Park. Panel A, Upstream 8 July 2016; panel B, Realigned Reach 8 July 2016; panel C, Wetland West 2 July 2015; panel D, Wetland West 8 July 2016; panel E, Wetland East 8 July 2016; Panel F, Wetland Center 8 July 2016; panel G, Lower Sentinel 8 July 2016.

3.1 Field methods

3.1.1 Flow redistribution: stream gaging

Solinst Level Logger Edge Model 3001 pressure transducers were used to record stream stage every 15 minutes. Pre-realignment measurements were recorded from 27 April 2015 through 21 September 2015 at the Upstream, Wetland Center, Wetland West, and Lower Sentinel study sites. Post-realignment measurements were recorded from 28 April 2016 through 8 September 2016 at the Upstream, Wetland Center, Wetland East, Wetland West, Restored Reach, and Lower Sentinel study sites. The Level Logger Edge Model 3001 pressure transducer has 0.01 m level resolution and 0.003 m accuracy over the 5 m depth range. It compensates for temperature between 0 and 50°C with 0.003°C temperature resolution and ± 5°C temperature accuracy. A Solinst Barologger Edge Model 3001 barometer, located at the Upstream study site, was used to correct water levels at all study sites for barometric pressure. The barometer has 0.0001 kPa resolution and ± 0.05 kPa accuracy.

Discharge, periodically calculated using the velocity gaging technique, was used to develop hydrographs from stream stage data. Flow velocity was measured using a Marsh McBirney FloMate Model 2000 flow meter. The unit has 0.01 m/s measurement resolution, and 2% of reading accuracy within a velocity range of -0.15 to 6 m/s. Measurements were taken along fixed transects located at each study site. Across-transect sampling stations were determined by the operator at a spacing that appropriately characterized the bed surface topography. Velocity measurements were averaged over 40 seconds. Cross sectional area was calculated from the wetted perimeter and flow depth, recorded with a wading rod along the velocity gaging transects. In 2015, six discharge measurements were made between July and August. In 2016, ten measurements were made between May and August.

3.1.2 Hyporheic exchange and solute retention: tracer test

Conservative tracers are commonly used to characterize surface water-groundwater exchange. Covino et al. (2011) have used chloride to characterize gross hydrologic exchanges between stream and groundwater and Harman et al. (2016) have used salt tracers to assess

how stream groundwater turnover times vary with discharge in montane streams. Non-conservative tracers, like nitrogen, can be used to quantify biotic consumption, but solute retention within the scope of this study is limited to physical storage of a conservative tracer. Others have successfully used electrical resistivity to characterize solute transport within the near-stream hyporheic zone (White, 1988; Ward et al., 2010). Because electrical resistivity is an intrinsic measure of a material's resistance to electric current flow, low electrical resistivity indicates highly conductive, saturated or moist soil, while high electrical resistivity indicates less conductive, drier substrate (McClymont et al., 2011).

Salt tracer tests were conducted during base-flow conditions between 14:40-18:40 on 6 September 2015, prior to channel realignment, and 11:30-15:30 on 28 August 2016, after channel realignment. Sodium chloride was dissolved in stream water and injected at a constant rate for four hours at the Upstream study site. Flow rate and concentration were similar during tracer tests in 2015 and 2016 (Table B.11). Injection concentrations were sufficient to raise stream dissolved solids concentrations 3 to 4 times above background, which was predicted to elicit a measurable response (Singha, personal comm. (2015)). Such elevated levels were needed to distinguish tracer-induced signals from background electrical resistivity levels. The tracer test was conducted during base-flow because research on a similarly sized mountain stream in Colorado showed more reliable hyporheic exchange estimations at low flows, when the stream was unlikely to gain groundwater, rather than high flows (Harvey et al., 1996). Additionally, completing the tracer tests during similar low flows helped control one variable, discharge, that was likely to influence hyporheic exchange (Ward et al., 2013).

3.1.3 Hyporheic exchange and solute retention: surface electrical conductivity

Surface conductivity was used to quantify changes in water residence times through Lulu City wetland using mass balance and velocity calculations. Mass balance analyses can then be used to characterize solute retention in river systems (Covino et al., 2011; Patil et al., 2013). During the salt tracer test, Onset HOBO model U24 conductivity probes were used to measure electrical conductivity and temperature at four (2015) and five locations

(2016) throughout Lulu City wetland. The conductivity loggers have two calibrated ranges: 0 - 1000 μS cm^{-1} (low range) and 0 - 10,000 μS cm^{-1} (full range), both within a calibrated temperature operating range of 5 to 35°C. Low-range conductivity measurements have 1 μS cm^{-1} resolution and ± 3% or 5 μS cm^{-1} accuracy. High-range conductivity measurements have 1 μS cm^{-1} resolution and ± 3% or 20 μS cm^{-1} accuracy. Both ranges have 0.01°C temperature resolution and 0.1°C temperature accuracy within the calibrated range.

Pre-realignment measurements in 2015 were recorded using the full conductivity range because the peak electrical conductivity produced by the injected tracer was not known. Post-realignment measurements in 2016 were recorded using the low conductivity range because data from 2015 indicated that peak electrical conductivity in 2016 would fall within the low conductivity range. Conductivity probes were placed at study sites and placement decisions were controlled by the number of available units and the distribution of flow through surface channels at the time of measurement.

Four conductivity probes were placed in 2015 at the following study sites: Upstream, Wetland West, Wetland Center, and Lower Sentinel (Figure 1). Wetland East was not instrumented in 2015 because it flowed into Wetland Center, which was instrumented. Five conductivity loggers were placed in 2016 at the following gage sites: Upstream, Realigned Reach, Wetland East, Wetland Center, and Lower Sentinel. Wetland East was instrumented in 2016 instead of Wetland West, because Wetland West no longer received base-flow as a result of the diversion berm associated with the realigned channel.

The Upstream conductivity probe was placed 34 m downstream from the injection site, which was the maximum length possible to remain within the single thread channel of the Colorado River. The mass recovered at the Upstream location was used as the input mass for mass recovery analyses, rather than what was actually injected at the Upstream site, because variations in pumping rates and incomplete salt dissolution made it difficult to accurately quantify how much salt was delivered to the system (Table B.11). Recording frequencies of the conductivity probes varied between 4 seconds and 90 seconds, based on the highest

frequencies allowed by instrument storage capacities that would allow a full characterization of the tracer breakthrough at each location (Table A.10).

3.1.4 Hyporheic exchange and solute retention: electrical resistivity imaging

Electrical resistivity was used as a semi-quantitative technique to identify changes in the hyporheic zone. By tracking salt tracer induced changes in subsurface electrical resistivity relative to background conditions, I characterized the subsurface area that exchanges water with surface flow, which by definition, describes the hyporheic zone. Electrical resistivity transects were measured using an IRIS Syscal Pro resitivity meter and a dipole-dipole measurement scheme. Stainless steel electrodes were placed in the ground and connected to a power source by an above ground extension cord. Groupings of four electrodes, called quadripoles, were varied along the transect according to a user-defined program. Under this scheme, one electrode pair was used to complete a circuit and the second was used to measure the difference in potential, which was then used to calculate an apparent resistivity (Binley and Kemna, 2005). This survey method was chosen for its ability to resolve vertical features and tracer plumes better than other electrical resistivity survey methods (Binley and Kemna, 2005), although this array generally experiences signal-noise issues because measurement electrodes are positioned outside of the pair of transmitting electrodes (Ward, 1990). Additionally, this array generally requires large input voltages for widely spaced dipole pairs, which can cause problems during the inversion process (Binley and Kemna, 2005). Four transects within Lulu City wetland were chosen: XS0, XS1, XS2, XSLW (Figure 4), repeating the ground penetrating radar transects of Rubin et al. (2012). Each electrical resistivity transect had 2595 quadripoles and electrode spacing between 1 and 4 meters, depending on the minimum spacing required to achieve the desired transect length. Closer electrode spacing allowed for more detailed visualization of the shallow subsurface than compared to widely spaced electrodes (Binley and Kemna, 2005).

Electrode positions were measured using a Topcon GR-5 real time kinematic global navigation satellite system (RTK-GNSS). The RTK-GNSS has 0.001 m resolution, 0.01 m

horizontal and 0.015 m vertical accuracy. Background electrical resitivity data were collected along all four transects prior to the salt tracer injections in 2015 and 2016. During the salt tracer injection, electrical resistivity data were recorded continuously along transect XS1 for 19-24 hours after the tracer injection began. This timing was informed by Ward et al. (2012), who suggests at least 12 hours of monitoring following the end of the injection in order to cover the period when the rate of electrical resistivity change within the hyporheic zone is likely to be the greatest.

3.1.5 Sediment transport

Depth-averaged suspended sediment was sampled for 2 minutes along thechannel thalweg at each study site using a DH-48 depth integrating hand line sampler with a 6-mm diameter nozzle. Bedload was sampled for 2 minutes from the channel thalweg using a Helley Smith bedload sampler with a 76 mm square opening and 0.4 m long, 250 micron nylon mesh net. Where collected, sediment concentrations were extrapolated to effective channel widths. Suspended sediment and bedload sediment samples were collected in 2016, but field sediment collection retrieved minimal volumes even during higher discharges, so these results were not used in any analyses. Logistical issues in 2015 delayed sediment sampling until after the snowmelt peak. Field observations suggest that both bedload and suspended sediment did move through the system, but not when collection occurred. It is more likely that transport in this system occurred during daily peak flows around midnight, and not at 12 noon, which was when the field sampling usually occurred. Additional semi-quantitative analyses, including aerial imagery differencing, bed grain size characterizations, and repeat bed elevation surveys were used to assess the sediment transport potential through the system.

Bed grain size distributions were measured following the Wolman pebble count method (Wolman, 1954). Intermediate axis diameters of 100 clasts were measured using a standard gravelometer and a random walk clast selection along representative reaches centered on established stream study sites (Figure 1). Analyses were conducted after peak flow in 2015 and 2016 at the Upstream Site, Wetland West, Wetland Center, Wetland East and Lower Sentinel. Bed grain size was measured at the Realigned Reach in 2016.

Repeat channel cross section surveys were completed at the Realigned Reach throughout snowmelt 2016 using a wading rod on a weekly basis and additionally with the RTK-GNSS on 13 July 2016. Cross sections were calibrated using the top right bank (transect distance = 8 m; a stable point) of the 13 July 2016 transect, which was surveyed using the RTK-GNSS. Left bank topography was harder to define, and thus subject to more uncertainty. Left bank elevations did not influence mean bed elevation calculations. Elevations were calculated from wading rod transects by subtracting the measured depth from the recorded gage height. An additional 0.08 m correction factor was subtracted from the 26 May 2016 and 1 June 2016 transects because the staff plate from which the gage height depths were recorded required a readjustment following the 1 June 2016 measurement.

3.1.6 GPS surveying

Topographic cross sections and reach-averaged slopes were measured at all study sites using the RTK-GNSS on 22 July 2015 and 13 July 2016.

3.1.7 Repeat photography

Reconyx HC500 HyperFire cameras were installed in April 2016 at two locations along the realigned channel in order to capture overbank flow and monitor the status of the constructed earthen diversion berm. Photographs were taken hourly from 6 am to 8 pm at each location; one camera viewing upstream (north) from the left bank and one camera viewing downstream (south) from the right bank, near the upstream edge of the diversion berm (Figure 3A). Repeat photography from these cameras was used to verify overbank flow analyses.

3.2 Analytical methods

3.2.1 Flow redistribution: hydrograph creation

Stage-discharge relationships were used to create hydrographs for all study sites in 2015 and 2016. Pressure transducer stage measurements were calibrated using weekly field measured stage values for each study site. Discharge was calculated using field measurements and the continuity Equation 1 as follows:

$$Q = \sum_{n=1}^{n} V_n A_n \tag{1}$$

where Q = discharge, V_n = velocity, and A_n = cross sectional area measured at n locations across a transect. Cross sectional area was calculated as a trapezoid across the transect. Discharge from continuity was used to calibrate the Manning equation (Equation 2), which was then used to calculate a discharge for every pressure transducer stage measurement. The Manning equation discharge, Q_m is given by:

$$Q_m = \frac{1}{n} A R^{(2/3)} S^{(1/2)} \tag{2}$$

where A = cross sectional area, roughness coefficient $n = 0.040$, R = hydraulic radius, and S = friction slope. To calculate Q_m for each stage measurement, S was first calculated by calibrating Q_m to field measured Q, and then A and R were varied for all Q_m calculations according to each stage measurement; A was calculated using the trapezoid method at each stage; R was calculated at each stage as A/WP, where WP = wetted perimeter; n was estimated by visual inspection, based on values for gravel bed streams with partially vegetated beds and banks (Arcement and Schneider, 1989).

3.2.2 Hyporheic exchange and solute retention: tracer mass recovery

Tracer mass recovery (T_{MR}) was calculated at each electrical conductivity measurement location from breakthrough curves, using (Equation 3), and solute retention was calculated as $1 - T_{MR}$:

$$T_{MR} = Q \int_0^t T_c(t)dt \tag{3}$$

where Q is the discharge measured at each study site on the day of the tracer test (calculated using Equation 1); T_c is the time-integrated tracer concentration at that site (mg L^{-1}), and t = time since tracer injection. Because conductivity loggers were set to different sampling frequencies, only measurements sampled at common times were extracted for comparisons of breakthrough curves; therefore dt = 180 seconds in 2015 and dt = 90 seconds in 2016. The discharge calculated at the Upstream study site was used to calculate T_{MR} at the Upstream conductivity site, because discharge was assumed to be unchanging in the 34 m between the two sites (Figure 4). T_c was quantified for each conductivity meter using the linear relationship measured between concentration (mg L^{-1}) and specific conductance at 25°C (μS cm^{-1}) (Table A.9). Breakthrough curve truncation, after Drummond et al. (2012), was required in 2016 because temperature-corrected specific conductance resulted in receding limb tails that did not return to pre-injection background levels. The receding limb was used to set sensitivity limits for the Realigned Reach, Wetland Center, Wetland East, and Lower Sentinel study sites; however, data from the Upstream study site did not require tail truncation in 2016. Because sampling continued for 19 to 24 hours following the end of the salt tracer injection, the receding limb measurements were more likely to capture variations in background electrical conductivity caused by changing flow conditions than the rising limb, where measurements were taken for less than one hour. Truncation of the 2016 data does underestimate mass recovery, which may overestimate solute retention, but this truncation was necessary because full tail analyses resulted in mass recovery estimates that were physically impossible (> 100% recovery).

3.2.3 Hyporheic exchange and solute retention: breakthrough curve tailing behavior

Solute retention capacity was further characterized by fitting a power-law function (Equation 5) to the receding tail of each normalized tracer breakthrough curve, following Patil et al. (2013), which allowed for relative, between-site, comparisons. Normalized break-

through curves were utilized, where time was normalized by time-to-peak and concentration was normalized by time-to-concentration. Receding tails were identified using Equation 4:

$$t_{start} = t_p + \frac{t_{end} - t_p}{2}, \tag{4}$$

where the time at the transition between the curve plateau and the falling limb is substituted for t_p in Equation 4, and t_{end} is the time at which no more measurable tracer was recovered. Power law functions were then fit to the receding limbs, following Patil et al. (2013):

$$C = aT^{-b}, \tag{5}$$

where C = normalized tracer concentration; T = normalized time; and a and b are empirically derived coefficients. Concentration (C) was normalized by peak concentration (C_P) and time (T) was normalized by time at peak concentration (T_P). The goal is to minimize the sum of squared residuals, defined by:

$$\sum_i (f_i - y_i)^2 \tag{6}$$

where f_i is the modeled value and y_i is the measured value.

3.2.4 Hyporheic exchange and solute retention: electrical resistivity inversion

Maps of estimates of subsurface conductivity, called tomograms, were generated along each electrical resistivity transect using the solver code R2 (v3.1, Generalized 2-D Inversion of Resistivity Data, available at http://www.es.lancs.ac.uk/people/amb/Freeware/ R2/R2.htm), which generates solutions through non-unique data inversion. The goal of the non-unique inverse solution is to accurately reflect electrical resistivity data noise while representing the subsurface electrical conductivity within the spatial scale that can be resolved by the survey design (Singha et al., 2014). Input model parameters were adjusted to produced background electrical resistivity inversions with root-mean-square error (RMSE), relative to data noise,

equal to 1. Inversions for which R2 converged on a solution, but where RMSE values were greater than 1, were retained in analyses.

Tomograms were produced from two types of inversions. Inversions were first completed on transects XS0, XS1, XS2, and XSLW, which were measured prior to the salt tracer injection. Measurements recorded along these transects are unrelated to the background transects completed for the tracer tests. For the tracer electrical resistivity analyses, each replicate measurement along transect XS1, referred to as a time step, was independently inverted against the background transect measurements, after Ward et al. (2012). Transects that failed to converge were omitted, which included the first time step measurements in 2015 and 2016. Transects were assigned times based on the completion of the entire run, which averaged 23 minutes in 2015 and 39 minutes in 2016. Subsurface water content and battery drain contributed to a wide range of transect completion times, which were beyond operator control.

Quadripoles were filtered to remove noisy or erroneous data. Instrument errors were reported in the output as current values of 9999. Because these values would have unrealistically impacted the measured voltage/injected current ratio needed for the inversion process, they were removed from analyses. Where these quadripoles were removed from one dataset they were removed from all time-steps in order to facilitate direct time-step comparisons between tomograms. Alternatively, quadripoles used in time-lapse inversions with injected current below 10 mA were removed, after Johnson et al. (2012).

4. RESULTS

4.1 Flow redistribution

Colorado River flow paths through Lulu City wetland imposed on aerial imagery show the redistribution of surface water flow between pre-realignment (2015) and post-realignment (2016) conditions (Figure 6). The cumulative flow path lengths shown in Figure 6 are 2,444 m in 2015 and 1,794 m in 2016. There is a distinct lack of flow in 2016 through the Western channel, which was 839 m (green dashed line, panel A), and the addition of a flow path through the Realigned Reach, which is 188 m (black line, panel B), toward the center of Lulu City wetland (Figure 6). Hydrographs in 2015 and 2016 (Figure 7) were used to quantify the redistribution of flow through Lulu City wetland by comparing the average daily discharges that passed through each study site under pre-realignment and post-realignment conditions (Table 1). It is important to note that hydrographs reflect any Grand Ditch-related water diversions and releases, which were assumed to be roughly equivalent between 2015 and 2016. Discharges in Table 1 are normalized by drainage area to allow for direct comparisons between sites, resulting in units of L T^{-1}. Due to close proximity between study sites, all study sites in Table 1 are assigned a drainage area of 25.5 km^2, except the Lower Sentinel site, which has an upstream drainage area of 29.2 km^2.

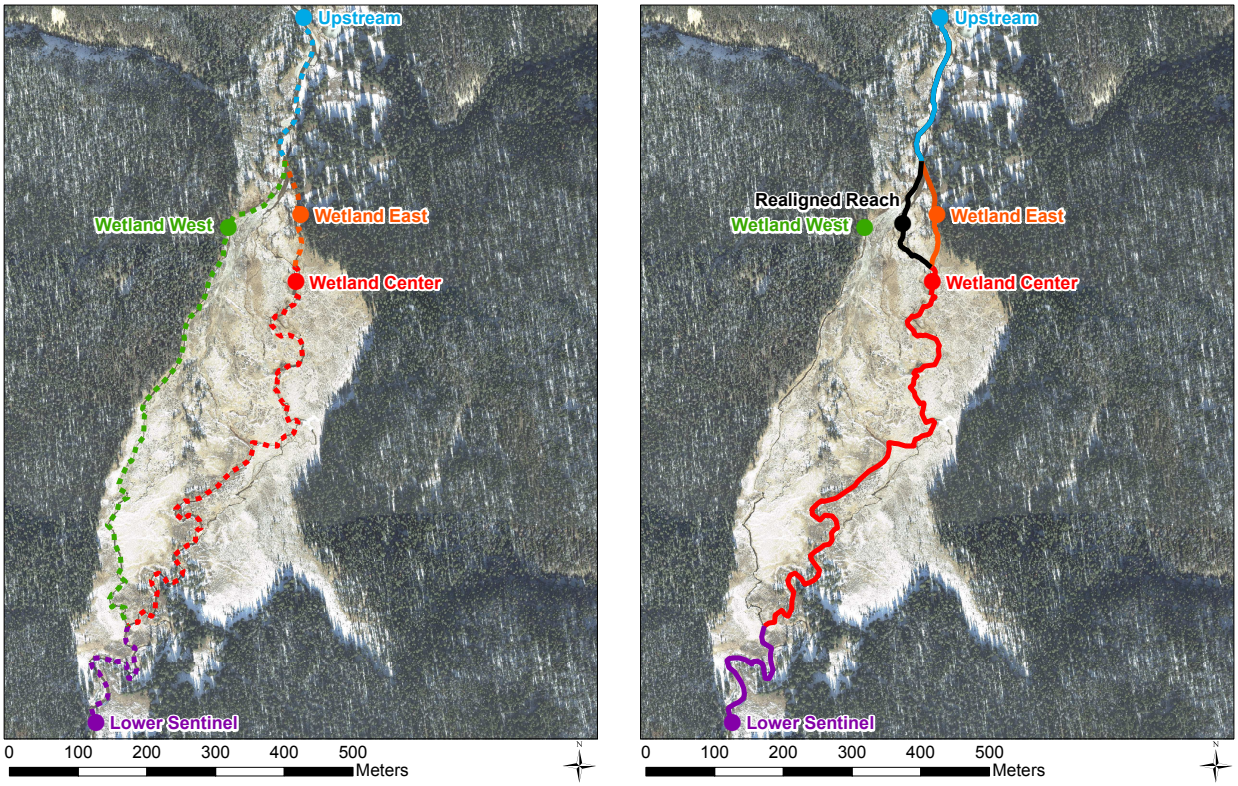

(A) 2015 flow paths

(B) 2016 flow paths

Figure 6: Major stream flow paths through Lulu City wetland, Rocky Mountain National Park. Pre-realignment flow paths are depicted in panel A and post-realignment flow paths are depicted in panel B. Study sites are indicated by solid circles. Colored streamlines indicate single threads of flow and are colored following the same scheme described in Section 3.

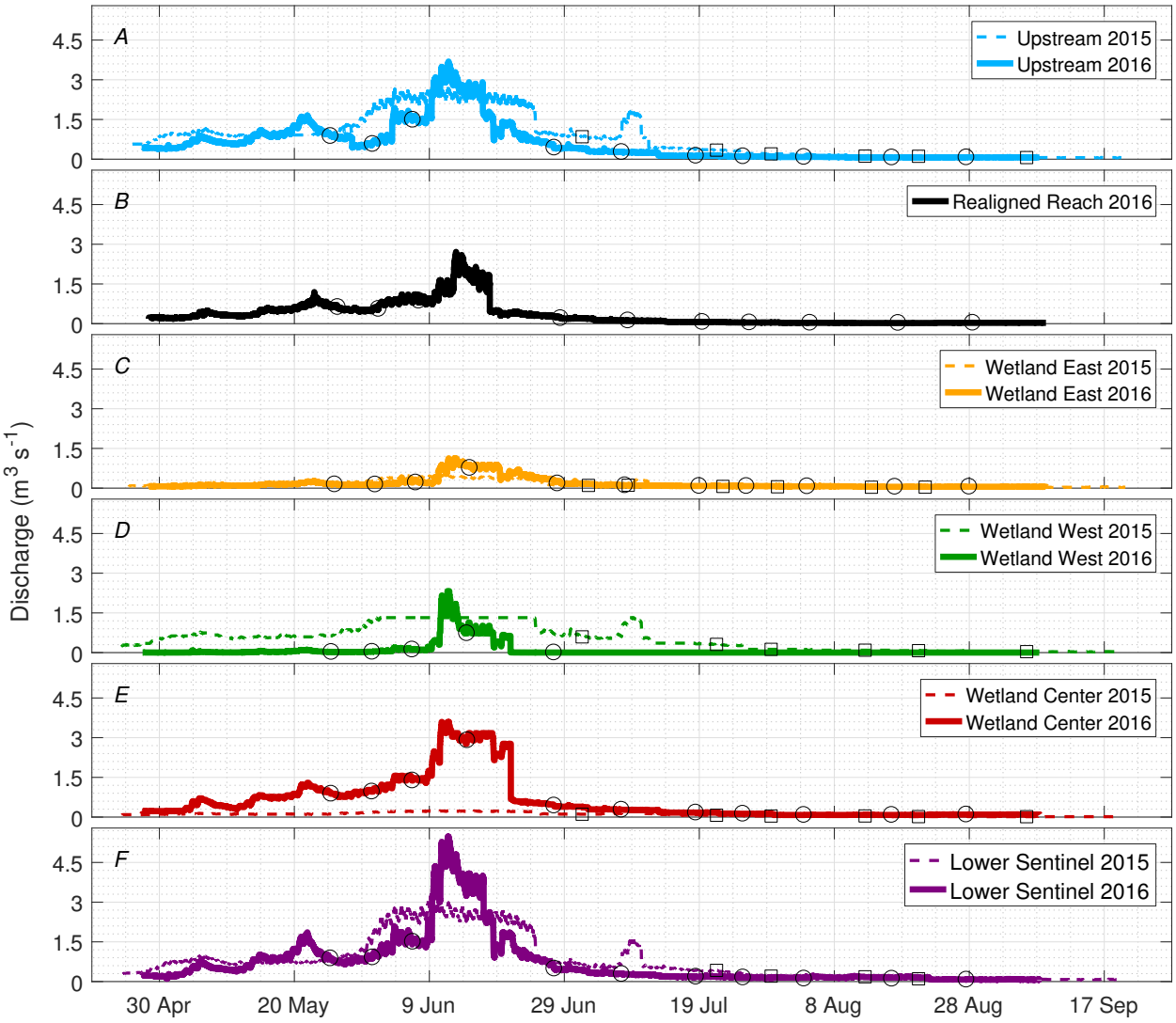

Figure 7: 2015 and 2016 hydrographs for all study sites. Study sites are arranged according to river distance from the Upstream study site. Panel A, Upstream; Panel B, Realigned Reach; Panel C, Wetland East; Panel D, Wetland West; Panel E, Wetland Center; and Panel F, Lower Sentinel. Steep decreases in discharge may be related to Gran Ditch related water diversions. Symbols represent field sampling points (squares in 2015 and circles in 2016). For the same figure with a semi-log discharge scale, see Figure C.32.

Table 1: Discharge comparisons between 2015 and 2016 at all study sites. Study sites are arranged according to river distance from the Upstream study site. Average Q is the average daily discharge at each site, averaged over 133 days between 28 April and 8 September, then normalized to drainage area. Discharge values are then expressed as a percentage of the upstream discharge in that flow year.

Study Site	**2015 Average Q (mm day^{-1})**	**2016 Average Q (mm day^{-1})**	**2015 % of Upstream**	**2016 % of Upstream**
Upstream	3.0	2.0	100	100
Realigned Reach	-	1.1	0	56
Wetland East	0.5	0.6	18	31
Wetland West	1.9	0.3	64	16
Wetland Center	0.4	2.1	12	103
Lower Sentinel	2.6	2.1	87	104

At all study sites, the 2016 snowmelt hydrograph was more peaked than it was in 2015. Both rising and falling limbs were steeper and total discharge higher in 2016 than in 2015. The 2016 snow pack reached 28 cm of snow water equivalent, which melted faster than the 2015 snow pack, which peaked at 23 cm of snow water equivalent (NRCS, 2016). Peak discharges were smaller in 2015 and lasted longer into the summer, and early July rains resulted in a secondary sub-peak, but rainfall was relatively insignificant in both years. In 2015, 7 rainfall events between 0.5 cm and 2 cm occurred while only 4 events of the same magnitude occurred in 2016 (NRCS, 2016). The Upstream study site is included in Table 1 to highlight the higher average discharge in 2016 than 2015. Average daily discharges for the 2015 study sites may be slightly overestimated because the rising limbs of those hydrographs were calibrated to the first field measurement, which was not recorded until 2 July 2015 (Figure 7). Flow through Wetland East increased between 2015 and 2016 by 13%. Wetland West was the dominant flow path through Lulu City wetland in 2015, but received only 16% of Upstream flow in 2016 as a result of the channel realignment. Due to the channel realignment, Wetland Center received 103% of upstream flow in 2016, which was an increase of 91% over 2015. The Realigned Channel and Wetland East, which both flow into the

center channel, totaled 87% of upstream flow in 2016, or 16% less than what was received immediately downstream at the Wetland Center study site. This difference may be attributed to the propagation of measurement errors or due to unidentified groundwater inputs that were not active in 2015. The percentage of upstream flow in 2016 through Wetland West (16%) occurred entirely during peak runoff, when overbank flow was high enough to pass around the constructed diversion berm (Figure 7). The Lower Sentinel study site received a larger percentage of the Upstream flow in 2016 than in 2015, due to the shortening and consolidation of flow paths through Lulu City wetland (Figure 6).

Hydrograph data were used to calculate the number of overbank, or flood days, at each study site (Table 2). Bankfull stage was calculated from the staff plate stage associated with flows greater than the top of the lowest bank, as defined through inspection during field site visits. Bankfull width-to-depth ratios (W/D), which provide a sense for transect channel geometry, were calculated at bankfull stage height from RTK-GNSS measured cross sections from 13 July 2016. The Lower Sentinel width/depth ratio was calculated from the 7 June 2016 wading rod cross section, because poor satellite reception limited the use of the RTK at that site.

Table 2: Bankfull analysis and overbank flow comparison between 2015 and 2016 for all study sites within Lulu City wetland, Rocky Mountain National Park. Study sites are arranged according to river distance from the Upstream study site. W/D is the width-to-depth ratio at bankfull stage. Days overbank are rounded up to the nearest day.

Study Site	**Bankfull Stage (m)**	**W/D Ratio**	**Days Overbank (2015)**	**Days Overbank (2016)**	**Change (days)**
Upstream	0.78	4.6	25	10	-15
Realigned Reach	0.21	4.2	-	75	-
Wetland East	0.22	5.8	59	34	-25
Wetland West	0.21	4.3	116	20	-96
Wetland Center	0.36	3.8	32	127	+95
Lower Sentinel	0.33	8.8	78	53	-25

There were 15 fewer overbank flow days recorded at the Upstream site in 2016 than in 2015, despite a higher average daily discharge in 2016. Overbank flooding in 2015 was gradual and sustained, while the flooding in 2016 appeared to have been more widespread during the 10 overbank days. Flow through the Wetland East study site responded similarly to the Upstream site, in that 25 fewer overbank flow days occurred in 2016 than in 2015, despite a larger percentage of upstream flow in 2016 than 2015. There were also 25 fewer overbank flow days recorded at the Lower Sentinel site in 2016 than 2015 (Table 2).

Overbank flooding is evident in photos from 2015 (Figure 8) and from time lapse photography captured by two cameras positioned along the Realigned Reach in 2016 (Figure 9 and Figure 10). Flooding was extensive through mid-June in both years. In 2016, flooding largely receded by the end of June (Figure 9D).

Figure 8: Pre-realignment flooding along the Colorado River in Lulu City wetland, Rocky Mountain National Park, from 10 June 2015. The location of the 2016 diversion berm is indicated by the dashed bar. Flow is from right to left, and view is to the south.

(A) 22 May 2016 (B) 11 June 2016 (C) 12 June 2016

(D) 24 June 2016 (E) 6 July 2016 (F) 7 September 2016

Figure 9: Realigned channel time lapse photography, view is downstream to the south. Panels A through F are photos of the realigned channel and adjacent floodplain within Lulu City wetland, Rocky Mountain National Park. Peak discharge occurred on 13 June, 2016.

(A) 22 May 2016 (B) 11 June 2016 (C) 12 June 2016

(D) 24 June 2016 (E) 6 July 2016 (F) 7 September 2016

Figure 10: Realigned channel time lapse photography, view is upstream to the north. Panels A through F are photos of the realigned channel and adjacent floodplain within Lulu City wetland, Rocky Mountain National Park. Peak discharge occurred on 13 June, 2016.

The effects of flow redistribution on the entire wetland system may be assessed by considering the discharge flux through Lulu City wetland by assuming only one surface water

input and one output. Hydrologic fluxes through the wetland were calculated by assigning discharge through the Upstream study site as the primary wetland input and discharge through the Lower Sentinel Gage as the primary wetland output. Daily fluxes are shown in Figure 11A, and cumulative fluxes are shown in Figure 11B, after Wegener (2016). Negative fluxes indicate surface water loss, primarily through evapotranspiration and wetland storage, while positive fluxes indicate surface water gains from groundwater, tributaries, or less loss to storage. In both 2015 and 2016, Lulu City wetland fluxes were negative in the early spring, positive during snowmelt, and close to zero during base-flow. In 2016, the positive flux during peak snowmelt was much higher than in 2015. Following snowmelt, the 2016 wetland flux remained close to zero, while the 2015 wetland flux dropped below zero before returning to base-flow conditions characterized by zero flux. Cumulative discharge fluxes through Lulu City wetland were noticeably different between 2015 and 2016. In 2015, the Colorado River lost 58 mm of water to evapotranspiration and storage in Lulu City wetland, while in 2016 the Colorado River gained 11 mm water over roughly the same time period, marking a 119% change. Data from 2012, which was an exceptionally dry year, shows a cumulative discharge flux of <1 mm and trends that suggests persistent base-flow conditions through much of the summer.

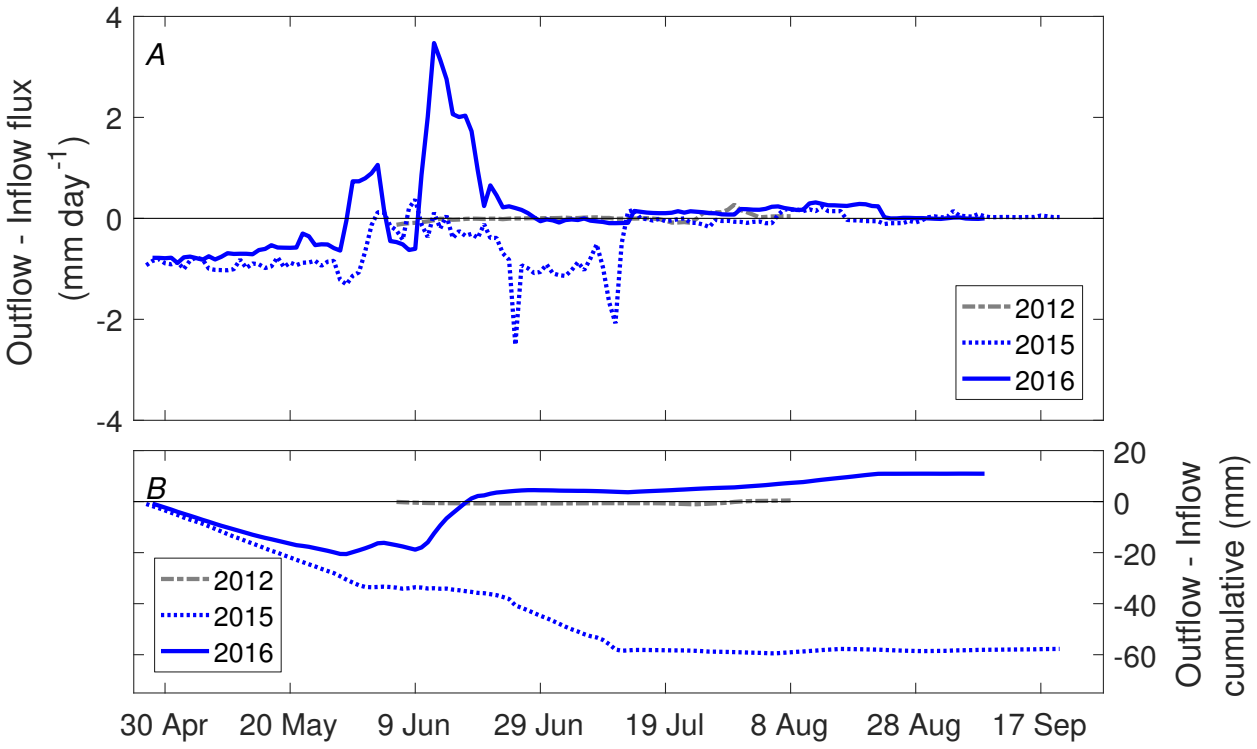

Figure 11: Discharge flux through Lulu City wetland. Panel A: The daily discharge flux through the wetland was calculated for 2012, 2015, and 2016 by subtracting the normalized daily discharge at the Upstream study site from the normalized daily discharge at the Lower Sentinel study site. Panel B: Cumulative discharge flux through the wetland for 2012, 2015, and 2016.

4.2 Hyporheic exchange and solute retention

4.2.1 Tracer mass recovery

The utility of tracer mass recovery comparisons relied on similar analytical and environmental conditions between tests conducted in 2015 and 2016. User controlled variables, like pump rate and injection solution concentration, were held constant between years (see Table B.11). Measured discharge at the Upstream site was 0.061 m^3 s^{-1} on 6 September 2015 and 0.066 m^3 s^{-1} on 28 August 2016 (Figure D.33).

Breakthrough curves

Solute concentration breakthrough curves for all sites are shown in (Figure 12). Total mass recoveries, calculated by integrating each breakthrough curve, are shown in Figure 13 and a summary of the mass recoveries is presented in Table 3. Constant-rate tracer injections

tend to produce plateau breakthrough curves, similar to all sites except Lower Sentinel in Figure 12, while pulse injections produce peaked breakthrough curves, often shaped like Lower Sentinel in the same figure (Drummond et al., 2012). Because all sites received the same constant-rate salt injection, the difference in breakthrough curve shape is a function of tracer travel time, which is affected by stream velocity and losses or gains through hyporheic exchange or solute retention.

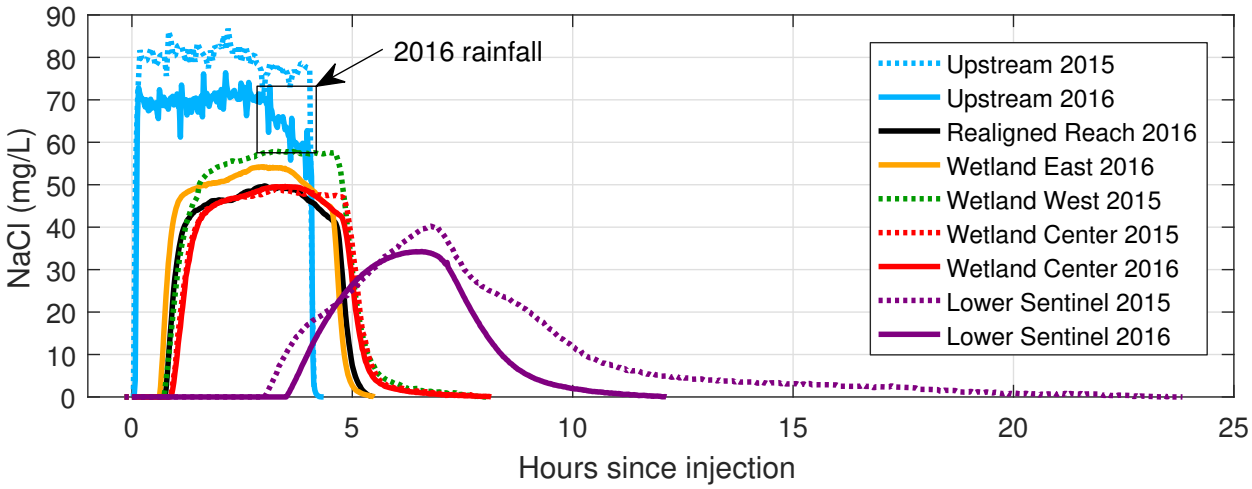

Figure 12: Salt tracer test concentration breakthrough curves for all study sites. 2016 breakthrough curves required tail truncation (excluding Upstream 2016). Legend entries are listed according to river distance from the Upstream study site.

The plateau variance shown in the Upstream breakthrough curve in both 2015 and 2016 is a result of incomplete mixing. Day (1977) found a downstream mixing length of 25 times the channel width to be adequate for complete vertical and lateral mixing for salt dilution gaging in mountain streams. The mixing length in this reach was limited to 12.5 times river width because the transition to distributary channels and multi-threaded flow $\sim$ 35 m downstream of the injection site would have introduced more error into the mass recovery calculation than inadequate mixing. The effects of light rainfall can be seen in the Upstream 2016 breakthrough curve (Figure 12). Rain began 2.5 hours into the tracer injection and lasted through the end of the injection at 4 hours (Figure 12), however, consistent 15-minute river stage measurements verify a negligible stream discharge response during the storm.

Because all analyses of tracer recoveries are based on the mass recovery at the Upstream site in each year, it was not imperative that the two concentrations were exactly the same. More importantly, the timing and slope of the rising and falling limbs within the Upstream breakthrough curves are identical, as are the magnitude and variance within the plateaus. The plateau concentrations at the Realigned Reach and Wetland sites are lower than the source plateau concentration (Upstream sites), which could be caused by freshwater inputs as a result of dilution from fresh water inputs to the channel between the Upstream site and the Wetland sites.

The presence of a shoulder on both the rising and falling limbs of the 2015 Lower Sentinel breakthrough curve is notable when compared to the 2016 Lower Sentinel breakthrough curve, where it is entirely absent. The tracer also arrived at the Lower Sentinel site later and was flushed through earlier in 2016 than in 2015. The remaining Lulu City wetland sites exhibit similar breakthrough curve patterns to each other.

Mass recovery

Mass integrations of the Figure 12 breakthrough curves are displayed in Figure 13. The total mass recovered at the Upstream Site was 70.0 kg in 2015 and 64.8 kg in 2016, and these values were used as reference mass values for all mass recovery calculations. These values are larger than those calculated from the continuous calibration field samples (Table B.11) and are differences that may be explained by the uncertainty propagated through the mass integration, primarily related to instrument error. Lower accuracy associated with the larger instrument calibration range used in 2015 can easily account for the higher mass recovery in 2015 (as described in Methods). A larger integration time step (180 seconds) was used in 2015 than in 2016 (90 seconds), which was necessitated by differences in the conductivity meter sampling frequencies. As a result, 2016 mass recoveries were calculated from more measurements, which subjected the final values to greater cumulative instrument errors. This error was offset in 2016 by using a tighter instrument calibration range with higher accuracy. Additional uncertainty was introduced by the specific conductivity to con-

centration conversion factor (0.47-0.51, Table A.9) and specific conductivity temperature coefficient (0.02 $°C^{-1}$), (Rice et al., 2012), but these uncertainties were consistent between sample years.

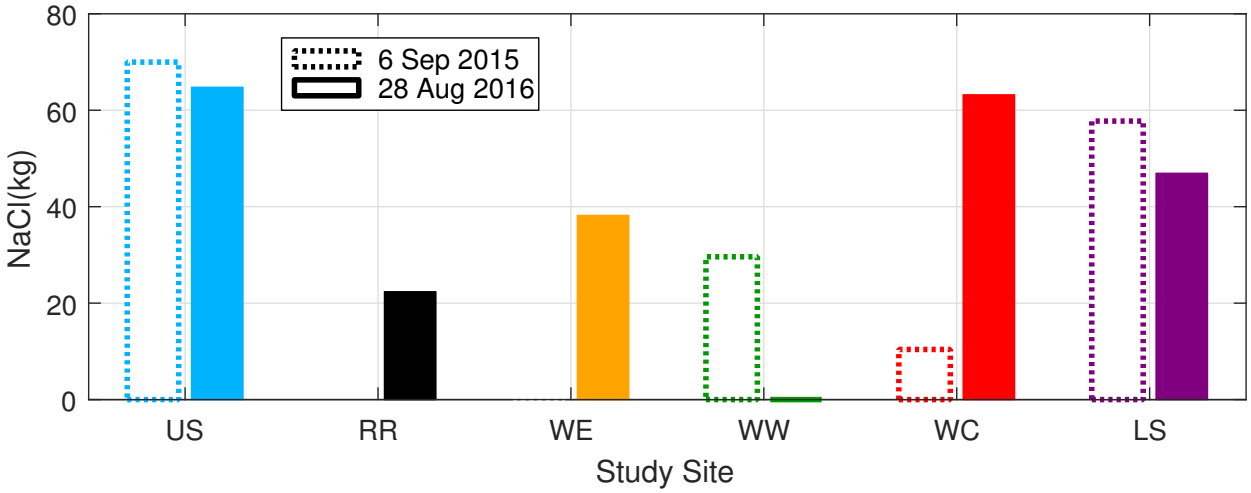

Figure 13: Total mass of salt recovered at each study site within Lulu City wetland, Rocky Mountain National park. Mass totals represent the area under each conductivity breakthrough curve in Figure 12. Study sites are arranged from left to right according to river distance from the Upstream study site. US = Upstream; RR = Realigned Reach; WE = Wetland East; WW = Wetland West; WC = Wetland Center; LS = Lower Sentinel.

Table 3: Salt tracer mass recoveries at all study sites within Lulu City wetland, Rocky Mountain National Park. Recovered mass is the same value depicted in Figure 13. Recovered mass represents the mass percent recovery at each site, as a percent of the Upstream mass recovery in that year. Retained mass is calculated as *1* - T_{MR} as a percentage of Upstream recovered mass. A graphical depiction of mass recovery can be found in Figure E.34.

Study Site	**Recovered mass (kg)**	**Recovered mass (as % of Upstream mass)**	**Retained Mass (as % of Upstream mass)**
Upstream 2015	70.0	100	0
Upstream 2016	64.8	100	0
Realigned Reach 2016	22.4	34.5	65.5
Wetland East 2015	-	-	-
Wetland East 2016	38.2	59.0	41.0
Wetland West 2015	29.6	42.3	57.7
Wetland West 2016	0	0	0
Wetland Center 2015	10.4	15.1	84.9
Wetland Center 2016	63.2	97.6	2.4
Lower Sentinel 2015	57.8	77.0	23.0
Lower Sentinel 2016	46.9	72.5	27.5

In 2015, the combined mass recovered between the Wetland West and Wetland Center study sites totaled 40 kg, or 57% of the mass recovered at the Upstream injection site. In 2016, the mass recovered at the Wetland Center study site was 63 kg, or 97.6% of the mass recovered at the Upstream injection site. The combined mass recovered at the Realigned Reach and Wetland East study sites, which both flow into the Wetland Center study site (Figure 6), totaled 60.6 kg, or 93.5% of the mass recovered at the Upstream site. Given the close proximity between study sites, the similarity between these values is expected, and the difference is assumed to be negligible. In 2015, the mass recovered at the Lower Sentinel site was 57.8 kg, or 77% of the Upstream site. In 2016, the percentage of mass recovered at the Lower Sentinel study site decreased to 72.5% (Table 3).

Characteristic in-stream travel times

Tracer travel times within Lulu City wetland added to the understanding of flow dynamics and potential solute retention. The characteristic in-stream travel time, as defined by Drummond et al. (2012), is the time for the salt tracer at a study site to reach half the maximum plateau tracer concentration. These normalized values, which indicate tracer velocities at each site, after Jackman et al. (1984), are shown in Figure 14. Associated tracer velocities are summarized in Table 4.

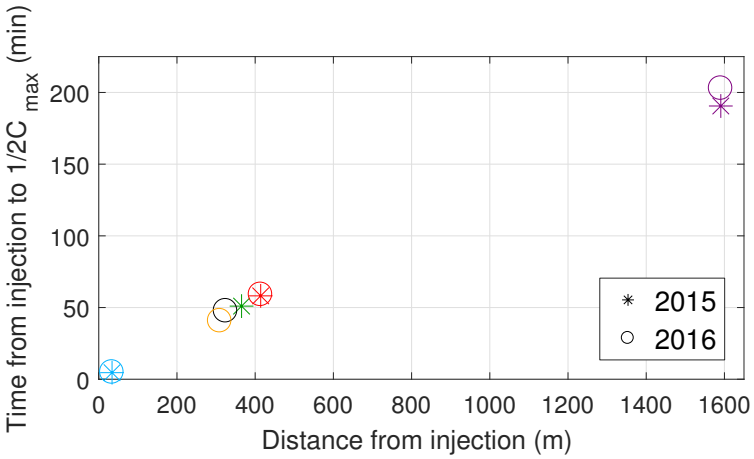

Figure 14: Characteristic in-stream travel times as distance from the Upstream injection site for all study sites within Lulu City wetland, Rocky Mountain National Park. Color coded symbols represent the following sites: **Upstream**, **Realigned Reach**, **Wetland East**, **Wetland West**, **Wetland Center**, and **Lower Sentinel**. Asterisks represent values from 2015 and open circles represent values from 2016.

Table 4: Salt tracer velocities, by study site within Lulu City wetland, Rocky Mountain National Park. Velocities were calculated as the time at which the leading edge of the concentration reached 50% of the average plateau concentration, are displayed. Study sites are listed according to river distance from the Upstream study site.

Study Site	**Velocity (m s^{-1})**
Upstream 2015	0.12
Upstream 2016	0.12
Realigned Reach 2016	0.11
Wetland East 2015	-
Wetland East 2016	0.13
Wetland West 2015	0.12
Wetland West 2016	0
Wetland Center 2015	0.12
Wetland Center 2016	0.12
Lower Sentinel 2015	0.14
Lower Sentinel 2016	0.13

Plateaus for in-stream travel time calculations were defined by obvious slope changes on the rising and falling limbs. Average plateau concentrations were used instead of maximum plateau concentrations to account for variability within the plateau concentrations. Plateau concentrations affected by rainfall dilution at the Upstream site in 2016 were excluded from that average calculation. Because the tracer response at the Lower Sentinel site was characterized by a peak, not a plateau, the maximum concentration value there was substituted for the maximum plateau value. Travel times show a strong linear relationship with distance (R^2=0.99). Travel time to the Upstream site in 2016 was within 30 seconds of the travel time to the same site in 2015, which serves to reinforce method continuity between years. Between-year travel times to Wetland Center were also similar within a minute, even with the extra flow path to this site through the Realigned Channel. Tracer velocities indicate that flow through the Wetland East study site was the fastest flow path through the upper Lulu City wetland and that flow through the realigned channel was relatively slow. The

2016 tracer velocity through Wetland East was 0.13 m s^{-1} while flow through the Realigned Reach was 0.11 m s^{-1}. Tracer velocity through the Lower Sentinel study site decreased from 0.14 m s^{-1} in 2015 to 0.13 m s^{-1} in 2016.

4.2.2 Breakthrough curve tail characterization

Results from breakthrough curve solute retention characterizations using Equation 5 are presented in Table 5. The slope of the power-law fit (exponent b, Equation 5) characterizes the breakthrough curve tail, where shallower slopes indicate greater capacity for solute retention than steeper slopes (Patil et al., 2013). With the exception of Wetland East in 2016, power law slopes are generally lower in the northern Lulu City wetland, and higher near the wetland outlet at Lower Sentinel (Table 5).

Table 5: Power law characterizations of mass recovery breakthrough curve tails, from Equation 5. The sum of squared residuals is an indication of goodness of fit, where the best model seeks to minimize this value. Study sites are listed according to river distance from the Upstream study site.

Study Site	**Coef. (a)**	**Slope (b)**	**Sum of squared residuals**
Realigned Reach 2016	0.451	0.121	2.75e-04
Wetland East 2015	-	-	-
Wetland East 2016	0.629	0.687	9.96e-04
Wetland West 2015	0.458	0.232	1.10e-03
Wetland West 2016	-	-	-
Wetland Center 2015	0.483	0.185	2.11e-03
Wetland Center 2016	0.457	0.118	3.41e-04
Lower Sentinel 2015	0.643	0.348	3.51e-03
Lower Sentinel 2016	0.633	0.318	8.07e-04

Linear regressions were calculated to explore any correlation between discharge, velocity, or bed slope and the slope of the power law fit, b, from Equation 5 (Figure 15). As channel slope, discharge and velocity increase, the slope of the power law function increases, indicating decreasing solute retention capacity. These relationships, although weak, are consistent with what Patil et al. (2013) found for similarly sized streams.

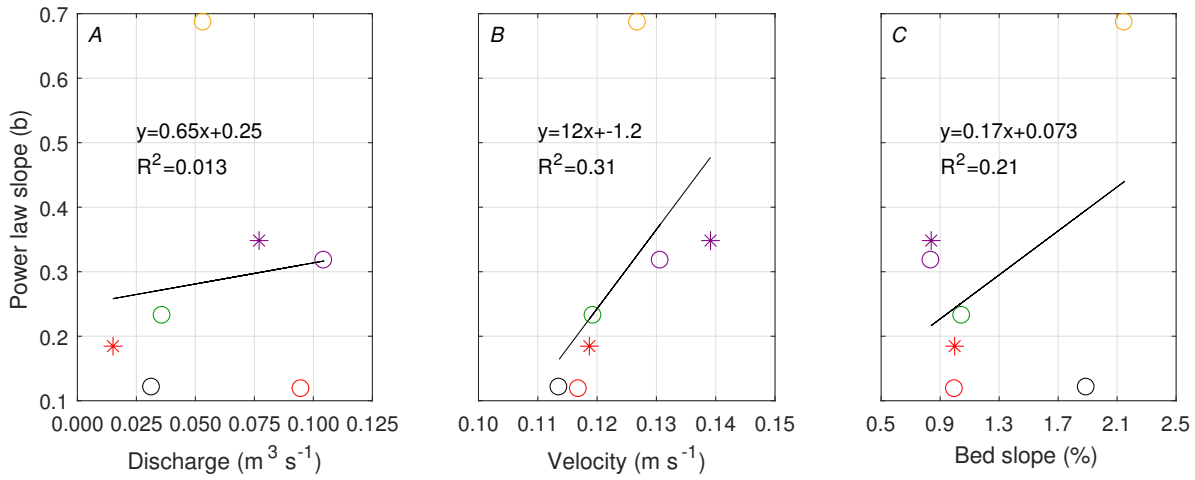

Figure 15: Power law slope regressions. Panel A: power law slope (b) as a function of discharge (m^3 s^{-1}); panel B: power law slope (b) as a function of velocity (m s^{-1}); panel C: power law slope as a function of bed slope (%). Color coded symbols represent the following study sites within Lulu City wetland, Rocky Mountain National Park: **Upstream**, **Realigned Reach (RR)**, **Wetland East**, **Wetland West**, **Wetland Center**, and **Lower Sentinel**. Asterisks represent values from 2015 and open circles represent values from 2016.

In a separate interpretation of solute retention, the ratio of recovered mass to recovered discharge was calculated at each study site. The ratio is loosely based on work from Harvey and Wagner (2000), who calculate net groundwater exchange by using both dilution gaged discharge and velocity gaged discharge. The mass recovered at each study site during the salt tracer test is calculated as a percentage of the mass recovered at the Upstream site, and divided by the discharge recovered at that same study site, calculated as a percentage of discharge recovered at the Upstream site. Normalization is therefore built into each ratio, which facilitates between-site comparisons (Table 6). Small values indicate less salt was recovered at a site relative to discharge, which may indicate higher solute retention capacity. Conversely, larger ratios indicate lower solute retention capacity. If the proportions are the same, the ratio would be 1, which might suggest no solute retention. Results from this analysis are shown in Table 6. Similarly to the power-law slopes presented in (Table 5), the mass/discharge ratios are different between the upper wetland (e.g. Realigned Reach and Wetland sites), where ratios are higher, and the lower wetland (e.g. Lower Sentinel), where the ratios are lower.

Table 6: Mass/discharge solute retention ratios, by study site within Lulu City wetland, Rocky Mountain National Park. Study sites are ordered according to river distance from the Upstream study site. Mass is calculated as the percentage of upstream mass recovered in that year. Discharge is calculated as the percentage of upstream discharge in that year. Smaller values indicate higher solute retention.

Study site	**Mass(%)**	**Discharge (%)**	**Mass/Discharge**
Upstream 2015	100.0	100.0	1.00
Upstream 2016	100.0	100.0	1.00
Realigned Reach 2016	34.5	47.6	0.72
Wetland East 2015	-	55.7	-
Wetland East 2016	59.0	80.5	0.73
Wetland West 2015	42.3	59.0	0.72
Wetland West 2016	0	-	-
Wetland Center 2015	15.1	24.8	0.61
Wetland Center 2016	97.6	143.1	0.68
Lower Sentinel 2015	77.0	126.2	0.61
Lower Sentinel 2016	72.5	157.7	0.46

4.2.3 Electrical resistivity

Electrical resistivity results are presented as tomograms, or qualitative, false-color images of subsurface electrical resistivity, in Figure 16 through Figure 24. Resistivity has been converted to conductivity, or the inverse of resistivity, for interpretation. For consistency "electrical resistivity" will be used to reference the physical transects, but "conductivity" will be used from here forward to describe the data measured along the electrical resistivity transects. Conductivity values were not temperature corrected because the substrate temperature was not continuously monitored throughout the electrical resistivity surveys. Figure colorbars represent conductivity values from 10 - 120 μS cm^{-1}. For reference, the background concentration at the injection site was 44 μS cm^{-1} in 2015 and 47 μS cm^{-1} in 2016. Conductivity values below roughly 50 μS cm^{-1} therefore indicate substrate with lower conductivity than the background stream concentration and values greater than 50 μS cm^{-1} represent more conductive fluid or substrate. The conductivity of the injected salt tracer solution was around 4,800 μS cm^{-1}.

Fence diagrams

Fence diagrams display the electrical resistivity transects in 3-dimensional space within Lulu City wetland (Figure 16). This representation highlights broad changes in conductivity and lithology throughout the study area, but is not sensitive enough to accurately identify small-scale changes in substrate lithology. In general, conductivity is high in areas that cross the flowing Colorado River channel in the east channel and portions of the west channel. A similar response is noticeably absent along transect XS1 under the realigned channel (Figure 16B). There is some consistency between years in high conductivity values at the east ends of transects XS1 and XS2. The seemingly large difference in conductivity near the west end of transect XS2 may be attributed more to edge-effects than to changes in physical conditions within Lulu City wetland. The potential fields measured by electrical resistivity extend in 3-dimensions, but the tomograms compress that information into a 2-dimensional representation. Therefore, the edges of transects are hard to accurately characterize as

they often include information from outside the appropriate measurement plane. Out-of-plane effects may also explain why conductivity is lower along transect XSLW than transect XS0 at the intersection of those two transects in the norther part of Lulu City wetland. Conductivity is highest along transect XSLW in both 2015 and 2016 where the west channel crosses transect XSLW. Comparatively little change in conductivity between 2015 and 2016 in the area under the realigned channel suggests limited spatial influence on the surrounding shallow groundwater.

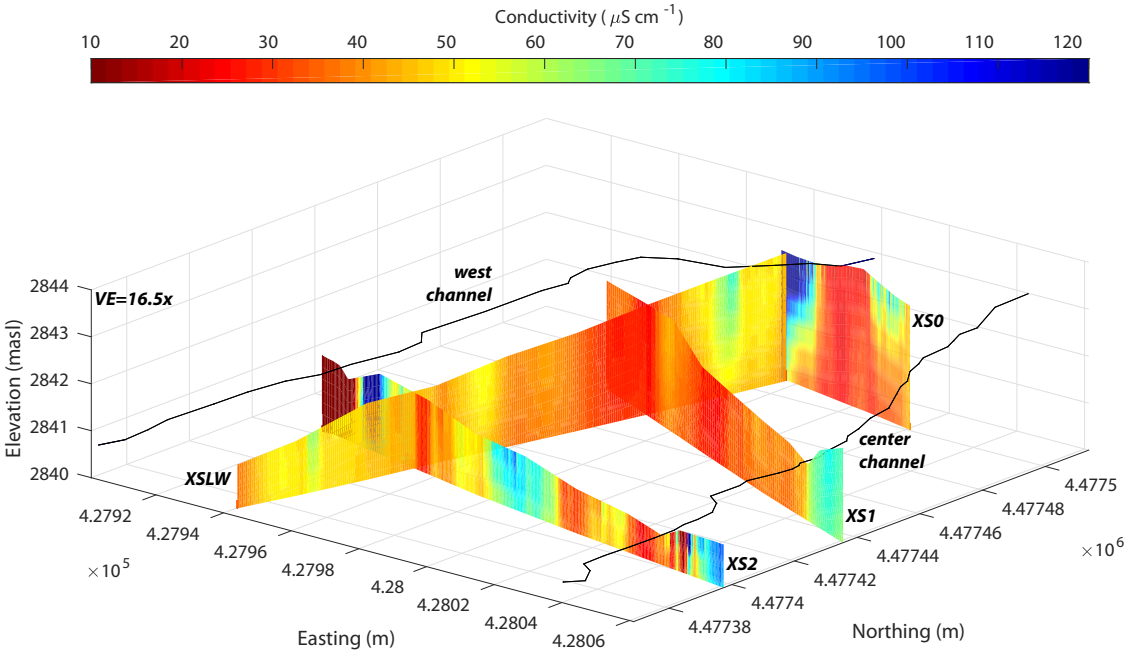

(A) Pre-realignment (2015)

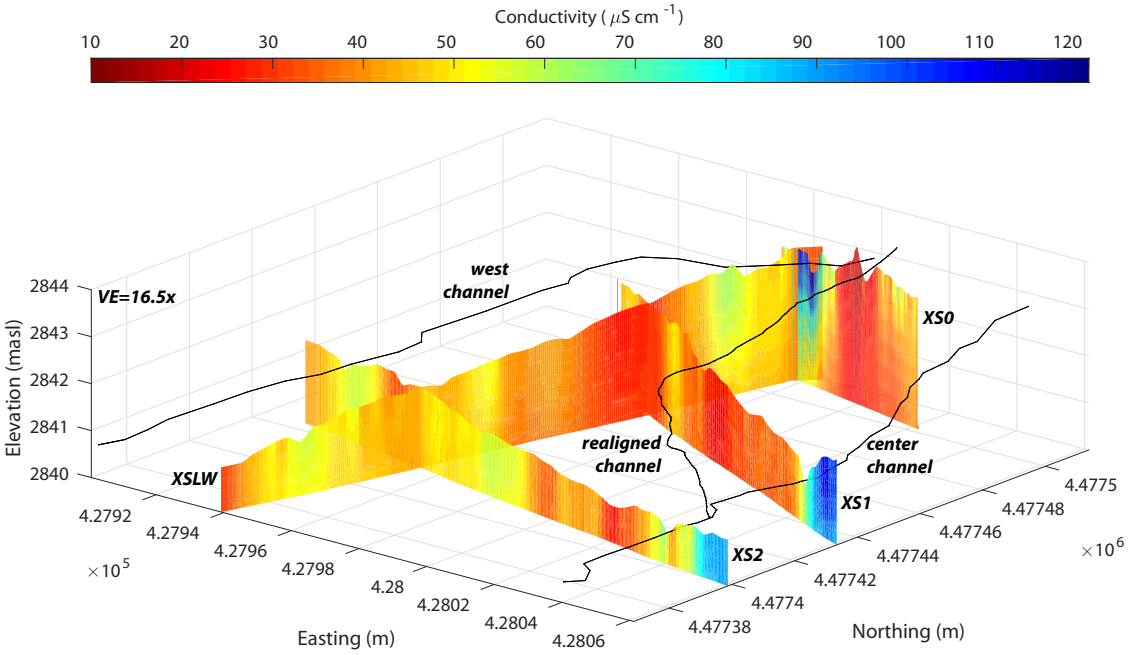

(B) Post-realignment (2016)

Figure 16: Electrical resistivity transect tomograms in 3-dimensional space within the pre-realignment (2015) and post-realignment Lulu City wetland, Rocky Mountain National Park. Generalized stream channels are added for reference; stream flow is from north to south. Locations of transects XS0, XS1, XS2, and XSLW are shown within Lulu City wetland in Figure 4. The view orientation is from an azimuth of 40° and elevation angle of 50°.

Comparative tomograms

While fence diagrams (Figure 16) facilitate the interpretation of conductivity on the wetland spatial scale, changes to the hyporheic zone in this system are more likely to occur on sub-meter spatial scales, adjacent to channels. Such changes become evident in Figure 17 through Figure 21, which show pre- and post-realignment comparisons of selected portions of electrical resistivity transects. These figures focus on specific areas of interest along electrical resistivity transects, such as stream channels and the constructed diversion berm.

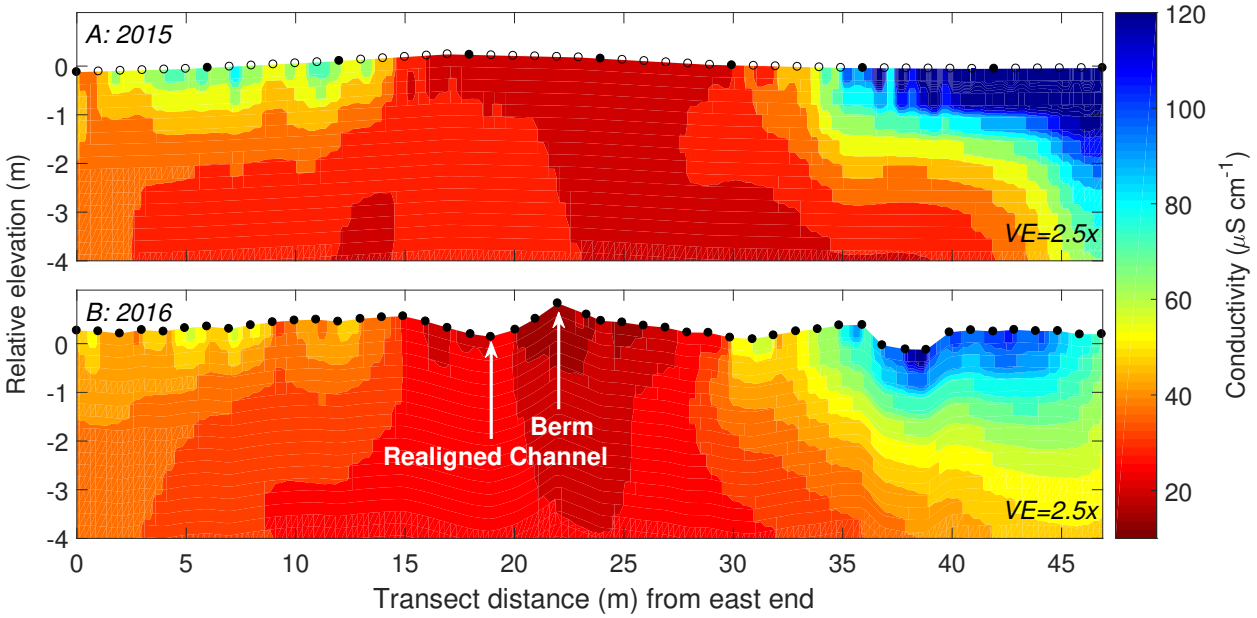

Figure 17: Comparative electrical resistivity tomograms measured along transect XS0 (location shown in Figure 4). Panel A was measured in 2015, prior to channel realignment. Panel B was measured in 2016, following channel realignment. The complete XS0 transect is displayed between 0 to 50 m. Circles represent electrode locations; solid circles represent surveyed electrode locations and open circles represent interpolated electrode locations. Final root mean squared error was 1.06 in 2015 and 1.00 in 2016.

Transect XS0 crosses the area of Lulu City wetland where the diversion berm was constructed at the head of the realigned channel. The constructed berm and realigned channel are labeled in Figure 17b. The small channel at 38 m in Figure 17b also existed in 2015 at the same location in Figure 17a, but was not surveyed in 2015. Differences in topography at the west end of the transect are a function of interpolation between surveyed points and suggest a smoother ground surface than exists at that location. Conductivity

results in Figure 17 show a decrease in conductivity at the diversion berm, and conductivity changes to a depth of 4 m (Table G.13). There are no obvious changes under the realigned channel, near 17 m. This is likely because at this location the realigned channel was dug entirely into debris flow sediments. Simply excavating sediment has done little to augment hyporheic exchange because substrate characteristics under the channel remained the same as the pre-realignment condition. The extent and magnitude of the low conductivity zone at the west end of the transect decreased between 2015 and 2016, which reflects decreased flow to this area as a result of the diversion berm. Statistical analyses confirmed a decrease in conductivity to a depth of 1 m at all spatial scales across transect XS0 between 2015 and 2016 (Table 7).

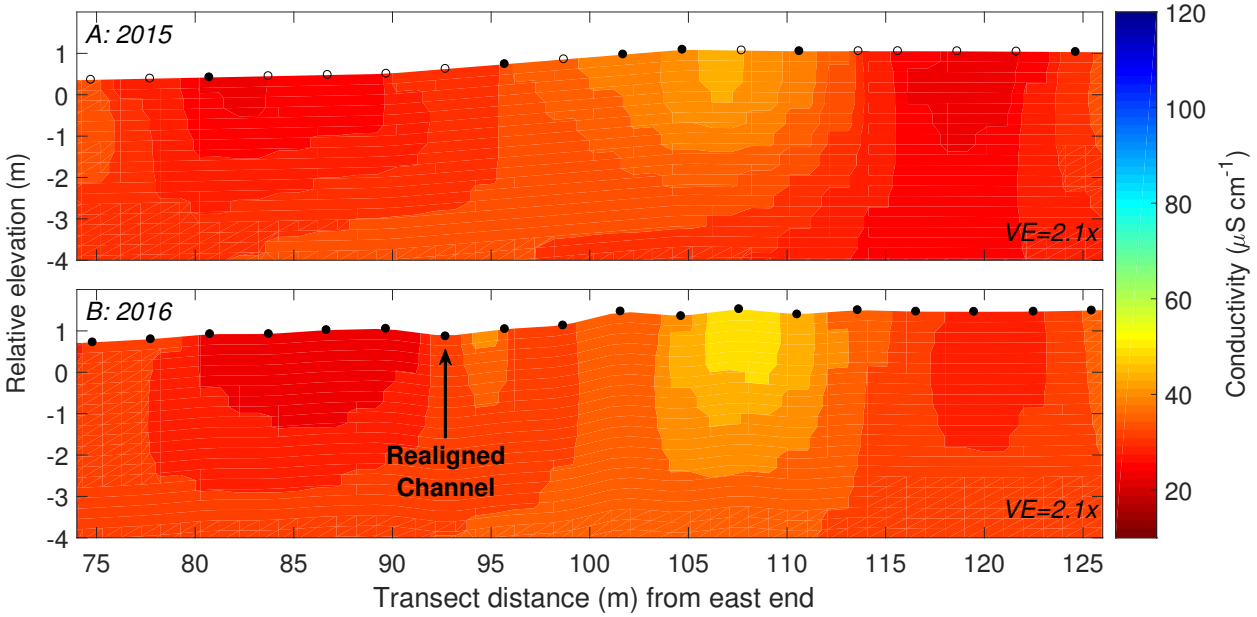

Figure 18: Comparative electrical resistivity tomograms measured along transect XS1, including the realigned channel (location shown in Figure 4). Panel A was measured in 2015, prior to channel realignment. Panel B was measured in 2016, following channel realignment. This portion of transect XS1 includes the realigned reach. Circles represent electrode locations; solid circles represent surveyed electrode locations and open circles represent interpolated electrode locations. Final root mean squared error was 1.00 in 2015 and 1.00 in 2016.

The center portion of transect XS1 crosses the realigned channel at 93 m, which can be seen in Figure 18. In general, conductivity near the realigned channel is low in both pre- and

post- realignment conditions, and is similar to the conductivity measured at the realigned channel in Figure 17. Statistical analyses confirmed a slight increase in conductivity to a depth of 1 m between 75 and 125 m along transect XS1 between 2015 and 2016, but this change did little to affect hyporheic flow through the realigned channel (Table 7).

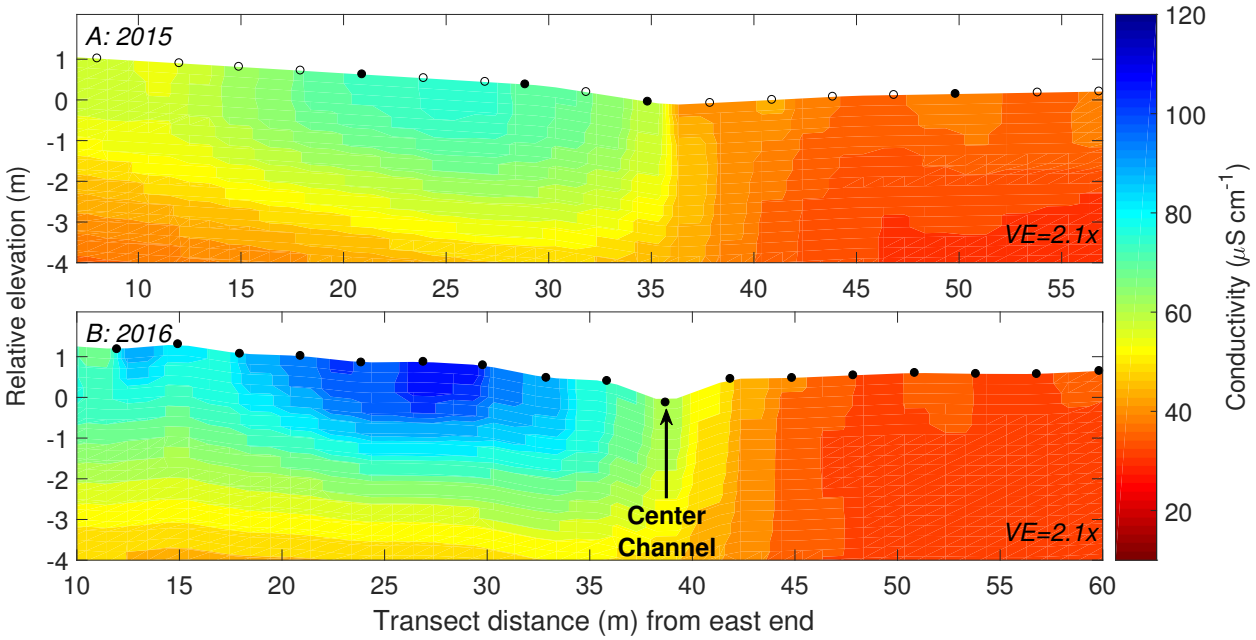

Figure 19: Comparative electrical resistivity tomograms measured along transect XS1, including the center channel (location shown in Figure 4). Panel A was measured in 2015, prior to channel realignment. Panel B was measured in 2016, following channel realignment. This portion of transect XS1 includes the center channel. Note the different x-axes; a 3-m offset was required due to different east-end transect starting positions. Circles represent electrode locations; solid circles represent surveyed electrode locations and open circles represent interpolated electrode locations. Final root mean squared error was 1.00 in 2015 and 1.00 in 2016.

The east portion of transect XS1 crosses the Wetland Center channel at 38 m (Figure 19). In general, high conductivity values were measured in both 2015 and 2016 near the east end of transect XS1 and lower values were measured in both years towards the west end of transect XS1. Statistical analyses confirmed an increase in conductivity to a depth of 1 m under and east of the center channel along this portion of transect XS1 between 2015 and 2016 (Table 7). Because the 2015 and 2016 transect locations were not perfectly aligned in space, there is a 3 m offset in transect positions.

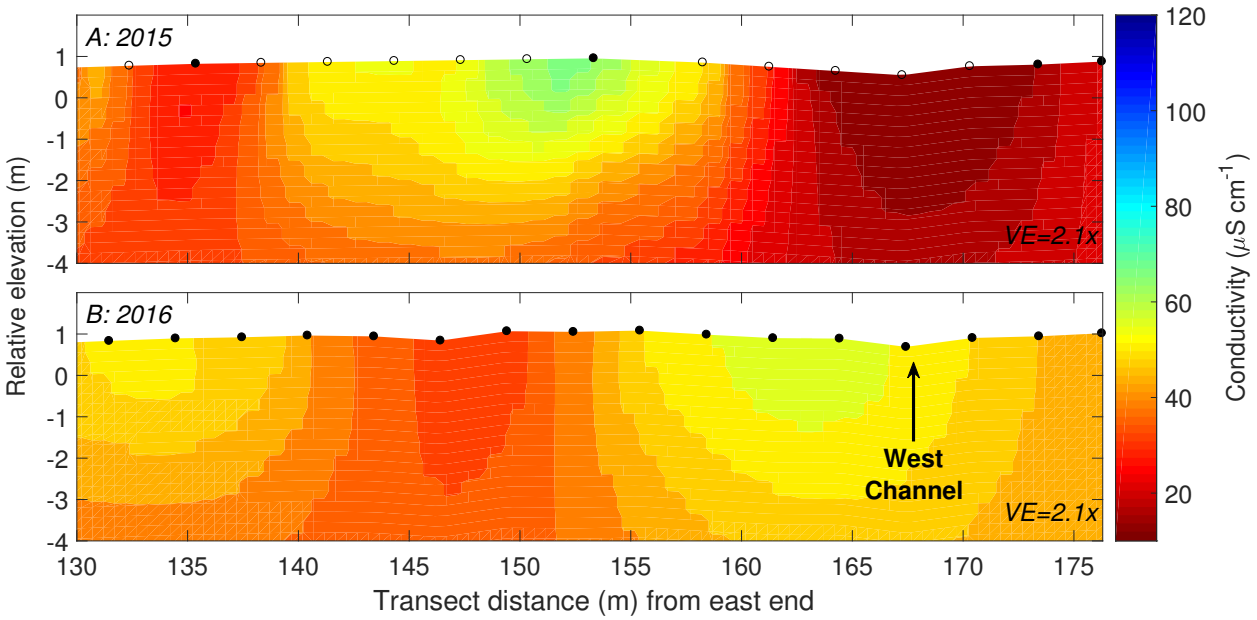

Figure 20: Comparative electrical resistivity tomograms measured along transect XS2, including the west channel (location shown in Figure 4). Panel A was measured in 2015, prior to channel realignment. Panel B was measured in 2016, following channel realignment. This portion of transect XS2 includes the west channel. Circles represent electrode locations; solid circles represent surveyed electrode locations and open circles represent interpolated electrode locations. Final root mean squared error was 1.00 in 2015 and 1.00 in 2016.

The west portion of transect XS2 crosses the west channel at 168 m (Figure 20). In general, conductivity is low in this portion of the transect, even in 2015 when the west channel was an active flow pathway. The increase in conductivity beneath the west channel between 2015 and 2016 is interpreted to be a result of out-of-plane effects and not a reflection of actual conductivity. Both transects may be representing portions of the high conductivity hillslope that begins to the west of the transect end at 176 m. The alternating low and high conductivity centers seen in panel A might be a result of instrument collection errors. Statistical analyses confirm an increase in conductivity to a depth of 1 m along this portion of transect XS2 between 2015 and 2016 (Table 7).

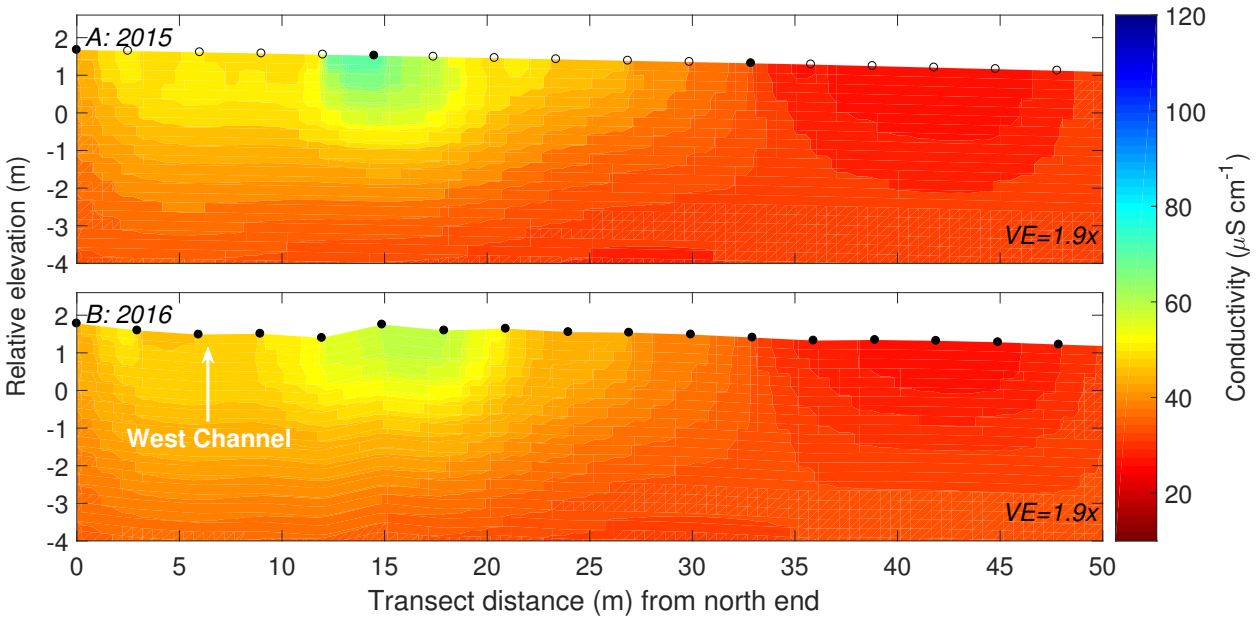

Figure 21: Comparative electrical resistivity tomograms measured along transect XSLW, including the west channel (location shown in Figure 4). Panel A was measured in 2015, prior to channel realignment. Panel B was measured in 2016, following channel realignment. This portion of transect XSLW is from the north end of the transect, including the west channel. Circles represent electrode locations; solid circles represent surveyed electrode locations and open circles represent interpolated electrode locations. Final root mean squared error was 0.63 in 2015 and 0.60 in 2016.

The north portion of transect XSLW, oriented north-south between transects XS0 and XS1, crosses the west channel at 6.5 m Figure 21. Conductivity is high in the upper 1 m of the transect between 0 and 20 m and is lower to the south. The northern portion of this transect is influenced by the diversion berm, where high water tables and saturated soil conditions exist. Statistical analyses confirm little to no change in conductivity to a depth of 1 m along this portion of transect XSLW between 2015 and 2016 (Table 7). Transect XSLW between 0 and 50 m is underlain by thick, well-drained sediment deposits delivered from the 2003 Grand Ditch debris flow.

Electrical resistivity summary statistics

Mean conductivity values for electrical resistivity distributions across tomograms displayed in Figure 17 through Figure 21 were calculated and compared between 2015 and 2016 using two-sample t-tests. These results, calculated to a depth of 1 m beneath the surface,

are presented in (Table 7). Distributions were compared because background noise and uncertainty in electrical resistivity transects prohibit accurate comparisons of how conductivity may have changed at a single point. Statistical analyses focused on the upper 1 m of substrate because sensitivity maps, calculated for each transect (Appendix J), show this region to be most sensitive to electrical resistivity measurements. Similar statistical summary tables for depths of 2 m and 4 m may be found in Appendix G. Minimum and maximum X values in Table 7 correspond to transect lengths in Figure 17 through Figure 21. Conductivity changes between 2015 and 2016 within the same transect segments are indicated as positive (+) or negative (-). In general, changes in mean conductivity values indicate changes in soil saturation. They do not necessarily indicate changes in hyporheic area, but instead identify subsurface areas where hyporheic exchange is likely to occur.

In general, statistical analyses along transects XS0 and XS1 were robust to changes in bounding regions, while XS2 and XSLW were not. A significant decrease in conductivity was observed along transect XS0 between 2015 and 2016 and was consistent across the entire transect. A significant increase in conductivity was observed along transect XS1 between 2015 and 2016 under most of the selected transect sections. A significant increase in conductivity was observed along transect XS2 between 2015 and 2016 when the entire transect was considered, but not within shorter transect segments. Most of the transect segments considered along transect XSLW did not exhibit a significant change in conductivity between 2015 and 2016.

Table 7: Summary statistics for electrical resistivity distribution means along select portions of electrical resistivity transects to 1 m depth. Mean conductivity is measured over the specified x and y transect distances in Figure 22 through Figure 26. SE describes the standard error in the mean. + conductivity change indicates an increase in mean conductivity between 2015 and 2016 population means and - conductivity change indicates a decrease in mean conductivity between 2015 and 2016. Analyses assume populations are normally distributed, but have unequal variances. For similar analyses to depths of 2 m and 4 m, see Table G.12 and Table G.13.

Transect	**Min X (m)**	**Max X (m)**	**Mean cond. (μS cm^{-1}) (2015)**	**SE (μS cm^{-1}) (2015)**	**Mean cond. μS cm^{-1} (2016)**	**SE (μS cm^{-1}) (2016)**	**Cond. change 5% sig. level**	**p-value**
XS0	0	47	62.9	3.1	48.3	1.5	-	< 0.05
XS0	14	30	26.4	0.4	25.0	0.6	-	< 0.05
XS0	33	50	119.4	4.8	78.4	1.9	-	< 0.05
XS1	0	141	41.9	0.9	49.0	1.3	+	< 0.05
XS1	10	60	56.9	1.6	68.0	2.6	+	< 0.05
XS1	34	44	54.6	3.4	62.3	3.7	+	< 0.05
XS1	75	125	32.1	0.6	34.4	0.6	+	< 0.05
XS1	90	100	33.2	0.6	33.5	0.8	not significant	0.60
XS2	0	176	51.7	1.1	56.9	0.9	+	< 0.05
XS2	130	176	49.2	2.9	46.7	0.5	not significant	0.09
XS2	162	176	12.3	2.0	51.4	0.6	+	< 0.05
XSLW	0	141	43.2	0.3	43.1	0.3	not significant	0.53
XSLW	0	25	50.8	0.5	49.7	0.4	-	< 0.05
XSLW	0	50	42.2	0.7	41.3	0.6	not significant	0.05
XSLW	30	50	30.4	0.3	30.2	0.3	not significant	0.58

Time lapse electrical resistivity

Results from time-lapse electrical resistivity tracer tests, measured along transect XS1, are displayed in Figure 22 through Figure 26. Results are centered on the center, west, and realigned Colorado River channels (locations shown in Figure 4). These time-step results track the expansion and contraction of the area within the hyporheic zone responding through time to salt tracer surface water exchange with groundwater. In general, results show that the most change in hyporheic exchange occurred between 2015 and 2016 near the west channel, that a moderate degree of change occurred near the center channel, and that the least amount of change occurred near the realigned channel. These figures are displayed in three segments, with 2015 pre-realignment tomograms on top of 2016 post-realignment tomograms of the same area. The bottom segment of each panel displays surface conductivity breakthrough curves for 2015 and 2016 as specific conductance at 25° C, measured at the nearest study site. Average error measured in background electrical resistivity transects was 0.2% in 2015 and 0.5% in 2016.

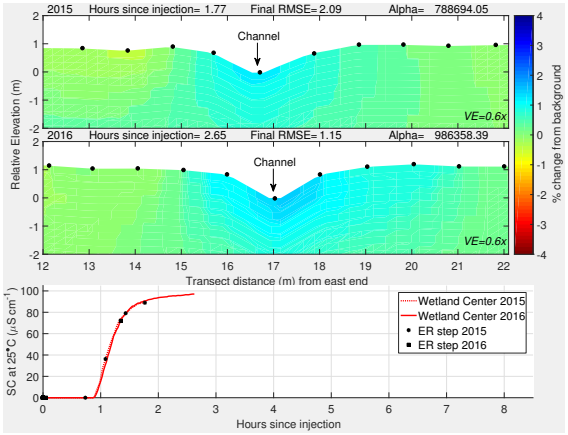

(A)

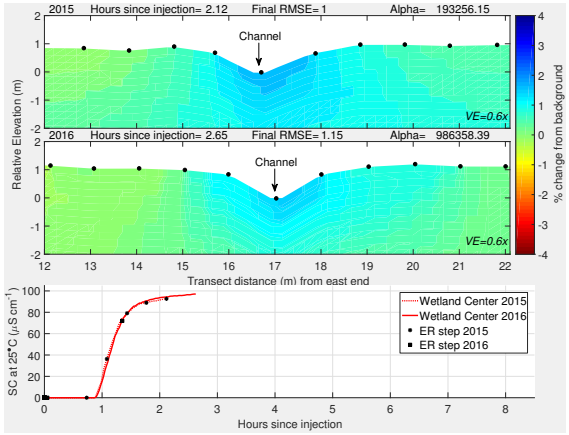

(B)

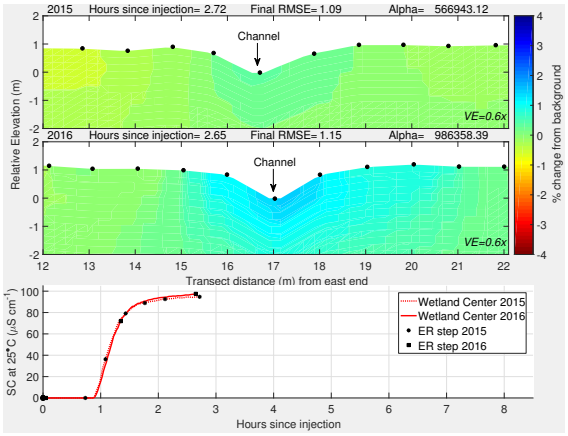

(C)

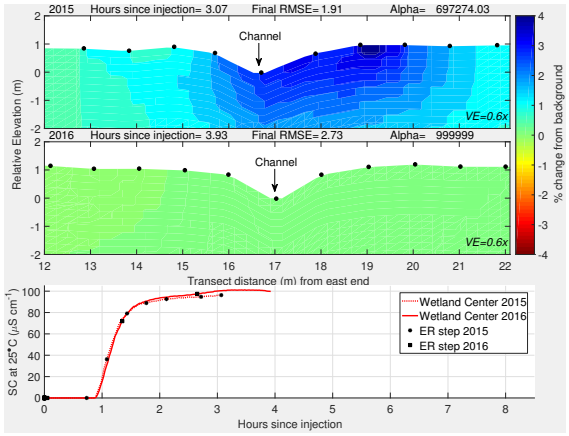

(D)

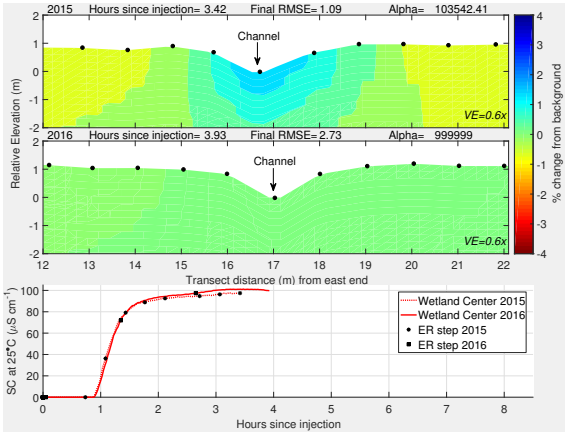

(E)

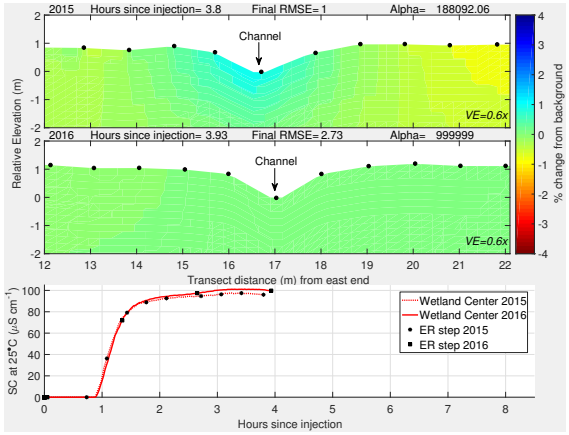

(F)

Figure 22: Comparative tomograms and tracer breakthrough curves from selected time steps during the electrical resistivity tracer test, including the center channel. Panels A through J show the percent change in conductivity from background along XS1 during the salt tracer injection. The top frame is pre-realignment, the middle frame is post-realignment, and the bottom frame shows the solute breakthrough curve measured at the Wetland Center study site. Tomogram time step, final RMS error (indication of model fit) and alpha (smoothing factor) are included for each year.

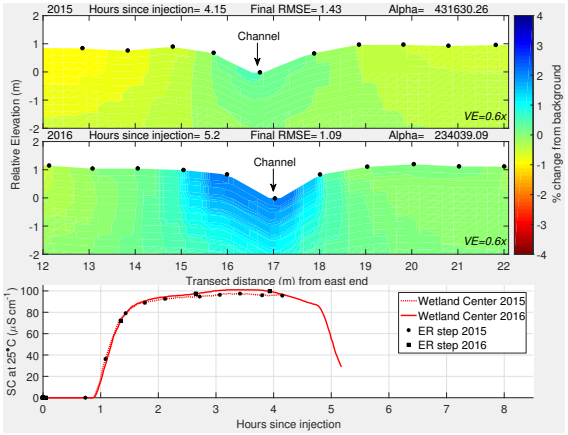

(G)

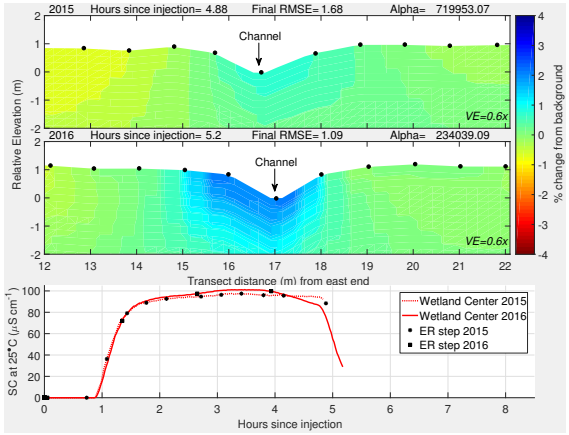

(H)

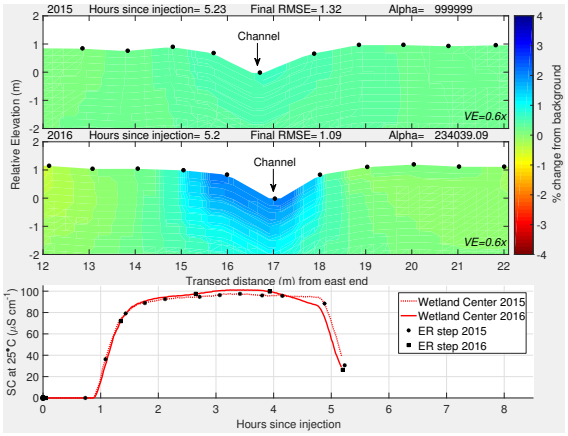

(I)

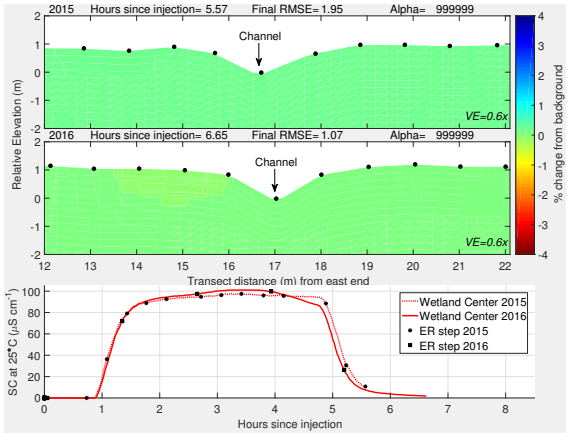

(J)

Figure 22a: Comparative tomograms and tracer breakthrough curves from selected time steps during the electrical resistivity tracer test, including the center channel. Panels A through J show the percent change in conductivity from background along XS1 during the salt tracer injection. The top frame is pre-realignment, the middle frame is post-realignment, and the bottom frame shows the solute breakthrough curve measured at the Wetland Center study site. Tomogram time step, final RMS error (indication of model fit) and alpha (smoothing factor) are included for each year.

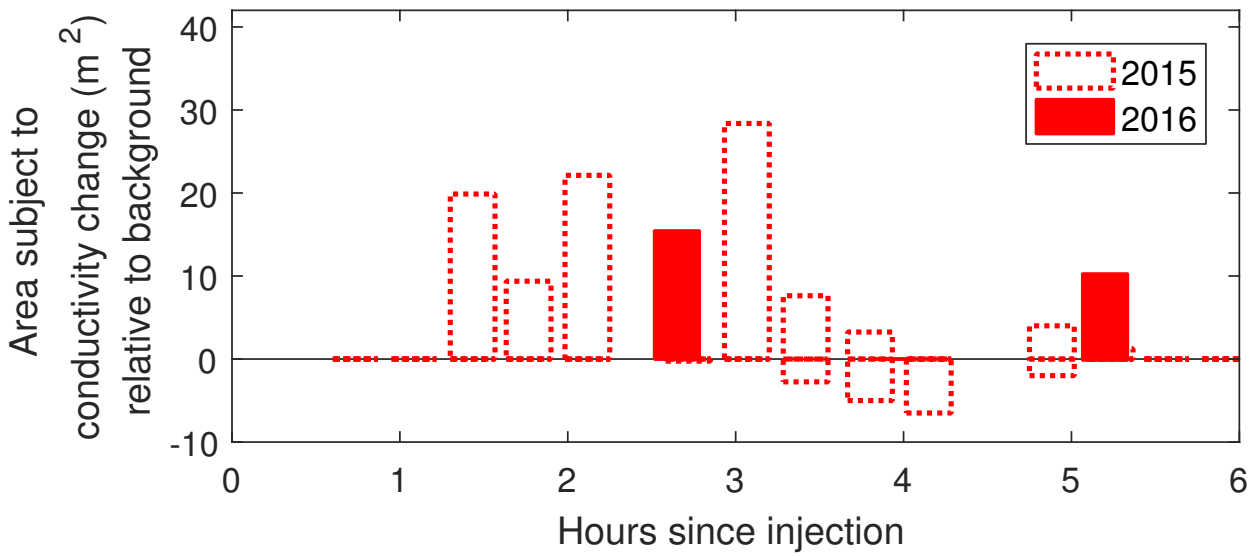

Figure 23: Area accessed by tracer stream water along electrical resistivity transect XS1 during the salt tracer test, including the center channel. Bar graphs show the expansion (+ area) and contraction (- area) of the area within the hyporheic zone that was accessed by stream water during the salt tracer, using a threshold of 0.5% change in area. The area of consideration is the same window represented in Figure 22. Note that this visualization does not indicate the magnitude of change.

Comparative tomograms and tracer breakthrough curves from selected time steps during both the 2015 and 2016 electrical resistivity tracer tests are displayed in Figure 22, with emphasis on the center channel. Figure 23 represents the expansion and contraction of area accessed by stream water within the the hyporheic zone through time, during the tracer tests displayed in Figure 22. In 2015, near-channel conductivity increased on the leading end of the salt injection plateau, and reached a maximum increase of 4% at 3 hours into the tracer test (Figure 22D). Tracer effects were flushed by 4 hours, and no delayed conductivity increase was observed for the remainder of the monitoring period. In 2016, the same channel exhibited a two-step response, correlated to the rising and falling limbs of the tracer breakthrough curve. The extent of hyporheic exchange was smaller in 2016 than in 2015, and was focused on the east edge of the channel (left bank), while in 2015 hyporheic exchange was greater on the west edge (right bank).

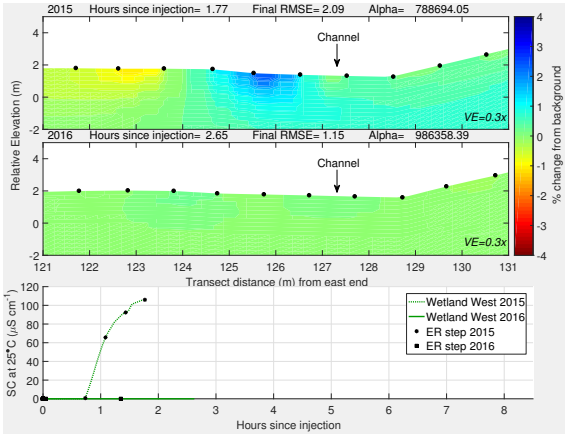

(A)

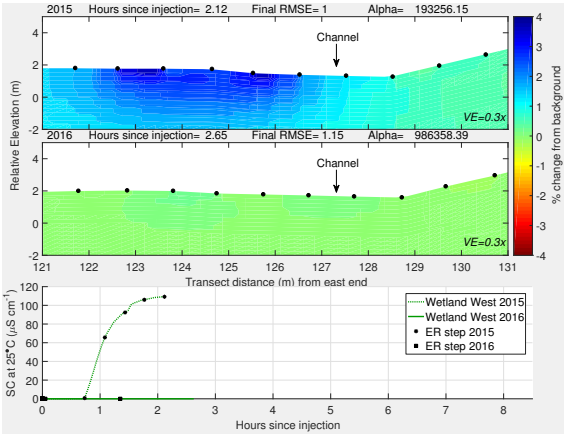

(B)

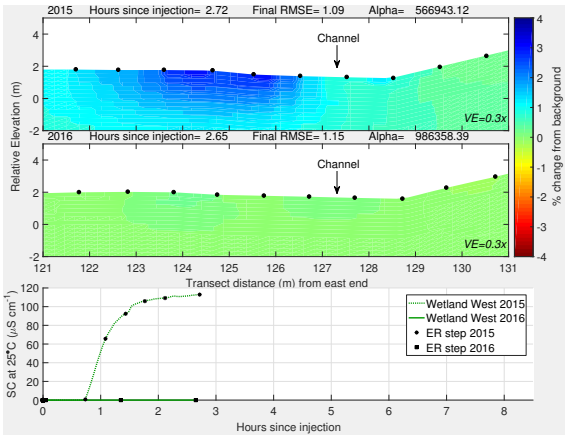

(C)

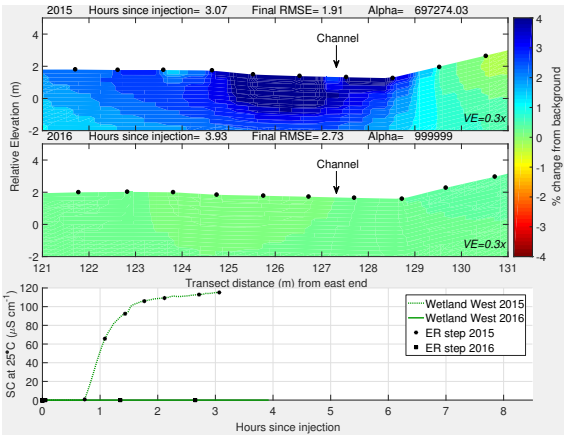

(D)

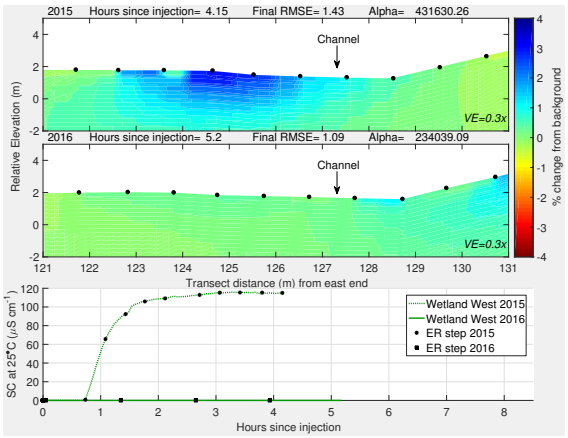

(E)

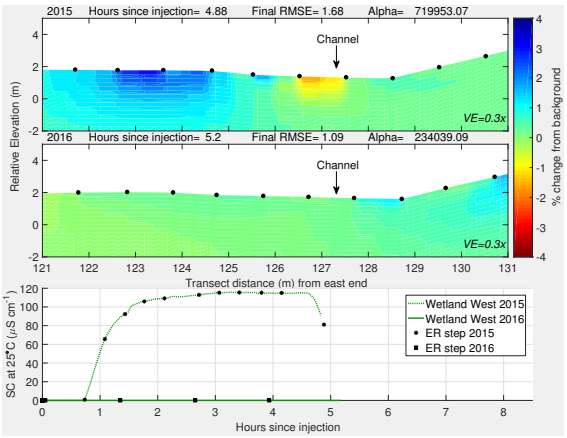

(F)

Figure 24: Comparative tomograms and tracer breakthrough curves from selected time steps during the electrical resistivity tracer test, including the west channel. Panels A through L show the percent change in conductivity from background along XS1 during the salt tracer injection. The top frame is pre-realignment, the middle frame is post-realignment, and the bottom frame shows the solute breakthrough curve measured at the Wetland West study site. Tomogram time step, final RMS error (indication of model fit) and alpha (smoothing factor) are included for each year.

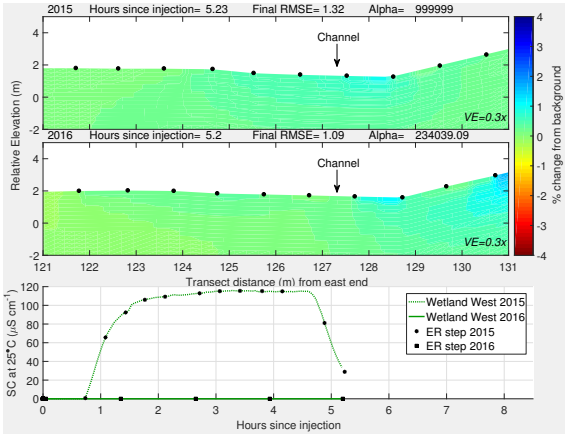

(G)

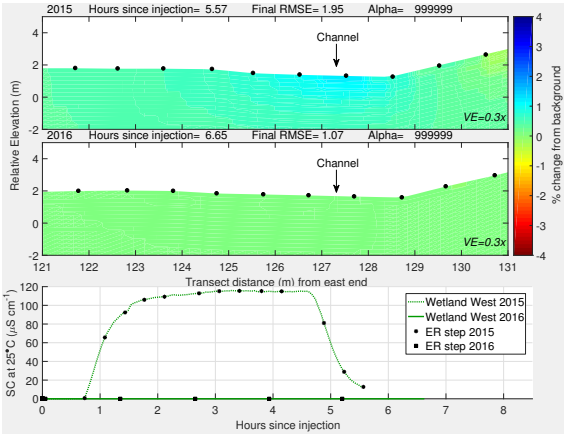

(H)

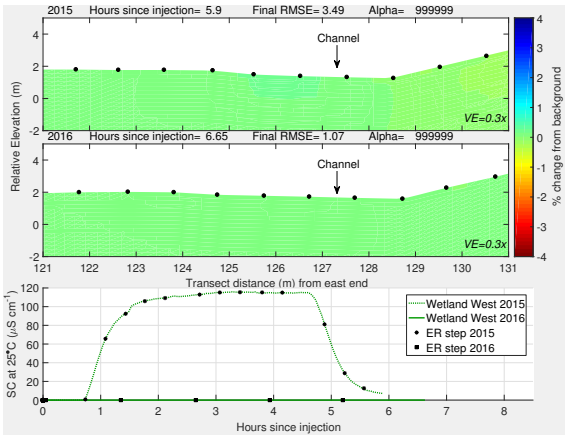

(I)

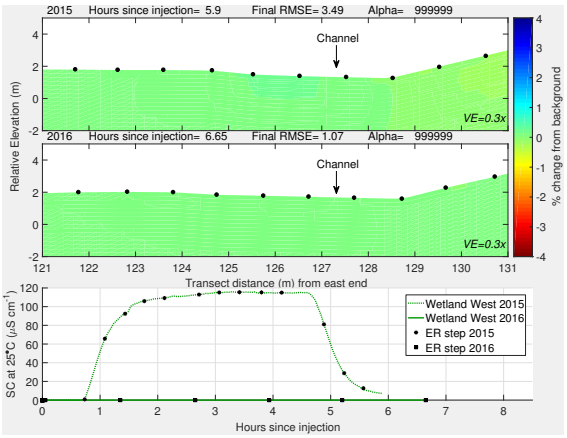

(J)

Figure 24a: Comparative tomograms and tracer breakthrough curves from selected time steps during the electrical resistivity tracer test, including the west channel. Panels a through l show the percent change in conductivity from background along XS1 during the salt tracer injection. The top frame is pre-realignment, the middle frame is post-realignment, and the bottom frame shows the solute breakthrough curve measured at the Wetland West study site. Tomogram time step, final RMS error (indication of model fit) and alpha (smoothing factor) are included for each year.

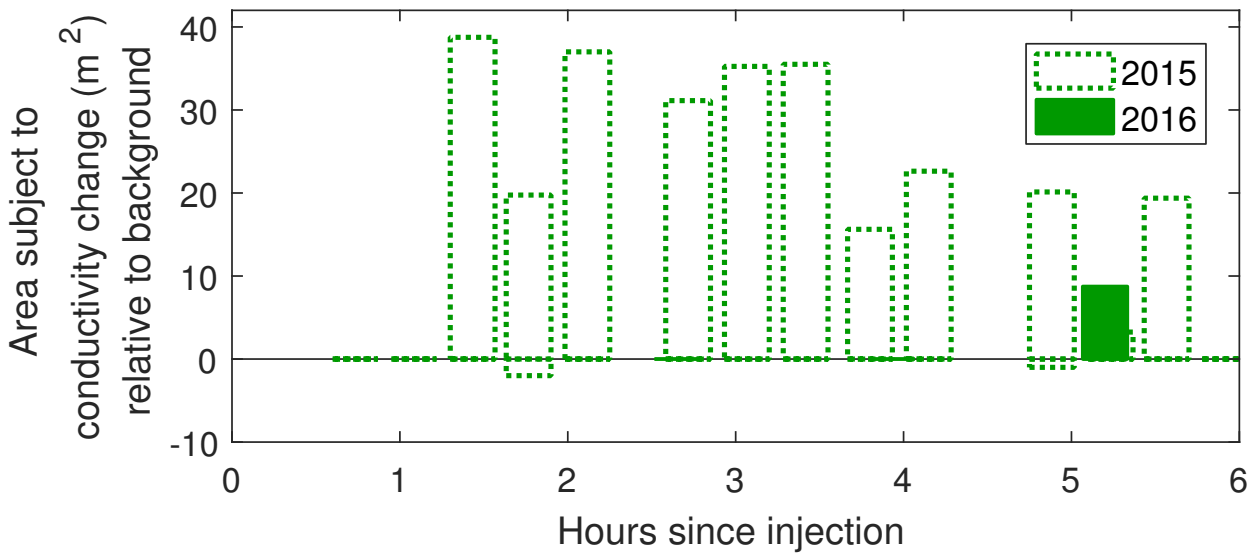

Figure 25: Area accessed by tracer stream water along electrical resistivity transect XS1 during the salt tracer test, including the center channel. Bar graphs show the expansion (+ area) and contraction (- area) of the area within the hyporheic zone that was accessed by stream water during the salt tracer, using a threshold of 0.5% change in area. The area of consideration is the same window represented in Figure 24. Note that this visualization does not indicate the magnitude of change.

Comparative tomograms and tracer breakthrough curves from selected time steps during both the 2015 and 2016 electrical resistivity tracer tests are displayed in Figure 24, with emphasis on the west channel. Figure 25 represents the expansion and contraction of area accessed by stream water within the hyporheic zone through time, during the tracer tests displayed in Figure 24. Maximum conductivity increase occurred 2 hours into the salt tracer test, the salt was flushed from the zone by 4 hours, and there was no delayed response following the test. In 2016, there was no hyporheic response near the western channel. This is not surprising given the fact that no salt-tracer flowed through the western channel during these conductivity measurements because flow was diverted into the realigned channel at the constructed diversion berm.

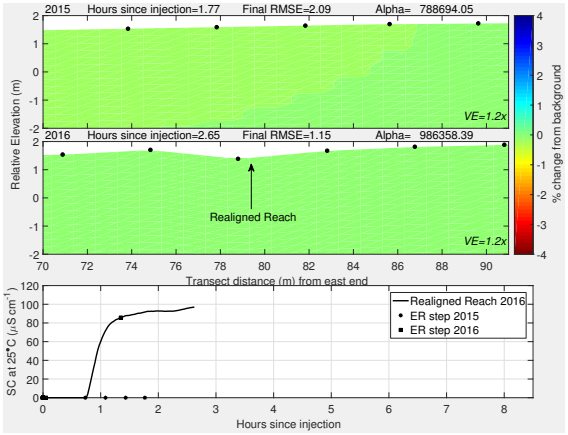

(A)

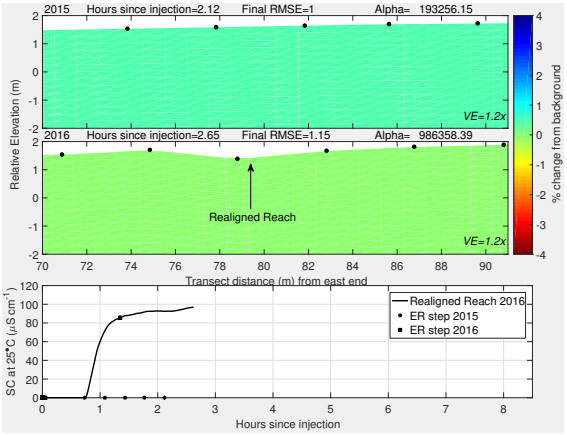

(B)

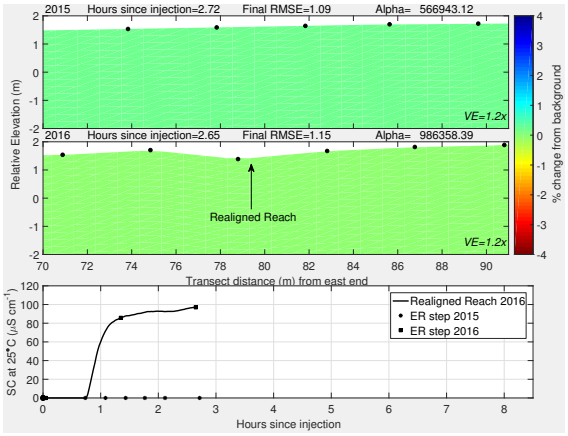

(C)

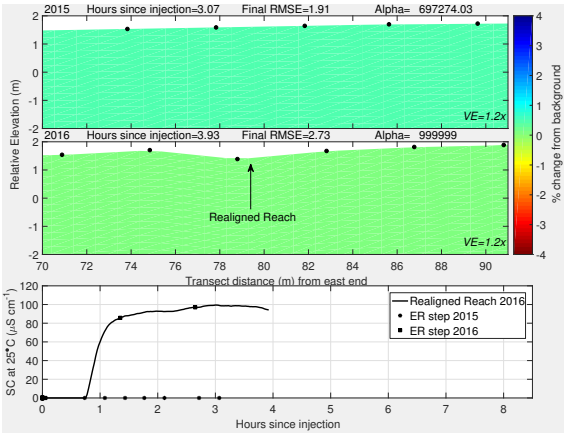

(D)

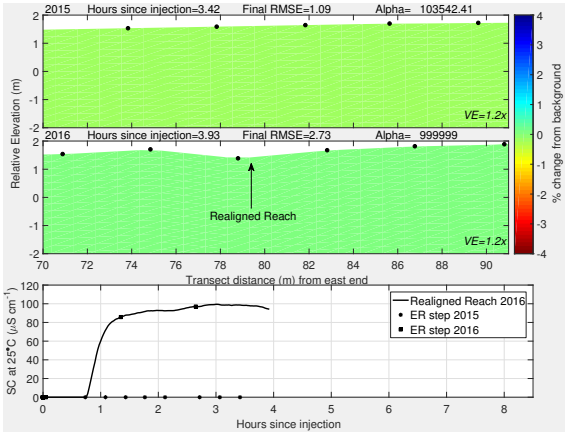

(E)

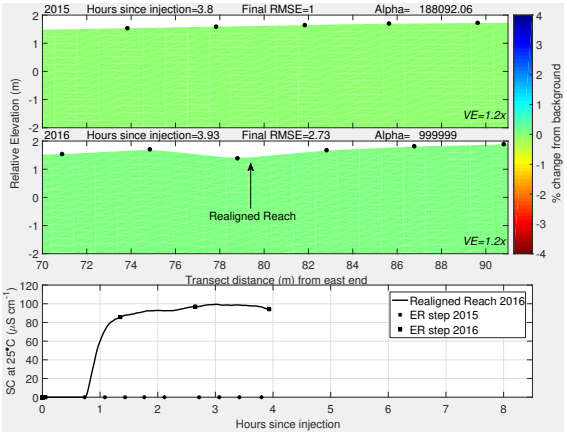

(F)

Figure 26: Comparative tomograms and tracer breakthrough curves from selected time steps during the electrical resistivity tracer test, including the realigned channel. Panels A through J show the percent change in conductivity from background along XS1 during the salt tracer injection. The top frame is pre-realignment, the middle frame is post-realignment, and the bottom frame shows the solute breakthrough curve measured at the Realigned Reach study site. Tomogram time step, final RMS error (indication of model fit) and alpha (smoothing factor) are included for each year.

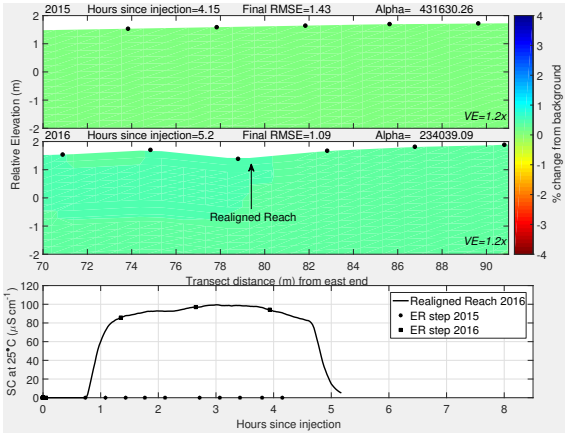

(G)

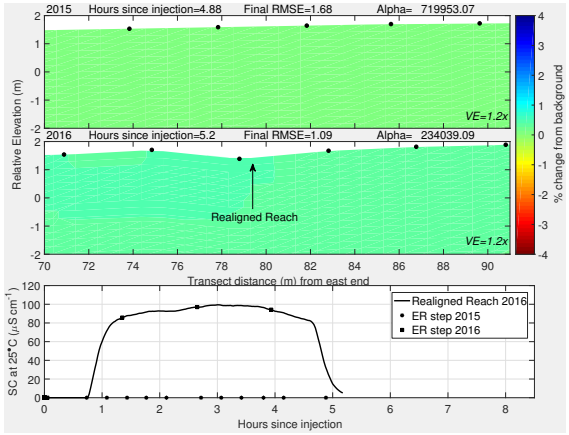

(H)

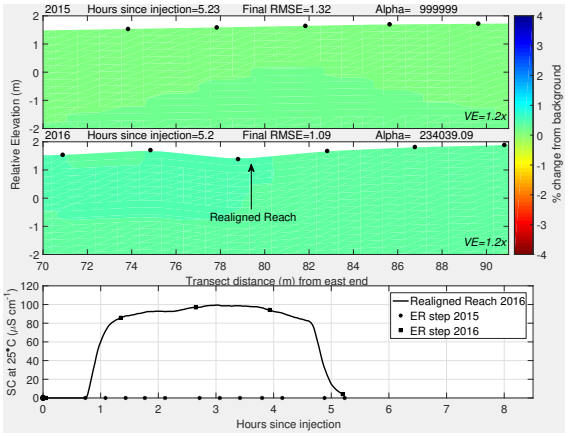

(I)

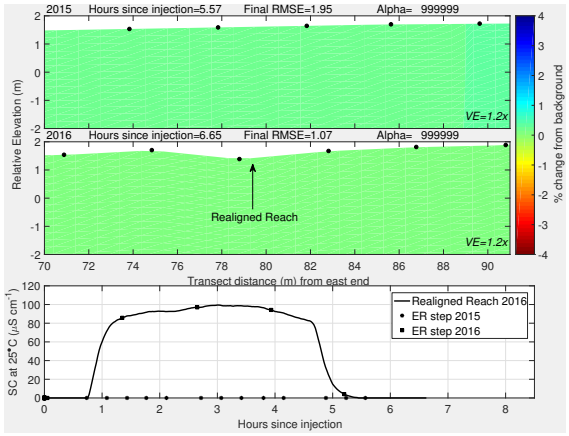

(J)

Figure 26a: Comparative tomograms and tracer breakthrough curves from selected time steps during the electrical resistivity tracer test, including the realigned channel. Panels A through J show the percent change in conductivity from background along XS1 during the salt tracer injection. The top frame is pre-realignment, the middle frame is post-realignment, and the bottom frame shows the solute breakthrough curve measured at the Realigned Reach study site. Tomogram time step, final RMS error (indication of model fit) and alpha (smoothing factor) are included for each year.

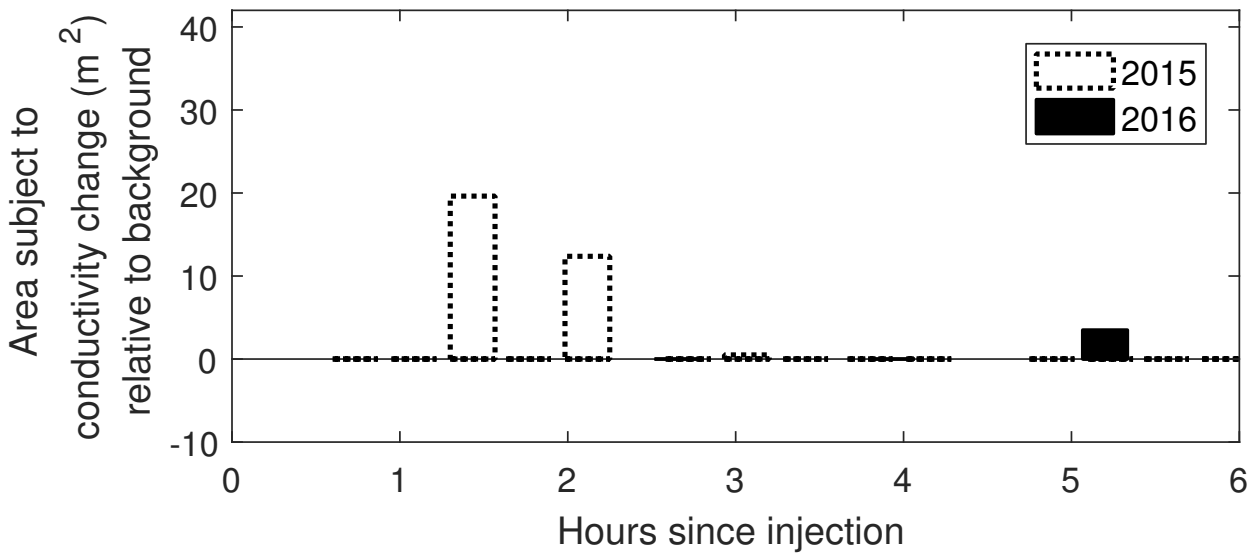

Figure 27: Area accessed by tracer stream water along electrical resistivity transect XS1 during the salt tracer test, including the center channel. Bar graphs show the expansion (+ area) and contraction (- area) of the area within the hyporheic zone that was accessed by stream water during the salt tracer, using a threshold of 0.5% change in area. The area of consideration is the same window represented in Figure 26. Note that this visualization does not indicate the magnitude of change.

Comparative tomograms and tracer breakthrough curves from selected time steps during both the 2015 and 2016 electrical resistivity tracer tests are displayed in Figure 26, with emphasis on the realigned channel. Figure 27 represents the expansion and contraction of area accessed by stream water within the hyporheic zone through time, during the tracer tests displayed in Figure 26. Surface conductivity measurements confirmed the presence of tracer water in the channel. It is worth noting that the electrode spacing over this section of the transect XSLW was 4 m, but 1 m in Figure 22 to Figure 24.

4.3 Sediment transport

4.3.1 Gravel bar redistribution

Aerial imagery comparisons focused on the northern extent of the Lulu City wetland show changes to flow paths and gravel bars between 18 September 2015 and 7 September 2016 (Figure 28). Rocky Mountain National Park staff began channel diversions and construction of the earthen diversion berm on 21 September 2015. Post-realignment aerial imagery clearly

shows increased channelization of the Colorado River and increased gravel bar surface area. A first order area estimate, which does not account for depth changes that may affect total volume, shows an increase in total gravel bar area of 273 m^2 between 2015 and 2016.

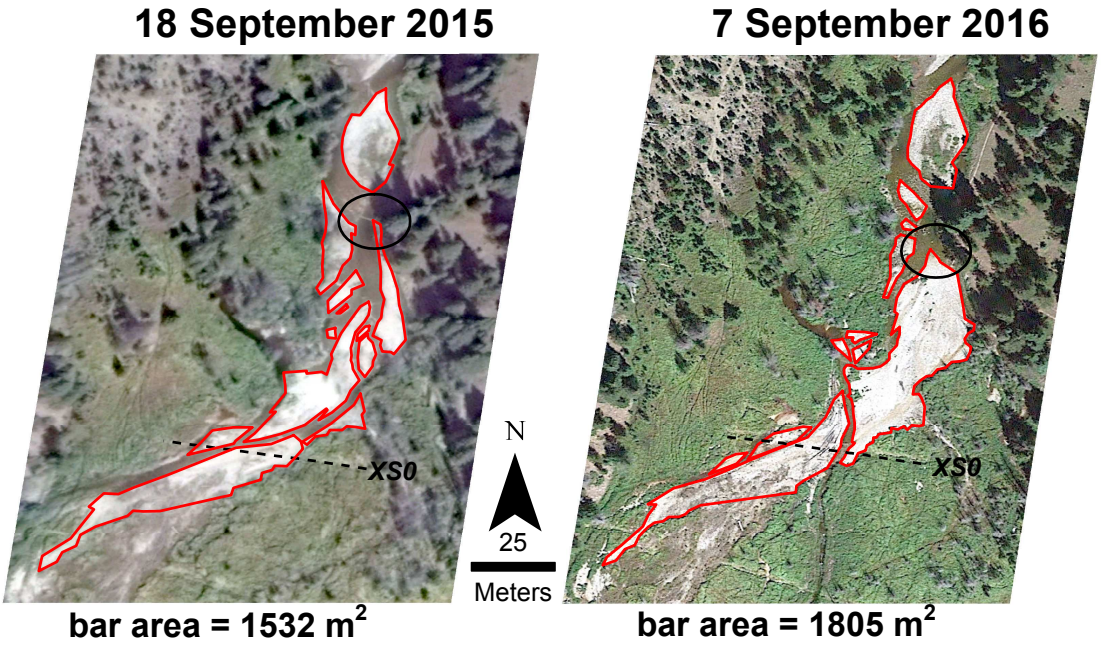

Figure 28: GoogleEarth aerial images of the northern extent of Lulu City wetland, Rocky Mountain National Park. Gravel bar extent is shown prior to channel realignment (2015) and one year after channel realignment (2016). The circled areas represent the approximate natural diversion point for flow through the eastern channel. Electrical Resistivity transect XS0 is included as a dashed line for reference. The realigned channel can be seen as the north-south feature bisecting the large gravel bar in the center of the 2016 image. Colorado River flow is to the south.

4.3.2 Bed grain size analysis

On 30 July 2015 and 14 July 2016, 100-clast pebble counts were collected and used to characterize bed grain size distributions. Cumulative distribution plots of pebble count data show little to no change in surface bed clast size distributions at most study sites between 2015 and 2016 (Figure 29). Sample means of log transformed data have been used to asses bed size differences between pools and riffles (Hey and Thorne, 1983). The R package lsmeans was used to calculate covariance-adjusted means, allowing for direct comparisons among pebble count data at all sites (RCoreTeam, 2017; Lenth and others, 2016). The results are displayed in Table 8.

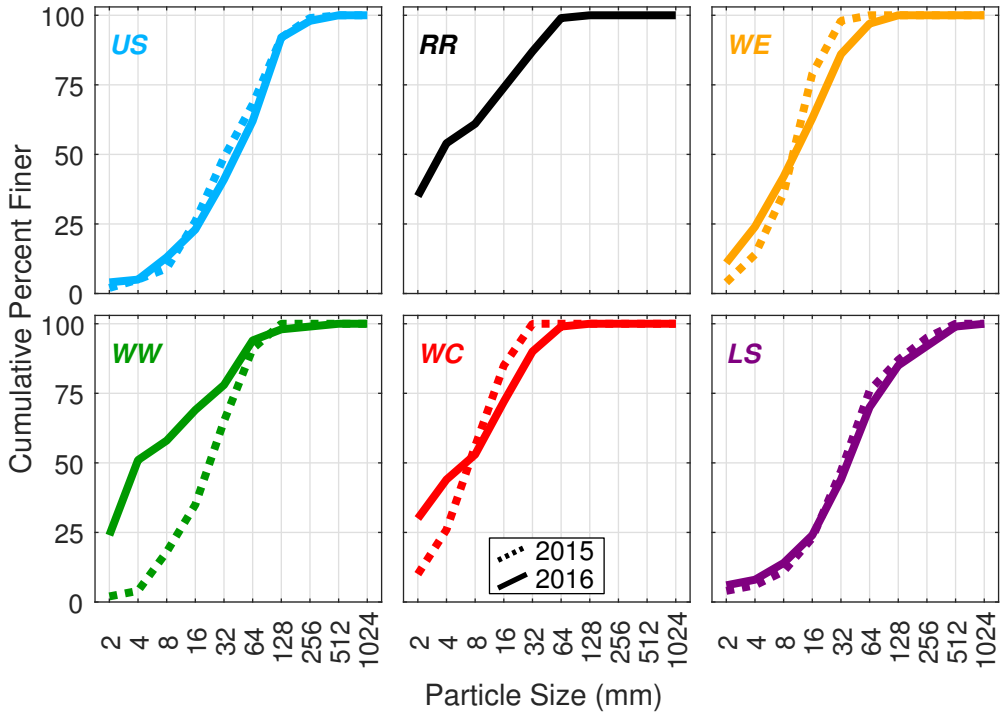

Figure 29: Pebble count cumulative frequency plots, by study site within Lulu City wetland, Rocky Mountain National Park. Cumulative frequency plots are derived from 100-clast pebble counts. Clasts were collected from the bed surface over reach lengths centered on each gage site. Study sites are arranged from left to right according to river distance from the Upstream study site. US = Upstream; RR = Realigned Reach; WE = Wetland East; WW = Wetland West; WC = Wetland Center; LS = Lower Sentinel.

Table 8: Least squares means (lsmeans) comparison between study sites within Lulu City wetland, Rocky Mountain National Park. Study sites are ordered by increasing lsmeans value. Study sites with similar group numbers do not have significantly different bed grain size distributions.

Site	**Log Mean**	**SE**	**95% Confidence Interval**	**Group**
RR 2016	0.82	0.05	(0.73, 0.92)	1
WC 2016	0.88	0.05	(0.78, 0.97)	12
WC 2015	0.91	0.05	(0.81, 1.00)	12
WW 2016	0.93	0.05	(0.84, 1.03)	12
WE 2015	1.03	0.05	(0.94, 1.13)	12
WE 2016	1.07	0.05	(0.97, 1.16)	2
WW 2015	1.39	0.05	(1.29, 1.48)	3
LS 2015	1.58	0.05	(1.48, 1.67)	3
GB 2015	1.59	0.05	(1.49, 1.68)	3
LS 2016	1.59	0.05	(1.50, 1.69)	3
GB 2016	1.60	0.05	(1.51, 1.70)	3

A comparison of lsmeans across study sites indicates that the bed fining between 2015 and 2016 at the Wetland West study site was the only significant change in bed grain size distributions (Table 8). The bed grain size in the pool at the realigned reach was significantly smaller than that seen at all other sites. The Upstream site and Lower Sentinel had the largest bed grain sizes, and both sites included portions of riffles. There were no significant differences between the Upstream and Lower Sentinel study sites, regardless of year.

4.3.3 Realigned reach change

Changes to channel geometry along the Realigned Reach were measured during weekly field surveys throughout summer 2016. Repeat topographic bed surveys from the Realigned Reach are displayed in Figure 30 and mean bed elevation changes through time are displayed in Figure 31, after Andrews (1979).

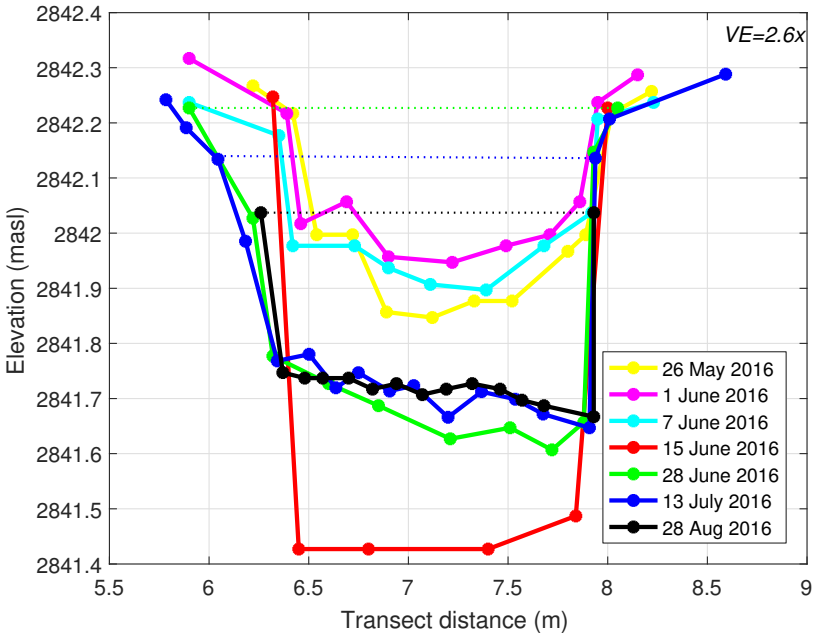

Figure 30: Repeat bed elevation surveys, Realigned Reach study site, Lulu City wetland, Rocky Mountain National Park. Repeat bed topographic cross sections are represented by solid lines. Circles are measurement points. Dashed lines represent water surface elevations for color corresponding transects. Transects without corresponding dashed lines had water surface elevations that were overbank. An RTK-GNSS was used to survey the 13 July 2016 cross section. A wading rod was used to survey all remaining cross sections.

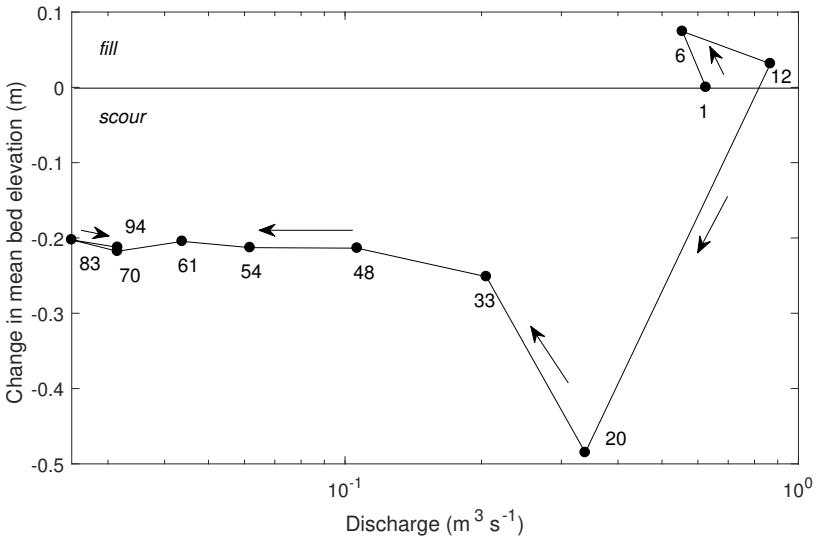

Figure 31: Change in mean bed elevation in response to discharge, Realigned Reach study site, Lulu City wetland, Rocky Mountain National Park. Numbers indicate the days elapsed since the initial channel survey. Surveys began on 26 May 2016 (day 1). The 1 June 2016 survey was day 6, the 15 June 2016 survey was day 20, and the final survey (day 94) was 28 August 2016

Mean bed elevations were calculated from bed survey points shown in Figure 30, and not the banks. The trend displayed by mean bed elevations in Figure 31 closely follows the trend of minimum bed elevation. Increases in mean bed elevation indicate periods of deposition (fill), and decreases indicate periods of erosion (scour). Following a period of early season deposition (< 0.1m) through 1 June 2016, the bed eroded by 0.59 m through 15 June 2016, two days after peak discharge. After peak discharge, deposition increased the mean bed elevation by 0.27 m when measured on 13 July 2016. After this, little change occurred through the end of the summer. The majority of channel change, including deposition, occurred at high flows, above 0.13 $m^3 s^{-1}$. Little widening occurred in the the southern, vegetated, portion of the realigned reach, but the upstream portion, which was dug into a gravel bar, widened to a maximum width of 3 m and the average channel slope increased to a reach-averaged 1.9%.

5. DISCUSSION

5.1 Flow redistribution

The channel realignment and constructed earthen berm succeeded in diverting Colorado River flow away from the western channel and through the realigned reach toward the center of Lulu City wetland. This lends full support to hypothesis 1. By redirecting more than 48% of river flow from west to east, the total area and distribution of wetland floodplain accessed by the river during all flows has been adjusted. Areas adjacent to the realigned channel, which were dry in 2015, flooded for 75 days in 2016 following channel realignment, and flooding increased by 95 days through the center channel downstream of the realigned channel. Flooding of the realigned and center channels will increase the delivery of nutrients to the adjacent wetland, likely improving certain conditions needed to improve plant and animal biodiversity there (Junk et al., 1989). It is equally likely that sedge and conifer encroachment will expand on the drier western side of the wetland. Overbank flooding decreased between 2015 and 2016 at the Upstream, Wetland East, and Lower Sentinel study sites due to the shorter duration flood peak in in 2016 (Figure 7).

Discharge flux calculations through Lulu City wetland, which assume one surface water input at the Upstream study site and one surface water output at the Lower Sentinel site, suggest that flow redistribution decreased the stream-wetland fluxes between 2015 and 2016 by 119% (Figure 11). This indicates an important shift from the Colorado River losing water in 2015 to gaining water in 2016, which was accompanied by an 17% increase in the average daily discharge reaching the Lower Sentinel study site in 2016 (Table 1). In other words, evapotranspiration and water retained as wetland storage were much less in 2016 than in 2015, likely resulting from the channel realignment. In 2015, the Lower Sentinel gage does not reflect a late summer increase in discharge, which I would expect if the 2015 discharge flux trend was controlled primarily by wetland storage. This suggests that the trend is due mostly to evaporative losses, or storage on longer timescales (i.e. more than one year).

Total flow path length through Lulu City wetland decreased by 650 m as a result of flow redistribution and the constructed diversion berm. The consolidation of stream flow into the Wetland Center channel decreased both the stream surface area exposed to evaporation and the total bed and bank area available for hyporheic exchange. An ongoing discharge flux deficit through Lulu City wetland, if continued for multiple years, will result in persistent low water tables on the western edge and an increasingly drier wetland.

This flow redistribution has implications for nutrient retention, which is widely recognized as a positive ecosystem service provided by wetlands (National Research Council and Committee on Mitigating Wetland Losses, 2001), but also for returning nutrients to the river through hyporheic exchange, which is an essential process for river biodiversity (Stanford and Ward, 1988). Microbes in near-surface hyporheic flow paths release biologically available nutrients, which return to the stream at upwelling zones and are sequestered by the algae that commonly make up periphyton communities in freshwater streams (Wyatt et al., 2008). *Hydrurus foetidus* algae thrives in the Colorado River through Lulu City wetland, and higher concentrations can be an indication of hyporheic upwelling (Graham et al., 2009). The algal growths located at upwelling sites support areas of increased productivity and biodiversity, which can have positive effects for plant and animal communities up the entire food chain (Boulton et al., 2010; Hauer et al., 2016).

Flow redistribution also affects the balance of nutrients within the river system, which is maintained by excess storage in floodplain sediments. Re-wetting of nutrient-rich floodplain sediments after extended periods of drying have been found to increase phosphorus loading to the stream at higher concentrations than under more frequent and longer wetting periods (Schönbrunner et al., 2012). This may be caused by the loss of sediment sorption capacity through crystallization of other compounds, but importantly, these results are independent of the quality of water entering the floodplain (Schönbrunner et al., 2012). Excess nutrients washed from floodplains to rivers may cause overwhelming algal blooms, or may be transported downstream. The headwaters of the Colorado River above Lulu City wet-

land are relatively pristine and are not exposed to excess nutrient inputs (e.g. runoff from agricultural fields). Due to the earthen diversion berm, western areas of the wetland, which will now experience increased drying cycles, may release more nutrients into the river during peak runoff than they previously have. This increases the potential for downstream nutrient transport, which may ultimately end up in drinking water reservoirs at Shadow Mountain Reservoir and Lake Granby.

5.2 Hyporheic exchange and solute retention

Current research involving hyporheic exchange often focuses on one aspect of the system, such as a controlling process (e.g. bed-form changes (Hill et al., 1998)) or a resulting process (e.g. nutrient uptake (Triska et al., 1989)). Alternatively, researchers often resort to modeling of simplified systems (e.g. Kasahara and Wondzell (2003)) to better understand individual processes. In Lulu City wetland, it proved difficult to identify the individual effects of driving variables on hyporheic flow paths. It is highly likely that the effects of the constructed diversion berm, channel bedforms, bed gradient, sinuosity, bed grain size compositions, discharge, and velocity all contributed to modifying hyporheic flow paths and increasing or decreasing exchange rates in complex ways that were hard to identify in the data presented above. Despite this uncertainty in the relative importance of driving factors, it is clear that the channel realignment caused measurable changes to hyporheic processes within the wetland, lending partial support to hypothesis 2.

The realigned channel shortened the total channel length through Lulu City wetland by 650 m by blocking the west channel at the constructed diversion berm. The realigned channel now has a steeper slope than the western channel it was built to replace. The realigned channel also introduced a degree of channel complexity to the upper wetland through the addition of three pool-riffle sequences, a constructed meander bend, and other constrictions along the 188 m course. These are all features that are known to generate head gradients that drive hyporheic exchange (Harvey and Bencala, 1993; White, 1993). The degree to which these channel features induce hyporheic exchange in small, mountain streams is still

unclear, especially when many driving factors experience some degree of change. White (1993) suggests that permanent headwater streams, like the Colorado River through Lulu City wetland, may not experience much hyporheic exchange, even in permeable substrate, due to short residence times and persistent groundwater inputs into the open channel.

The electrical resistivity data do provide insight into how the hyporheic zone in Lulu City wetland responded to the channel realignment. Use of electrical resistivity in this heterogeneous system was particularly appealing in light of earlier work showing that this method may add missing information to a hyporheic zone interpretation based on surface conductivity analyses alone (Ward et al., 2010). In Lulu City wetland, electrical resistivity transects were selected specifically to match ground penetrating radar transects used to image wetland substrate following the 2003 debris flow; previous analysis by Rubin et al. (2012) confirmed the presence of coarse debris flow deposits throughout much of the area under transects XS0, XS1, and XS2, with limited peat and overbank deposits under the far eastern portions of those transects. These debris flow deposits are permeable enough to drain surface water (as evidenced by time lapse photography) on the timescale of hours, which would suggest that they are permeable enough to support hyporheic flow paths. The hydraulic conductivity of the debris flow deposit was not measured in the field, but an estimate for poorly sorted fine sands to medium gravels suggests a hydraulic conductivity of about 0.05 cm s^{-1} (EPA, 1986).

High infiltration through these debris flow deposits may explain why between-year comparisons at XS0 indicate no increase in conductivity along the realigned channel. Conductivity data along transect XS0 do not indicate increases in hyporheic exchange, but it is again possible that flow paths were smaller and faster than what can be seen with the electrical resistivity background monitoring (Figure 17). Conductivity decreased at the diversion berm, which was built from the same permeable debris flow deposits that promote fast drainage, and conductivity remained high on the east end of transect XS1, which is adjacent to a perennial wet area north of the transect. Increased vertical exchange into the

stream-bed upstream of small log dams has been observed in coarse, permeable substrate (Fanelli and Lautz, 2008), so it is possible that hyporheic exchange occurred adjacent to the constructed diversion berm. The high conductivity areas between 35 and 50 m along transect XS0 in both 2015 and 2016 are likely a result of out-of-plane effects, which are a reflection of wet areas to the north of transect XS0. These out-of-plane effects may also explain the persistent high conductivity areas at the north end of transect XSLW in both 2015 and 2016 (Figure 21), which is also representing a wetter area to the north, and the very low conductivity edge of transect XS2 in 2015 (Figure 20), which may be indicative of the dry hillslope to the west.

Time-lapse electrical resistivity results from transect XS1 during the tracer test provided an approximation of changes in hyporheic zone area, which add to the interpretations of hyporheic exchange based on the background data. Ward et al. (2012) employed a two-step filtration to quantify changes in hyporheic zone area by first subjecting the resolution matrix to a sensitivity threshold, and second by using a percent change threshold. Percent change thresholds vary within the literature, and depend heavily upon background error. Ward et al. (2012) used a 3% change threshold, but in a similar analysis, Singha and Gorelick (2005) could not confidently distinguish real change from noise below a 5% change threshold. Data errors from background transects in Lulu City wetland were very well constrained, which allowed a 0.5% percent change threshold to be used to calculate the area within the hyporheic zone that was subject to changes in conductivity. Because the resolution matrix analysis was prohibitively computationally slow (e.g. 21 days to process the 2015 data), the percent change threshold was the only filter used on the Lulu City wetland tracer data. Quantifying the area subject to changes in conductivity provides a first oder approximation of the expansion and contraction of the stream water zone of influence within the hyporheic zone in near-channel areas of Lulu City wetland. These results suggest the presence of an active hyporheic exchange area through the western channel during the 2015 tracer injection, and virtually no response in 2016 (Figure 25). Subsurface conductivity through the western

channel returned to background levels within two hours of the 2015 salt injection completion, suggesting that the hyporheic zone responded quickly along short flow paths. In 2016 the western channel was completely dry, which explains why there was no hyporheic response during the tracer test.

Almost no change in the area accessed by stream water occurred along the realigned reach (Figure 27), but this does not preclude the presence of hyporheic exchange processes there. It is more likely that all hyporheic exchange occurred at a much smaller spatial scale, and that 4 m electrode spacing in 2015 along the tracer electrical resistivity transect was too coarse to resolve the near-surface conductivity (Binley and Kemna, 2005). The loss of hyporheic exchange pathways, however small, is detrimental to the health of the ecosystem. Small-scale exchange pathways, which link gravel bed rivers to their associated floodplains, are important for biodiversity and connectivity across the larger wetland system (Hauer et al., 2016). Zones of concentrated nutrients along the small hyporheic exchange flow paths affect flora and fauna on increasingly larger scales, ultimately influencing the biodiversity of the regional river-floodplain ecosystem (Wyatt et al., 2008).

Time lapse electrical resistivity results along the center channel show an expansion and contraction of the total area accessed by salt-traced stream water within the near-channel hyporheic zone in 2015, but less influence of salt-traced stream water in 2016 (Figure 23). Substrate hydraulic conductivity was not measured adjacent to the center channel, but is estimated between 0.02 and 0.3 cm s^{-1}, within the range of values measured in the top 0.1 m of a similar large-sedge fen located 19 km to the south (Crockett et al., 2016). While the hydraulic conductivity estimate for substrate adjacent to the center channel is less than half of the estimate for debris flow deposits within the west channel, it is still high enough to expect some level of hyporheic exchange. Background conductivity adjacent to the center channel was higher in 2016 than in 2015, indicating more saturated soil conditions in 2016 (Table 7). Therefore, it is possible that the smaller area changes observed in 2016 are the result of smaller magnitude changes over a similar area as measured in 2015. Hyporheic

exchange is likely occurring along the center channel, but in adjacent areas not measured by the electrical resistivity transects. For example, immediately downstream of the Wetland Center study site, the center channel transitions from a deep, sandy pool to a coarse, shallow riffle. In other locations, these conditions have been found to be ideal for promoting hyporheic exchange into the bed (Fanelli and Lautz, 2008). Ultimately it is difficult to assess what effect, if any, increased flow may have had on these results. Background electrical resistivity data collection was limited to one pass along the transect, which inhibited the ability to constrain the natural, daily fluctuations in background electrical resistivity.

Underestimation of electrical resistivity in paired electrical resistivity tracer tests is a common systematic issue. Binley et al. (2002) found during a paired electrical resitivity tracer test that up to 50% mass balance error led to an underestimation of true moisture content change. Additional studies have found similar underestimations of tracer recovery (e.g. Singha and Gorelick 2005, Müller et al. 2010), although in Müller et al. (2010), the underestimation ranged from 50% up to 90%. Reasons for this error may be attributed to the over-parameterization of the inversion problem (i.e. more variables are solved for than are measured) or to the regularization of tomograms, of which some degree is always required (Singha and Gorelick, 2005). Underestimation can also occur when the contrast between the target tracer and the background stream concentration is high or when the tracer plume is small (Singha and Gorelick, 2005).

Analyses of hyporheic exchange cannot rely entirely on electrical resistivity, but will benefit still from incorporating surface conductivity measurements, as done in this analysis. In certain cases, surface water tracer characterizations may serve as a better estimate of hyporheic exchange. Harvey et al. (1996) found hyporheic exchange estimates from surface water conductivity measurements to be more reliable at low flows than high flows, due to a larger percentage of the tracer interacting with hyporheic flow paths, and because higher plateau concentrations result in more reliable mass recoveries. During a salt tracer test using sodium chloride, Harvey and Bencala (1993) continued to measure stream water with low

tracer concentrations for days following the end of the test, which they interpreted to indicate retention in sub-stream flow paths. Such retention can be indicated by long receding limbs in tracer breakthrough curves (Kennedy et al., 1984).

Solute retention inferred from power-law slopes expands the spatial extent of hyporheic exchange interpretation to a larger area of the wetland. Between-year comparisons of power law slopes under equivalent low flows indicate increases in solute retention at the Wetland Center study site (Table 5). Associated mass recovery comparisons show that the east channel delivered almost twice as much tracer as the Realigned Reach to Wetland Center (Figure 13), which suggests that this remained the dominant flow path to Wetland Center following channel realignment. This increase in solute retention through the center channel occurred despite an increase in discharge, which is weakly correlated with decreasing solute retention (Figure 15). Patil et al. (2013) found that the discharge-solute retention relationship was stronger at lower discharges, but weaker at discharges in the 0.8 - 0.1 m^3 $s^{-}1$ range, similar to discharge measured at the Wetland Center study site in 2016. At lower flows, increased interaction between water and sediment is predicted to induce hyporheic exchange more than it would at higher flows (Bencala, 1983).

Solute retention at the Realigned Reach as indicated by power law slopes (Table 5) appears to be high, relative to other sites, and may be adequate to replace that which was lost from the western channel. Hyporheic exchange along the realigned channel could be driven by the prominent meander bend (Boano et al., 2006), but could also be aided by low discharge and velocity. This hyporheic exchange may be limited to a small area. Comparisons between solute retention ratios suggest that solute retention potential along the realigned reach is roughly equivalent to both the western and eastern channels (Table 6). Mass recovery data (Figure 13) suggest that the realigned channel may be a more effective flow conduit, but that the western channel may have induced more hyporheic exchange when it was active. A substantial loss in hyporheic flux through the western channel between 2015 and 2016 can be seen in Figure 25. The combined percent mass recovered at Wetland West

and Wetland Center in 2015 (57% of upstream mass in that year) was much less than the percent mass recovered at Wetland Center in 2016 (98% of upstream mass in that year), which now accumulates flow from all upstream channels.

Increased roughness introduced by bed and near-channel vegetation through the center channel expanded a storage zone for solute-laden water along the length of the stream, but did not necessarily increase exchange through the hyporheic zone. The apparent decrease in hyporheic flux through Wetland Center between 2015 and 2016 suggests that solute retention may have increased without an equal increase in hyporheic exchange (Figure 23). This distinction between solute retention and hyporheic exchange may explain why the mass/discharge ratios at the Wetland Center study site do not align with the trend suggested by the power-law characterization. A between-year comparison of mass/discharge ratios (Table 3) at the Wetland Center study site suggests a decrease in solute retention or hyporheic exchange, which conflicts with the increase indicated by the power-law slopes. Plausible explanations exist for both solute retention trends. More efficient surface water routing through consolidated flow paths upstream of the Wetland Center study site, which includes the steep, realigned channel, may have limited solute storage. It is also possible that the mass/discharge ratio may not accurately characterize the hyporheic exchange behavior through time, because it is simply a ratio of final mass recovery and discharge percentages. Alternatively, the power-law slope characterization assesses solute flux through time.

The increase in solute retention between 2015 and 2016 at the Lower Sentinel study site is consistently supported across multiple datasets. Power law slopes decreased from 0.348 to 0.318 (Table 5) and the mass/discharge ratio increased from 0.61 to 0.46 (Table 6) between 2015 and 2016. The percentage of tracer mass retained in Lulu City wetland above the Lower Sentinel study site increased from 23% to 27.5% between 2015 and 2016 (Table 3). In addition to increased overbank water ponding, the longer and more sinuous flow path through the center channel likely introduced zones of in-stream storage for salt-traced water in eddies and other constrictions. Sustained higher daily discharges through the center channel in

2016 than in 2015 meant a larger proportion of flow was overbank for a longer period of time (Table 2). Hydraulic resistance associated with floodplain vegetation likely increased overbank water storage, which contributed to the decrease in solute retention at the Lower Sentinel study site. Additionally, the tracer velocity measured at the Lower Sentinel site decreased between 2015 and 2016 (Table 4). Lulu City wetland may have lost hyporheic exchange capacity through the western channel, but gained solute retention capacity by routing more flow through the center of the wetland.

The receding limb of the Lower Sentinel mass recovery breakthrough curve, which returns to background concentration much sooner in 2016 than in 2015, suggests a decrease in hyporheic exchange in 2016 (Figure 12). Similar to the Wetland Center site, the Lower Sentinel trend may be explained by separating solute retention and hyporheic exchange. The obvious shoulders on both the rising and falling limbs of the Lower Sentinel breakthrough curve in 2015, which are absent in 2016, may be a function of faster tracer delivery through two flow paths in 2015, instead of one in 2016 (Figure 12). The rising limb shoulder indicates that tracer was delivered faster to the Lower Sentinel study site in 2015 than in 2016 (Figure 14), most likely through the portion of flow that traveled through the shorter west channel. The west channel also retained a portion of the mass tracer, possibly in hyporheic exchange pathways, which slowed the recovery of tracer at the Lower Sentinel site, as evidenced by the falling limb shoulder. I suspect the breakthrough curve shoulders are a function of surface flow through two dominant flow paths, where the inclusion of the pre-realignment west channel induced a markedly different advective travel time than the center channel. In-stream travel times through the Wetland Center channel were consistent between 2015 and 2016 (Figure 14, Table 4).

5.3 Sediment transport

Sediment delivered to the northern end of Lulu City wetland by the 2003 debris flow was a source of concern for Rocky Mountain National Park staff, and one that scientists and consultants agreed might be addressed through management of the Upper Colorado

River (RMNP, 2013; Rathburn and Cooper, 2014). Anthropogenic disturbances, especially debris flows initiating from Grand Ditch, have increased debris flow frequency and have elevated sediment loads into Lulu City wetland such that natural floods do not reliably return the system to a baseline sediment flux (Rubin et al., 2012; Rathburn et al., 2013). Debris flow sediments in Lulu City wetland are more likely to accumulate in between the now infrequent large floods required to transport the sediment out of the system (Rathburn et al., 2013). *In situ* weathering of upstream debris flow ryholite introduces a persistent (on a decadal time scale) supply of gravel sized sediment into the system (Rathburn et al., 2013). Increasing sediment transport through Lulu City wetland provided motivation for rerouting the Colorado River through the steepened realigned channel. Sand and gravel transport did occur, lending partial support to hypothesis 3, but all sediment transport was limited and localized to the Realigned Reach only. Deposition occurred at the east-turning bend along the realigned channel and at the Wetland Center study site, as indicated by the increased surface area of sand bars. Immediately downstream of the deep pool at the Wetland Center study site, shallow flows and increased overbank roughness contributed to significant sand deposition. Field observations suggest that this is the downstream extent of sediment transport; from here south, very little change in channel erosion or deposition occurred following upstream channel realignment.

Prior to the channel realignment, Rathburn et al. (2013) found that the upstream site was identified as being transport-limited during the rising limb, but supply-limited during the falling limb of the snowmelt peak. Repeat bed elevation surveys and bed grain size analyses confirm a similar history at the Realigned Reach study site. The realigned channel eroded its bed and banks during snowmelt runoff in 2016, but given more time, the realigned channel will likely evolve in a similar way to the eastern channel, which is characterized by a step-pool bedform and a steep, 2.1%, reach-averaged slope. Field observations indicate that alluvial fine sands and silt, which previously existed in the top 0.2 m of the realigned channel, were flushed away as early as 4 October 2015 (less than two weeks after channel completion),

exposing permeable coarse sands and gravels. Despite increased incision through snowmelt 2016, which formed a series of knickpoints held in place by sedge root wads, the realigned channel did not erode to the peat or overbank deposits identified beneath the 4 m deep debris flow deposits (Rubin et al., 2012). These knickpoints did migrate upstream during the course of peak runoff, but migration stopped during low flows before they accessed the gravel bars at the north end of the realigned channel.

Changes in gravel bar area can be seen in repeat aerial imagery at the head of Lulu City wetland, indicating increased channelization and possibly increased deposition of debris flow sediments (Figure 28). Volumetric changes in gravel bars would need to be confirmed by repeat elevation surveys or differencing of digital elevation models, but field observations of post-realignment sand and gravel deposition suggest some level of deposition. Additionally, a 13% increase in flow through the Wetland East study site between 2015 and 2016 (Table 1) may be attributed to backwater effects that induced sediment deposition behind the earthen diversion dam. It appears that the size of the medial gravel bar that splits flow between the east and center channel expanded during peak flow in 2016, which effectively diverted a larger portion of upstream flow to the east channel (Figure 28).

It is possible that redistributed gravels at the head of Lulu City wetland may reflect increased delivery from upstream, and that transport capacity remained unchanged. Alternatively, it is possible that both the sediment transport capacity and delivery from upstream increased, but that delivery remained greater than transport. However, the comparison in Figure 28 shows that under two similar hydrograph years, movement of coarse material through the head of the wetland did not increase enough to prevent gravel bar expansion.

The significant change in bed grain size distribution along the western channel also indicates a change in transport capacity, although it is not necessarily indicative of decreased sediment transport through that channel (Figure 29). It is likely that sediment was mobilized through the west channel during periods of peak discharge, which were higher in 2016 than in 2015 (Figure 7D), but that field sediment sampling missed any transport that occurred. Fining along the western channel does indicate that fine sediment is suspended in the flow at some point before settling out of suspension after snowmelt, when flow velocity decreases.

Depending on the size and extent of deposition, redistributed debris flow sediments may not affect hyporheic exchange in the wetland. Modeling by Storey (2003) found that increasing alluvial thickness, when composed of permeable material, did not affect flow paths through the hyporheic zone. This has positive implications for hyporheic exchange, but increased overbank deposition of permeable sands and gravels near the Wetland Center site may contribute to disconnecting the water table from the surface, as early debris flow sedimentation has done on the western side of the wetland. Low permeability peat layers, buried within Lulu City wetland, may limit or alter hyporheic flow paths, or promote overbank water storage that does not return to the stream channel, similar to what Tonina and Buffington (2009) found. The effect of increased sedimentation near the Wetland Center study site may be detrimental for willow establishment and growth, which benefit from high water tables (Bilyeu et al., 2008). If sediment deposition remains modest, the increased overbank flooding observed near the Wetland Center study site may be sufficient to maintain water tables needed for willow growth, but the larger concern for willow establishment in Lulu City wetland continues to be intense browsing by moose, elk, and deer.

6. CONCLUSION

Rocky Mountain National Park staff constructed an earthen diversion berm and excavated a channel to realign a portion of the Upper Colorado River through a historic channel as it flows into Lulu City wetland. This low-flow channel prevailed through one average snowmelt season in 2016, but continued monitoring is needed to assess the maximum flows it is likely to sustain. The realignment successfully diverted over 48% of incoming flow from the west to the center of the wetland, such that losses to the western channel were almost completely accounted for in the center channel. Resulting decreases in hyporheic exchange along the western channel were substantial, and were not immediately mitigated by increases to hyporheic exchange in either the realigned channel or central wetland flow-path. Electrical resistivity results indicate that hyporheic exchange occurs along sub-meter flow paths within Lulu City wetland, where transit times are on the order of minutes to hours. The scale of hyporheic exchange within Lulu City wetland was likely under-represented within this study, as the tracer test implementation was biased toward hyporheic exchange that occurred along only a portion of the flow paths that are likely present. The loss of hyporheic flow paths, while small-scale, has negative implications for the biodiversity and river-floodplain connectivity in Lulu City wetland.

The constructed earthen diversion berm and channel realignment did not succeed in creating a sustainable or well-defined channel through debris flow deposits at the head of Lulu City wetland, which could have connected the main upstream channel to the main thread within the wetland. The realignment and berm construction did not increase transport of debris flow sediments through the wetland, nor did it prevent further deposition of 2003 debris flow sediments at the wetland head. The realigned channel produced additional sediment as it eroded its own bed during snowmelt in 2016. These sediments were transported downstream, but were quickly deposited overbank and in lateral bars as the Colorado River gradient and depth decreased immediately downstream of the realigned channel.

7. MANAGEMENT IMPLICATIONS

This research successfully incorporated portions of techniques that, if expanded and combined, could lead to a deeper and more complete understanding of the hyporheic exchange and sediment transport processes acting in a complex wetland system. One year of restoration effectiveness monitoring from Lulu City wetland highlights an important consideration for future wetland restoration projects: that the conditions needed to facilitated sediment transport may not align with those needed to increase, or even maintain, hyporheic exchange pathways or floodplain solute retention.

A deep, narrow, steep and longitudinally continuous channel would be required to effectively transport sediment from the head of Lulu City wetland 750 m south to the wetland outlet. This channel would have to be the primary flow path through the wetland, which would limit the lateral connectivity between the river and floodplain. The extent of hyporheic exchange and overbank flooding would decrease, with detrimental effects for wetland biodiversity. Sediment transport modeling for river restoration projects is often based on thresholds needed to move sediment through a reference reach, but generally assumes a high degree of connectivity between up and downstream reaches. This assumption may work for fine-grained sediment, but can overestimate longitudinal transport of coarser material (Hooke, 2003). Proposed channel changes that would facilitate sediment transport at high flows on the Colorado River upstream of Lulu City wetland would still result in sediment storage in sand and gravel bars within the low-gradient wetland. This type of unconnected system is characterized by localized responses to sediment storage zones that persist until coarse-grained sediment is reduced to size fractions that are suitable for transport under current flow conditions (Hooke, 2003).

Alternatively, a process-based restoration approach aimed at treating the sediment supply at its source would be a sustainable solution for limiting sediment deposition at the head of Lulu City wetland. For example, effective sediment mitigation for Lulu City

wetland would address potential debris flows initiation points upstream by stabilizing the hydrothermally-altered slopes above and below Grand Ditch. Given sufficient time to return to a more natural debris flow regime, weathering processes will facilitate storage and transport of debris flow sediments through Lulu City wetland. Plants would stabilize mobile gravel bars and weathering processes would break down gravels to sands, which could then be transported by the Upper Colorado River through Lulu City wetland.

Re-establishing willows within Lulu City wetland may be an effective means of stabilizing gravel bars and limiting sediment transport. Willow seedlings may be limited by gravel bar mobilization that appears to occur frequently during low magnitude flows in Lulu City wetland, but research on vegetation turnover on gravel bars shows that established vegetation can have higher disturbance thresholds than colonizing plants (Surian et al., 2015). Planting willow cuttings on gravel bars in Lulu City wetland is one option, but this would require animal exclosures to prevent ungulate browsing. Exclosures have been shown in other riparian wetlands to significantly increase willow growth and resilience in as short as one to two seasons (Case and Kauffman, 1997). Exclosures in other areas of Rocky Mountain National Park have successfully decreased ungulate related plant mortality within the exclosure when compared to mortality of the same species outside of the exclosure (Baker et al., 1997). Once established, willows are exceptionally tolerant to variable inundation conditions (Amlin and Rood, 2001) and would likely do well on gravel bars in Lulu City wetland assuming exclosures remain until plants grow large enough to survive ungulate browsing.

I emphasize caution when planning more extensive and, inevitably, disruptive restoration based on these preliminary conclusions. One year of monitoring might provide insight, but 5-10 years of continued monitoring are needed to better understand the full effects of restoration (Zedler, 2004). Restoring wetlands is an important and noble effort, but many systems are slow, or unable, to provide the same level of ecosystem services or return to the equivalent level of biodiversity that undisturbed and natural wetlands offer (Zedler, 2004).

8. FUTURE WORK

Electrical resistivity imaging proved promising in Lulu City wetland. If repeated, electrical resistivity analyses would benefit from longer background data collections to account for daily variations in pre-tracer conductivity. Increasing the spatial extent of time-lapse electrical resistivity transects is essential to better understand large-scale hyporheic flow paths and also to validate the existence of small-scale, near stream hyporheic zones. Increasing the spatial coverage of surface conductivity measurements to include more of the wetland would better identify where solutes are preferentially retained. Adding a nutrient tracer, such as nitrogen, along with a conservative tracer would better identify which hyporheic zone processes are occurring at which locations (Triska et al., 1989).

Linking measured tracer concentrations to a one-dimensional transport model (e.g. OTIS) has proven to be a powerful way to quantify the storage component of hyporheic exchange. This approach is not without problems, as there are often many parameter combinations that may produce the same results, not all of which accurately reflect the natural processes acting to produce the input data (Harvey and Wagner, 2000).

Additional techniques could be added to expand the spatial coverage of hyporheic zone characterization, including the use of seepage meters or hydraulic head gradient mapping throughout a well network (Harvey and Wagner, 2000). The use of a physical tracer, like heat, could characterize the spatial extent of hyporheic exchange, as well as contribute to calculating seepage rates through the bed. Because stream and groundwater have different temperatures, zones of mixing at exchange sites could easily be distinguished from the two distinct end-members (Fanelli and Lautz, 2008). Temperature sensors placed on the bed along a river reach could identify those spatial patterns, while quantifying heat flow in saturated soils could be used to indirectly measure bed seepage rates (Constantz, 2008).

Sediment transport through the wetland was not successfully measured in 2015 or 2016. Access to the channel during high flows, when bedload was most likely moving, was

prohibitively dangerous. Wilcock (2001) describes an inexpensive and mobile method for bedload collection using traps created by placing 20 L buckets in the bed - a method that is well suited to remote back-country sites. Scour chains paired with tracer clasts have also been successfully used to estimate event-based bedload transport volumes in gravel bed rivers (Liébault and Laronne, 2008). Repeating pebble counts weekly throughout the melt season would better characterize bed roughness, leading to better estimates of sediment transport capacity. Finally, quantification of gravel bar sediment volume at the head of the wetland is needed to validate whether the area changes identified in repeat aerial imagery represent changes in erosion or deposition, or simply flow consolidation. Repeat elevation surveys or digital elevation model differencing could be used to quantify volume changes at the head of Lulu City wetland.

REFERENCES

Amlin, N. A. and Rood, S. B. December 2001. Inundation Tolerances of Riparian Willows and Cottonwoods1. *JAWRA Journal of the American Water Resources Association*, 37 (6):1709–1720.

Andrews, E. D. 1979. Scour and fill in a stream channel, East Fork River, western Wyoming. USGS Numbered Series 1117, US Goverment Printing Office, Washington, DC.

Andrews, T. G. 2011. *An Environmental History of the Kawuneeche Valley and the Headwaters of the Colorado River, Rocky Mountain National Park*.

Arcement, G. J. and Schneider, V. R. 1989. *Guide for Selecting Manning's Roughness Coefficients for Natural Channels and Flood Plains*. US Government Printing Office, Washington, DC.

Baker, W. L., Munroe, J. A., and Hessl, A. E. 1997. The Effects of Elk on Aspen in the Winter Range in Rocky Mountain National Park. *Ecography*, 20(2):155–165.

Bencala, K. E. 1983. Simulation of solute transport in a mountain pool-and-riffle stream with a kinetic mass transfer model for sorption. *Water Resources Research*, 19(3):732–738.

Bernhardt, E. S. and Palmer, M. A. 2011. River restoration: The fuzzy logic of repairing reaches to reverse catchment scale degradation. *Ecological Applications*, 21(6):1926–1931.

Bilyeu, D. M., Cooper, D. J., and Hobbs, N. T. 2008. Water tables constrain height recovery of willow on Yellowstone's northern range. *Ecological Applications*, 18(1):80–92.

Binley, A. 2016. R2, executable code. (3.1).

Binley, A. and Kemna, A. DC resistivity and induced polarization methods. In *Hydrogeophysics*, pages 129–156. Springer, 2005.

Binley, A., Cassiani, G., Middleton, R., and Winship, P. 2002. Vadose zone flow model parameterisation using cross-borehole radar and resistivity imaging. *Journal of Hydrology*, 267(3–4):147–159.

Boano, F., Camporeale, C., Revelli, R., and Ridolfi, L. 2006. Sinuosity-driven hyporheic exchange in meandering rivers. *Geophysical Research Letters*, 33(18):L18406.

Boulton, A. J., Findlay, S., Marmonier, P., Stanley, E. H., and Valett, H. M. 1998. The Functional Significance of the Hyporheic Zone in Streams and Rivers. *Annual Review of Ecology and Systematics*, 29(1):59–81.

Boulton, A. J., Datry, T., Kasahara, T., Mutz, M., and Stanford, J. A. 2010. Ecology and management of the hyporheic zone: Stream–groundwater interactions of running waters and their floodplains. *Journal of the North American Benthological Society*, 29(1):26–40.

Braddock, W. and Cole, J., 1990. Geologic Map of Rocky Mountain National Park and Vicinity, Colorado.

Case, R. L. and Kauffman, J. B. 1997. Wild ungulate influences on the recovery of willows, black cottonwood and thin-leaf alder following cessation of cattle grazing in Northeastern Oregon. *Northwest Science*, 71(2):115–126.

Clayton, J. A. and Westbrook, C. J. 2008. The effect of the Grand Ditch on the abundance of benthic invertebrates in the Colorado River, Rocky Mountain National Park. *River Research and Applications*, 24(7):975–987.

Constantz, J. 2008. Heat as a tracer to determine streambed water exchanges. *Water Resources Research*, 44(4):W00D10.

Cooper, D. J. 2007. Restoration concepts and approaches for the Lulu City wetland and riparian zones of the Colorado River and Lulu Creek impacted by the May 2003 breach of Grand Ditch, Rocky Mountain National Park, Colorado State University, Fort Collins, CO.

Covino, T. 2016. Hydrologic connectivity as a framework for understanding biogeochemical flux through watersheds and along fluvial networks. *Geomorphology*.

Covino, T., McGlynn, B., and Mallard, J. 2011. Stream-groundwater exchange and hydrologic turnover at the network scale. *Water Resources Research*, 47(12):W12521.

Crockett, A. C., Ronayne, M. J., and Cooper, D. J. September 2016. Relationships between vegetation type, peat hydraulic conductivity, and water table dynamics in mountain fens: Relating Vegetation Type and Peat Hydraulic Conductivity in Mountain Fens. *Ecohydrology*, 9(6):1028–1038.

Dahl. 2000. Status and trends of wetlands in the conterminous United States 1986 to 1997. Technical report, US Fish and Wildlife Service.

Dahl. 1990. Wetlands Losses in the United States 1780s to 1980s. Report to Congress. Technical Report PB-91-169284/XAB, US Fish and Wildlife Service.

Day, T. 1977. Field procedures and evaluation of a slug gilution gauging method in mountain streams. *Journal of Hydrology*, 16(2):113–133.

Drummond, J. D., Covino, T. P., Aubeneau, A. F., Leong, D., Patil, S., Schumer, R., and Packman, A. I. 2012. Effects of solute breakthrough curve tail truncation on residence time estimates: A synthesis of solute tracer injection studies. *Journal of Geophysical Research: Biogeosciences*, 117(G3):G00N08.

EPA. 1986. Method 9100: Saturated hydrualic conductivity, saturated leachate conductivity, and intrinsic permeability. Technical report, US Environmental Protection Agency, Washington, D.C.

Fanelli, R. M. and Lautz, L. K. 2008. Patterns of Water, Heat, and Solute Flux through Streambeds around Small Dams. *Ground Water*, 46(5):671–687.

Findlay, S. 1995. Importance of surface-subsurface exchange in stream ecosystems: The hyporheic zone. *Limnology and Oceanography*, 40(1):159–164.

Gooseff, M. N. 2010. Defining Hyporheic Zones – Advancing Our Conceptual and Operational Definitions of Where Stream Water and Groundwater Meet. *Geography Compass*, 4(8):945–955.

Gowan, C. and Fausch, K. D. 1996. Long-Term Demographic Responses of Trout Populations to Habitat Manipulation in Six Colorado Streams. *Ecological Applications*, 6(3):931–946.

Graham, L. E., Wilcox, L. W., and Graham, J. M. 2009. *Algae*. Benjamin Cummings, San Francisco, 2 edition. ISBN 978-0-321-55965-4.

Grimsley, K. J., Rathburn, S. L., Friedman, J. M., and Mangano, J. F. 2016. Debris Flow Occurrence and Sediment Persistence, Upper Colorado River Valley, CO. *Environmental Management*.

Harman, C. J., Ward, A. S., and Ball, A. 2016. How does reach-scale stream-hyporheic transport vary with discharge? Insights from rSAS analysis of sequential tracer injections in a headwater mountain stream. *Water Resources Research*.

Harvey, J. W. and Bencala, K. E. 1993. The effect of streambed topography on surface-subsurface water exchange in mountain catchments. *Water Resources Research*, 29(1): 89–98.

Harvey, J. W. and Wagner, B. J. Quantifying hydrologic interactions between streams and their subsurface hyporheic zones. In Jones, J. B. and Mulholland, P. J., editors, *Streams and Ground Waters*, pages 3–44. Academic Press, San Diego, California, 2000.

Harvey, J. W., Wagner, B. J., and Bencala, K. E. 1996. Evaluating the Reliability of the Stream Tracer Approach to Characterize Stream-Subsurface Water Exchange. *Water Resources Research*, 32(8):2441–2451.

Hauer, F. R., Locke, H., Dreitz, V. J., Hebblewhite, M., Lowe, W. H., Muhlfeld, C. C., Nelson, C. R., Proctor, M. F., and Rood, S. B. 2016. Gravel-bed river floodplains are the ecological nexus of glaciated mountain landscapes. *Science Advances*, 2(6):13.

Hester, E. T. and Gooseff, M. N. Hyporheic restoration in streams and rivers. In *Stream Resotration in Dynamic Fluvial Systems*, number 194 in Monograph, pages 167–187. American Geophysical Union, 2013.

Hey, R. D. and Thorne, C. R. 1983. Accuracy of surface samples from gravel bed material. *Journal of Hydraulic Engineering*, 109(6):842–851.

Hill, A. R., Labadia, C. F., and Sanmugadas, K. 1998. Hyporheic zone hydrology and nitrogen dynamics in relation to the streambed topography of a N-rich stream. *Biogeochemistry*, 42(3):285–310.

Hooke, J. November 2003. Coarse sediment connectivity in river channel systems: A conceptual framework and methodology. *Geomorphology*, 56(1-2):79–94.

Jackman, A. P., Walters, R. A., and Kennedy, V. C. 1984. Transport and concentration controls for chloride, strontium, potassium and lead in Uvas Creek, a small cobble-bed stream in Santa Clara County, California, U.S.A.: 2. Mathematical modeling. *Journal of Hydrology*, 75(1–4):111–141.

Johnson, T. C., Slater, L. D., Ntarlagiannis, D., Day-Lewis, F. D., and Elwaseif, M. 2012. Monitoring groundwater-surface water interaction using time-series and time-frequency analysis of transient three-dimensional electrical resistivity changes. *Water Resources Research*, 48(7):W07506.

Junk, W. J., Bayley, P. B., and Sparks, R. E. 1989. The Flood Pulse Concept in River-Floodplain System. *Proceedings of the International Large River Symposium*, pages 110–127.

Kaczynski, K. M. 2007. Riparian willow decline in Colorado: Interactions of ungulate browsing, native birds and fungi. Master's thesis, Colorado State University. Libraries.

Kasahara, T. and Wondzell, S. M. 2003. Geomorphic controls on hyporheic exchange flow in mountain streams. *Water Resources Research*, 39(1):1005.

Kennedy, V. C., Jackman, A. P., Zand, S. M., Zellweger, G. W., and Avanzino, R. J. 1984. Transport and concentration controls for chloride, strontium, potassium and lead in Uvas Creek, a small cobble-bed stream in Santa Clara County, California, USA: 1. Conceptual model. *Journal of hydrology*, 75(1-4):67–110.

Kondolf, G. M., Boulton, A. J., O'Daniel, S., Poole, G. C., Rahel, F. J., Stanley, E. H., Wohl, E., Bang, A., Carlstrom, J., Cristoni, C., and others. 2006. Process-based ecological river restoration: Visualizing three-dimensional connectivity and dynamic vectors to recover lost linkages. *Ecology and Society*, 11(2):5.

Lenth, R. V. and others. 2016. Least-squares means: The R package lsmeans. *J Stat Softw*, 69(1):1–33.

Liébault, F. and Laronne, J. B. 2008. Evaluation of bedload yield in gravel-bed rivers using scour chains and painted tracers: The case of the Esconavette Torrent (Southern French Prealps). *Geodinamica Acta*, 21(1-2):23–34.

Mangano, J. F. 2014. Evaluating channel morphologic changes and bed-material transport using airborne lidar, Upper Colorado River, Rocky Mountain National Park, Colorado. Master's thesis, Colorado State University.

McClymont, A. F., Roy, J. W., Hayashi, M., Bentley, L. R., Maurer, H., and Langston, G. 2011. Investigating groundwater flow paths within proglacial moraine using multiple geophysical methods. *Journal of Hydrology*, 399(1-2):57–69.

Meierding, T. 1980. *Glaciation of the Upper Colorado River Basin, Geoecology of the Colorado Front Range: A Study of Alpine and Subalpine Environments*. Westview Press, Boulder, CO.

Menichino, G. T. and Hester, E. T. 2014. Hydraulic and thermal effects of in-stream structure-induced hyporheic exchange across a range of hydraulic conductivities. *Water Resources Research*, 50(6):4643–4661.

Müller, K., Vanderborght, J., Englert, A., Kemna, A., Huisman, J. A., Rings, J., and Vereecken, H. 2010. Imaging and characterization of solute transport during two tracer tests in a shallow aquifer using electrical resistivity tomography and multilevel groundwater samplers. *Water Resources Research*, 46(3):W03502.

National Research Council and Committee on Mitigating Wetland Losses. 2001. *Compensating for Wetland Losses under the Clean Water Act*. National Academy Press, Washington, D.C. OCLC: 53366820.

NRCS, U. 2016. Phantom Valley (688) - Site Information and Reports.

Packard, F. M. 1947. A Survey of the Beaver Population of Rocky Mountain National Park, Colorado. *Journal of Mammalogy*, 28(3):219.

Palmer, M. A., Bernhardt, E. S., Allan, J. D., Lake, P. S., Alexander, G., Brooks, S., Carr, J., Clayton, S., Dahm, C. N., Follstad Shah, J., Galat, D. L., Loss, S. G., Goodwin, P., Hart, D. D., Hassett, B., Jenkinson, R., Kondolf, G. M., Lave, R., Meyer, J. L., O'Donnell, T. K., Pagano, L., and Sudduth, E. 2005. Standards for ecologically successful river restoration. *Journal of Applied Ecology*, 42(2):208–217.

Patil, S., Covino, T. P., Packman, A. I., McGlynn, B. L., Drummond, J. D., Payn, R. A., and Schumer, R. 2013. Intrastream variability in solute transport: Hydrologic and geomorphic controls on solute retention. *Journal of Geophysical Research: Earth Surface*, 118(2):413–422.

Radtke, D. B., Davis, J. V., and Wilde, F. D. 2005. 6.3 Specific electrical conductance. *National Field Manual for the Collection of Water-quality Data: US Geol. Surv. Tech. Water-Resour. Invest., book*, 9.

Rathburn, S. L. and Cooper, D. J. 2014. Executive Summary – Restoration Workshop. Technical report.

Rathburn, S. L., Rubin, Z. K., and Wohl, E. E. 2013. Evaluating channel response to an extreme sedimentation event in the context of historical range of variability: Upper Colorado River, USA. *Earth Surface Processes and Landforms*, 38(4):391–406.

RCoreTeam, 2017. R: A language and environment for statistical computing.

Rice, E., Baird, R., Eaton, A., and Clesceri, L. Conductivity, SM 2510. In *Standard Methods for the Examination of Water and Wastewater*, pages 52–54. American Public Health Association, New York, 2012.

Ringelman, J. K. 1992. *Waterfowl Management Handbook: Ecology of Montane Wetlands*, volume 13.3.6. US Department of the Interior, Fish and Wildlife Service.

RMNP. 2013. EIS Grand ditch breach restoration. Technical report, National Park Service.

Rubin, Z., Rathburn, S. L., Wohl, E., and Harry, D. L. 2012. Historic range of variability in geomorphic processes as a context for restoration: Rocky Mountain National Park, Colorado, USA. *Earth Surface Processes and Landforms*, 37(2):209–222.

Schönbrunner, I. M., Preiner, S., and Hein, T. 2012. Impact of drying and re-flooding of sediment on phosphorus dynamics of river-floodplain systems. *Science of The Total Environment*, 432:329–337.

Singha, K., Day-Lewis, F. D., Johnson, T., and Slater, L. D. 2014. Advances in interpretation of subsurface processes with time-lapse electrical imaging. *Hydrological Processes*, page 28.

Singha, K. and Gorelick, S. M. 2005. Saline tracer visualized with three-dimensional electrical resistivity tomography: Field-scale spatial moment analysis. *Water Resources Research*, 41(5):1–17.

Stanford, J. A. and Ward, J. V. 1988. The hyporheic habitat of river ecosystems. *Nature*, 335:64–66.

Storey, R. G. 2003. Factors controlling riffle-scale hyporheic exchange flows and their seasonal changes in a gaining stream: A three-dimensional groundwater flow model. *Water Resources Research*, 39(2):1–17.

Surian, N., Barban, M., Ziliani, L., Monegato, G., Bertoldi, W., and Comiti, F. March 2015. Vegetation turnover in a braided river: Frequency and effectiveness of floods of different magnitude. *Earth Surface Processes and Landforms*, 40(4):542–558.

Tonina, D. and Buffington, J. M. 2009. Hyporheic Exchange in Mountain Rivers I: Mechanics and Environmental Effects. *Geography Compass*, 3(3):1063–1086.

Toran, L., Hughes, B., Nyquist, J., and Ryan, R. 2012. Using Hydrogeophysics to Monitor Change in Hyporheic Flow around Stream Restoration Structures. *Environmental & Engineering Geoscience*, 18(1):83–97.

Triska, F. J., Kennedy, V. C., Avanzino, R. J., Zellweger, G. W., and Bencala, K. E. 1989. Retention and Transport of Nutrients in a Third-Order Stream in Northwestern California: Hyporheic Processes. *Ecology*, 70(6):1893–1905.

Ward, A. S., Singha, K., and Gooseff, M. N. 2010. Imaging hyporheic zone solute transport using electrical resistivity. *Hydrological processes*, 24(7):948–953.

Ward, A. S., Fitzgerald, M., Gooseff, M. N., Voltz, T. J., Binley, A. M., and Singha, K. 2012. Hydrologic and geomorphic controls on hyporheic exchange during base flow recession in a headwater mountain stream. *Water Resources Research*, 48(4):20.

Ward, A. S., Gooseff, M. N., Voltz, T. J., Fitzgerald, M., Singha, K., and Zarnetske, J. P. 2013. How does rapidly changing discharge during storm events affect transient storage and channel water balance in a headwater mountain stream? *Water Resources Research*, 49(9):5473–5486.

Ward, S. H. Resistivity and induced polarization methods. In *Geotechnical and Environmental Geophysics*, number 5, pages 147–189. Society of Exploration Geophysics, 1990.

Wegener, P. 2016. The influence of lateral hydrologic connectivity on fluvial flux and ecosystem metabolism in a river-floodplain system. Master's thesis, Colorado State University.

Westbrook, C. J., Cooper, D. J., and Baker, B. W. 2006. Beaver dams and overbank floods influence groundwater-surface water interactions of a Rocky Mountain riparian area:. *Water Resources Research*, 42(6):W06404.

White, D. S. 1993. Perspectives on Defining and Delineating Hyporheic Zones. *Journal of the North American Benthological Society*, 12(1):61–69.

White, P. A. 1988. Measurement of ground-water parameters using salt-water injection and surface resistivity. *Ground Water*, 26(2):179–186.

Wilcock, P. R. 2001. Toward a practical method for estimating sediment-transport rates in gravel-bed rivers. *Earth Surface Processes and Landforms*, 26(13):1395–1408.

Windell, J. T., Willard, B. E., Cooper, D. J., Foster, S. Q., and Knud-Hansen, C. F. 1986. An ecological characterization of Rocky Mountain montane and subalpine wetlands. Technical report.

Wohl, E., Lane, S. N., and Wilcox, A. C. 2015. The science and practice of river restoration. *Water Resources Research*, 51(8):5974–5997.

Wolman, M. 1954. A method of sampling coarse river-bed material. *Transactions, Amerian Geophysical Union*, 35(6):951–956.

Wyatt, K. H., Hauer, F. R., and Pessoney, G. F. 2008. Benthic algal response to hyporheic-surface water exchange in an alluvial river. *Hydrobiologia*, 607(1):151–161.

Zedler, J. B. 2004. Compensating for wetland losses in the United States. *Ibis*, 146(s1): 92–100.

Zedler, J. B. and Kercher, S. 2005. Wetland Resources: Status, Trends, Ecosystem Services, and Restorability. *Annual Review of Environment and Resources*, 30(1):39–74.

APPENDIX A. CONDUCTIVITY DATA LOGGER SPECIFICATIONS

Specific conductance at 25°C, SC (μS cm^{-1}) was used, instead of electrical conductivity, for all analyses. This normalizes for temperature effects, by using (Equation 7) (Radtke et al., 2005):

$$SC = \frac{EC}{1 + 0.02(t - 25°C)} \tag{7}$$

where EC is the field measured electrical conductivity in μS cm^{-1} before temperature correction, 0.02 °C^{-1} is a temperature coefficient (applicable to Cl$^-$) (Rice et al., 2012), and t is water temperature (°C) at the time of EC measurement. Conversion factors for each data logger and site are listed in Table A.9.

Table A.9: Conductivity data logger specifications. The conversion factor is the slope of the linear regression between specific conductance at 25°C (μS cm^{-1}) and concentration (mg L^{-1}), measured with each instrument using NaCl. The R^2 value describes each correlation.

Logger #	**2015 location**	**2016 location**	**Conversion factor**	**R^2 value**
055	-	Upstream	0.47	0.9998
331	Upstream	Wetland Center	0.49	0.9997
332	Wetland West	Lower Sentinel	0.50	0.9997
333	Wetland Center	Restored Reach	0.50	0.9997
334	Lower Sentinel	Wetland East	0.51	0.9996

Table A.10: Conductivity data logger recording frequency. Study sites are listed according to river distance from the Upstream study site.

Study site	**Recording frequency (sec)**
Upstream 2015	4
Upstream 2016	5
Realigned Reach 2016	10
Wetland East 2016	10
Wetland West 2015	10
Wetland Center 2015 and 2016	10
Lower Sentinel 2015 and 2016	90

Table B.11: Salt tracer test instrument injection specifications. The total delivered mass was calculated from field samples, taken at the times indicated. These totals were not used for mass recovery calculations.

Date	**Elapsed time since tracer injection (hr)**	**Pump rate (L s^{-1})**	**Concentration (g L^{-1} NaCl)**	**Total delivered mass (kg NaCl)**
6 Sep 2015	0.0	0.104	40.5	
	1.0	0.109	41.8	
	2.0	0.107	40.9	
	3.0	0.100	42.7	
	4.0	0.097	-	62.7
average	-	**0.103**	**42.7**	
28 Aug 2016	0.5	0.103	46.0	
	2.0	0.095	44.7	
	2.5	0.099	47.1	
	3.5	0.092	44.8	
	4.0	0.091	44.8	63.3
average	-	**0.096**	**45.6**	

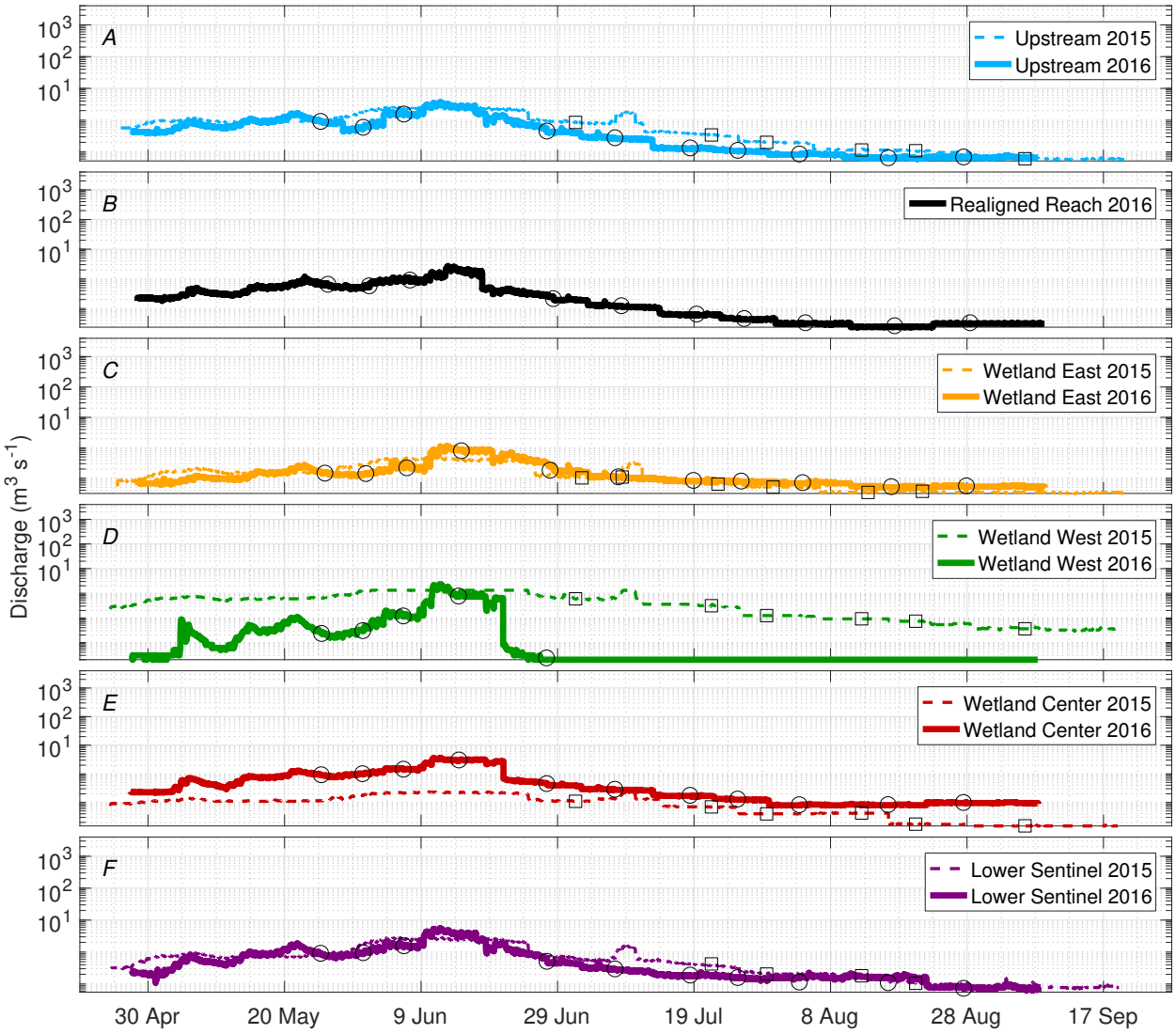

Figure C.32: Hydrographs with semi-log Y-axis for all study sites within Lulu City wetland, Rocky Mountain National Park. Study sites are arranged according to river distance from the Upstream study site. Panel A, Upstream; Panel B, Realigned Reach; Panel C, Wetland East; Panel D, Wetland West; Panel E, Wetland Center; and Panel F, Lower Sentinel. Symbols represent field sampling points (square in 2015 and circle in 2016).

APPENDIX D. MEASURED DISCHARGE DURING SALT TRACER TESTS

The velocity gaging method was used to calculate river discharge at each study site during the salt tracer injections in both 2015 and 2016 Figure D.33. 2015 Wetland East discharge is derived from the stage-discharge rating curve, because this site was not gaged by hand on 6 September 2015. Wetland East was gaged during the salt tracer test on 28 August 2016. Realigned Reach does not have 2015 discharge data because it was constructed after the 2015 tracer test. Wetland West was not gaged on 28 August 2016 because there was no measurable flow through that channel. Wetland Center and Lower Sentinel were gaged at the same location in both years. Lower Sentinel was gaged on 28 August 2016 following 2 hours of light, but steady rainfall.

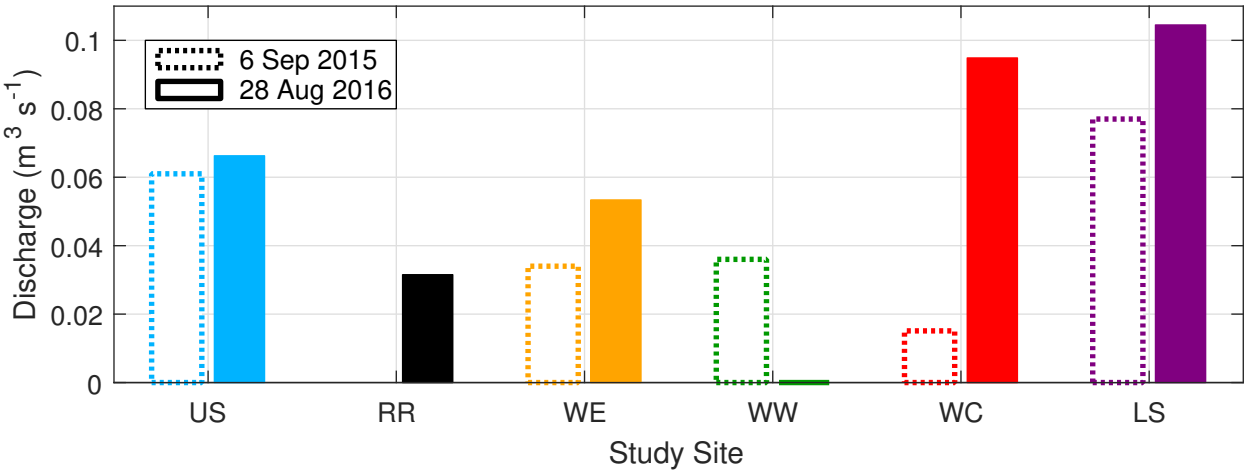

Figure D.33: Measured discharge during salt tracer tests, by study site within Lulu City wetland, Rocky Mountain National Park. Study sites are arranged from left to right according to river distance from the Upstream study site. US = Upstream; RR = Realigned Reach; WE = Wetland East; WW = Wetland West; WC = Wetland Center; LS = Lower Sentinel.

APPENDIX E. SALT TRACER MASS RECOVERY AS PERCENTAGE OF UPSTREAM RECOVERY

Figure E.34 simply displays the salt tracer mass recovery data in graphical form. Mass recoveries are calculated for each study site as a percentage of total mass recovered at the Upstream Site in that year.

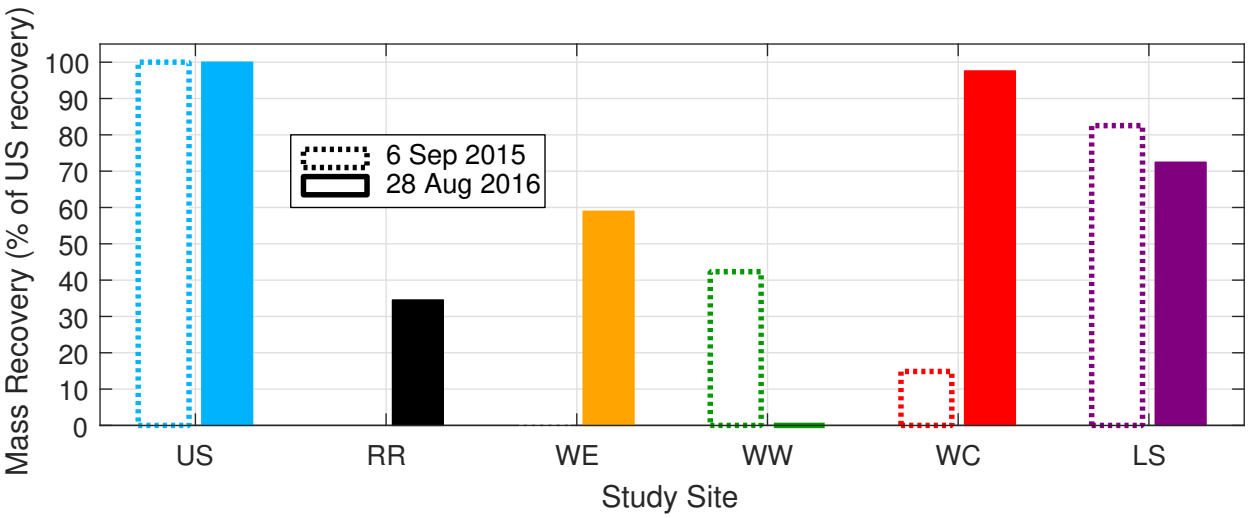

Figure E.34: Total salt recovered during tracer test as a percentage of Upstream recovery, by study site within Lulu City wetland, Rocky Mountain National Park. Study sites are arranged from left to right according to river distance from the Upstream study site. US = Upstream; RR = Realigned Reach; WE = Wetland East; WW = Wetland West; WC = Wetland Center; LS = Lower Sentinel.

APPENDIX F. MASS RECOVERY BREAKTHROUGH CURVE TAIL WITH POWER LAW EQUATION, BY STUDY SITE

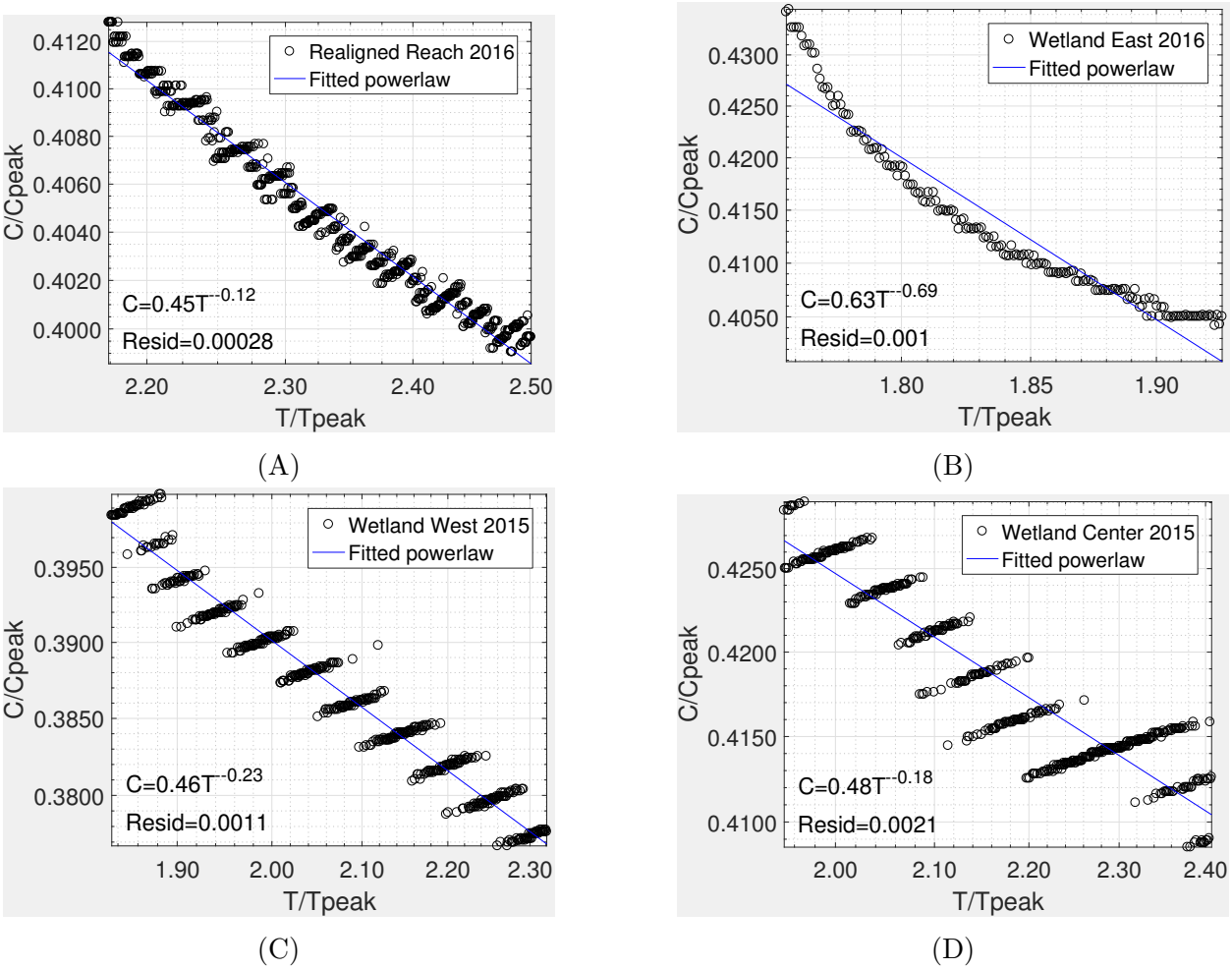

Figure F.35: Mass recovery breakthrough curve tails with power law equation fit, by study site. The slope of the curve is given by the exponent, which provides an indication of solute retention. Smaller absolute values indicate more solute retention.

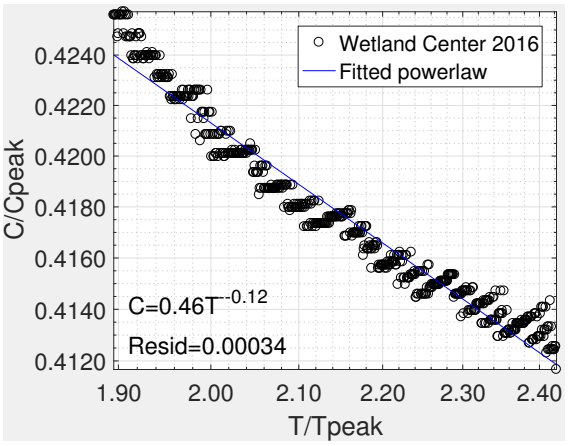

(E)

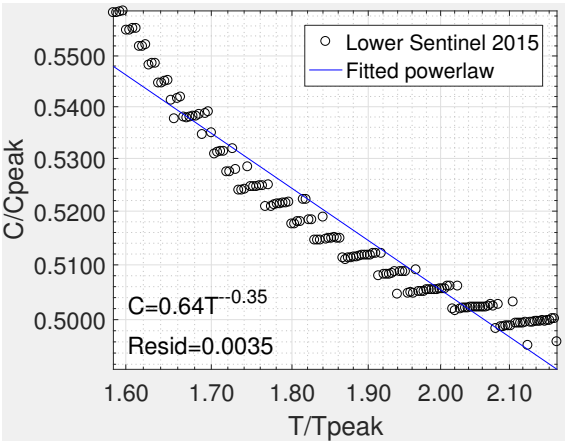

(F)

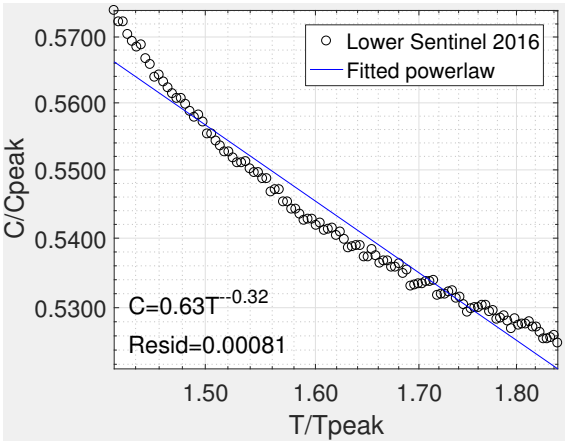

(G)

Figure F.35a: Mass recovery breakthrough curve tails with power law equation fit, by study site. The slope of the curve is given by the exponent, which provides an indication of solute retention. Smaller absolute values indicate more solute retention.

APPENDIX G. SUMMARY STATISTICS FOR ELECTRICAL RESISTIVITY DISTRIBUTION OF MEANS

Additional summary statistics for distributions of conductivity means, calculated to depths of 2 meters and 4 meters are displayed in Table G.12 and Table G.13. Minimum and maximum X values in Table 7 correspond to transect lengths in Figure 17 through Figure 21. A positive (+) conductivity change indicates that conductivity increased between 2015 and 2016. A negative (-) conductivity change indicates that conductivity decreased.

Table G.12: Summary statistics for electrical resistivity distribution means along select portions of electrical resistivity transects to 2 m depth. Mean conductivity is measured over the specified x and y transect distances in Figure 22 through Figure 26. SE describes the standard error in the mean. + conductivity change indicates an increase in mean conductivity between 2015 and 2016 population means and - conductivity change indicates a decrease in mean conductivity between 2015 and 2016. Analyses assume populations are normally distributed, but have unequal variances.

Transect	**Min X (m)**	**Max X (m)**	**Mean cond. (μS cm^{-1}) (2015)**	**SE (μS cm^{-1}) (2015)**	**Mean cond. μS cm^{-1} (2016)**	**SE (μS cm^{-1}) (2016)**	**Cond. change 5% sig. level**	**p-value**
XS0	0	47	55.4	1.9	45.6	1.0	-	< 0.05
XS0	14	30	27.0	0.3	25.9	0.4	-	< 0.05
XS0	33	50	98.8	3.2	71.1	1.4	-	< 0.05
XS1	0	141	41.2	0.7	47.7	1.0	+	< 0.05
XS1	10	60	54.7	1.2	64.3	2.0	+	< 0.05
XS1	34	44	53.7	2.3	61.2	2.6	+	< 0.05
XS1	75	125	31.8	0.5	34.3	0.5	+	< 0.05
XS1	90	100	33.0	0.4	33.6	0.6	not significant	0.09
XS2	0	176	48.3	0.7	55.9	0.7	+	< 0.05
XS2	130	176	45.5	2.1	46.3	0.4	not significant	0.48
XS2	162	176	12.6	1.4	51.0	0.4	+	< 0.05
XSLW	0	141	42.3	0.3	42.4	0.3	not significant	0.59
XSLW	0	25	48.5	0.5	47.8	0.4	-	< 0.05
XSLW	0	50	40.8	0.5	40.3	0.5	not significant	0.22
XSLW	30	50	30.6	0.2	30.8	0.2	not significant	0.47

Table G.13: Summary statistics for electrical resistivity distribution means along select portions of electrical resistivity transects to 4 m depth. Mean conductivity is measured over the specified x and y transect distances in Figure 22 through Figure 26. SE describes the standard error in the mean. + conductivity change indicates an increase in mean conductivity between 2015 and 2016 population means and - conductivity change indicates a decrease in mean conductivity between 2015 and 2016. Analyses assume populations are normally distributed, but have unequal variances.

Transect	**Min X (m)**	**Max X (m)**	**Mean cond. (μS cm^{-1}) (2015)**	**SE (μS cm^{-1}) (2015)**	**Mean cond. μS cm^{-1} (2016)**	**SE (μS cm^{-1}) (2016)**	**Cond. change 5% sig. level**	**p-value**
XS0	0	47	45.7	1.1	41.2	0.6	-	< 0.05
XS0	14	30	27.7	0.2	26.5	0.2	-	< 0.05
XS0	33	50	75.0	2.3	60.6	1.0	-	< 0.05
XS1	0	141	39.1	0.5	44.9	0.6	+	< 0.05
XS1	10	60	50.1	0.9	57.7	1.3	+	< 0.05
XS1	34	44	51.0	1.4	57.2	1.8	+	< 0.05
XS1	75	125	31.5	0.3	34.3	0.3	+	< 0.05
XS1	90	100	33.0	0.3	34.2	0.4	+	< 0.05
XS2	0	176	43.1	0.5	53.5	0.5	+	< 0.05
XS2	130	176	39.3	1.3	45.1	0.3	+	< 0.05
XS2	162	176	13.5	0.9	49.8	0.3	+	< 0.05
XSLW	0	141	40.0	0.2	40.4	0.2	+	< 0.05
XSLW	0	25	44.2	0.5	44.2	0.4	not significant	0.83
XSLW	0	50	38.3	0.4	38.5	0.3	not significant	0.44
XSLW	30	50	31.1	0.2	31.5	0.2	+	< 0.05

Table H.14: Electrical resistivity transect lengths.

Transect	**2015 Length (m)**	**2016 Length (m)**
XS0	46.9	46.8
XS1	140.6	140.3
XS1T	137.0	136.7
XS2	176.3	176.3
XSLW	140.5	140.7

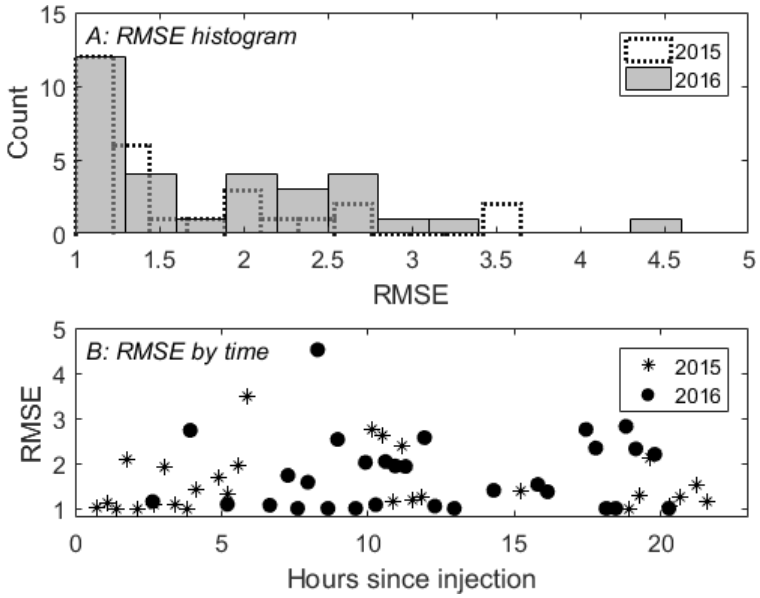

Figure I.36: Root mean squared error (RMSE) values for electrical resistivity tracer tests.

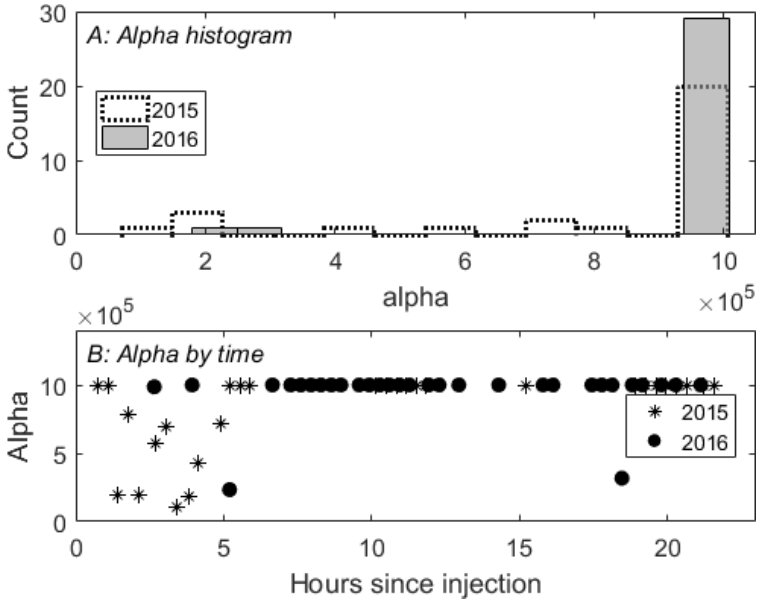

Figure I.37: Alpha smoothing values for electrical resistivity tracer tests.

APPENDIX J. SENSITIVITY MAPS FOR ELECTRICAL RESISTIVITY TRANSECTS

Sensitivity maps were calculated for each electrical resistivity transect, including the background transect recorded along XS1T. These maps include values from the diagonal of the matrix [J^T W^T W J], where high values indicate high sensitive to measurements (e.g wet, conductive near-stream areas, or areas adjacent to electrodes), and low values indicate low sensitivity to measurements (e.g. deeper, drier substrate) (Binley, 2016).

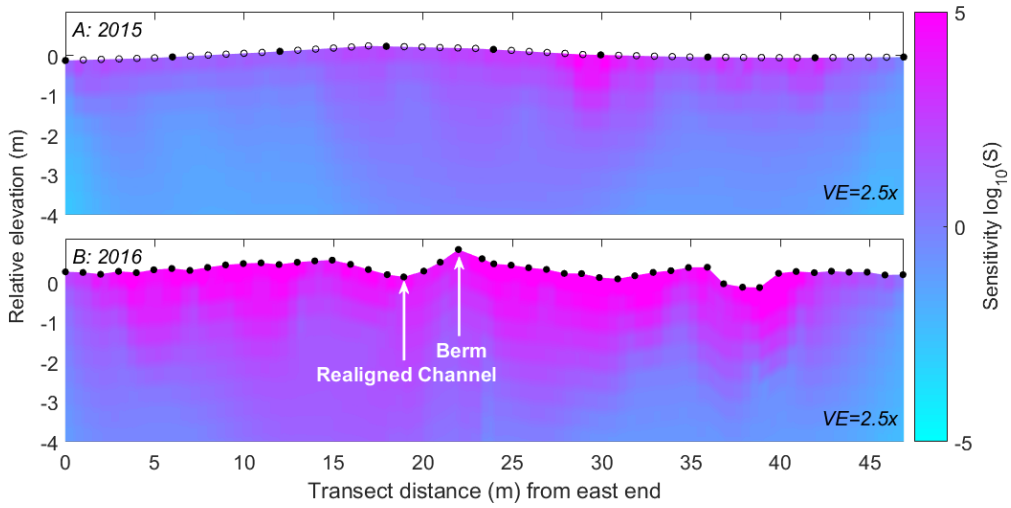

Figure J.38: Comparative electrical resistivity sensitivity matrix tomogram, entire length of transect XS0. Panel a was measured in 2015, prior to channel realignment. Panel b was measured in 2016, following channel realignment. Circles represent electrode locations; solid circles represent surveyed electrode locations and open circles represent interpolated electrode locations. High near surface sensitivity in both 2015 and 2016 is likely due to the presence of water over much of this transect.

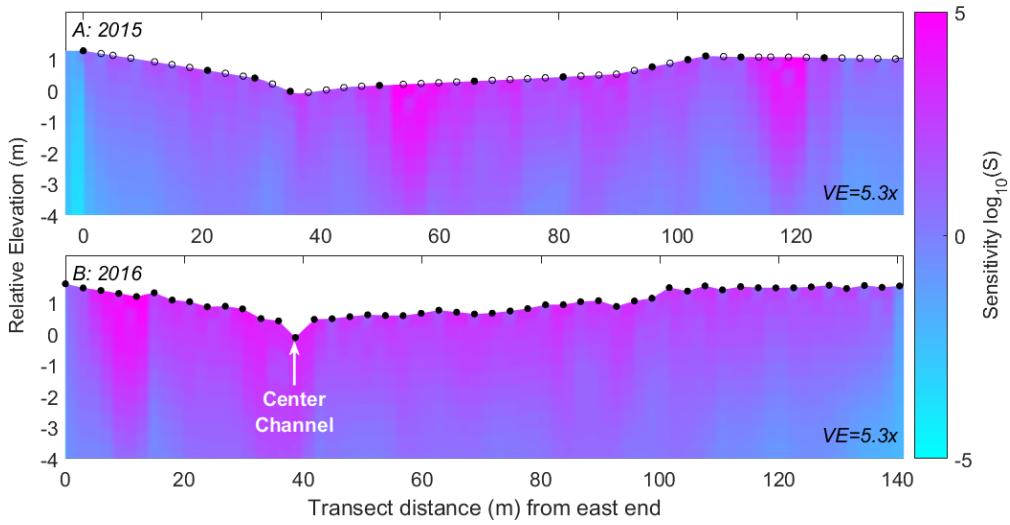

Figure J.39: Comparative electrical resistivity sensitivity matrix tomogram, entire length of transect XS1. Panel a was measured in 2015, prior to channel realignment. Panel b was measured in 2016, following channel realignment. Circles represent electrode locations; solid circles represent surveyed electrode locations and open circles represent interpolated electrode locations.

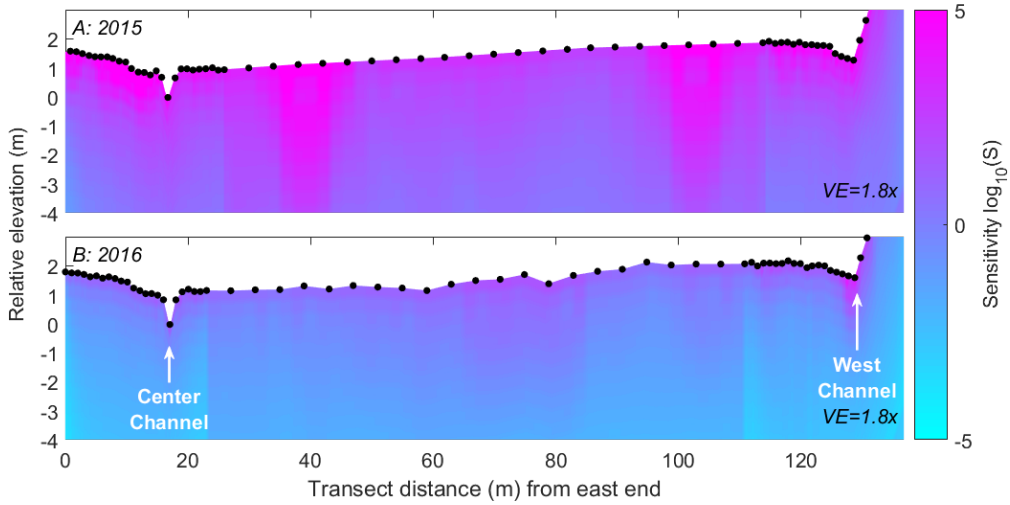

Figure J.40: Comparative electrical resistivity sensitivity matrix tomogram, entire length of transect XS1T. Panel a was measured in 2015, prior to channel realignment. Panel b was measured in 2016, following channel realignment. Circles represent electrode locations; solid circles represent surveyed electrode locations and open circles represent interpolated electrode locations.

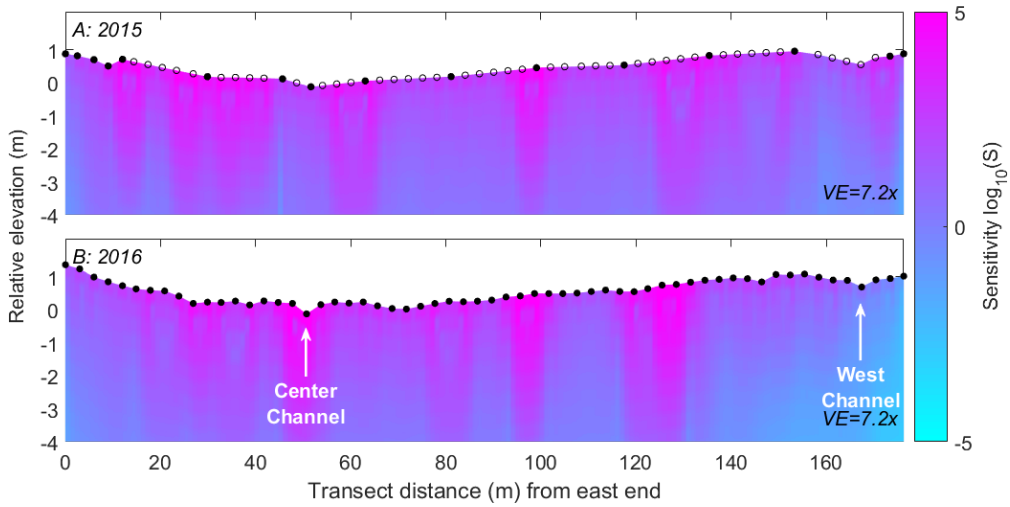

Figure J.41: Comparative electrical resistivity sensitivity matrix tomogram, entire length of transect XS2. Panel a was measured in 2015, prior to channel realignment. Panel b was measured in 2016, following channel realignment. Circles represent electrode locations; solid circles represent surveyed electrode locations and open circles represent interpolated electrode locations.

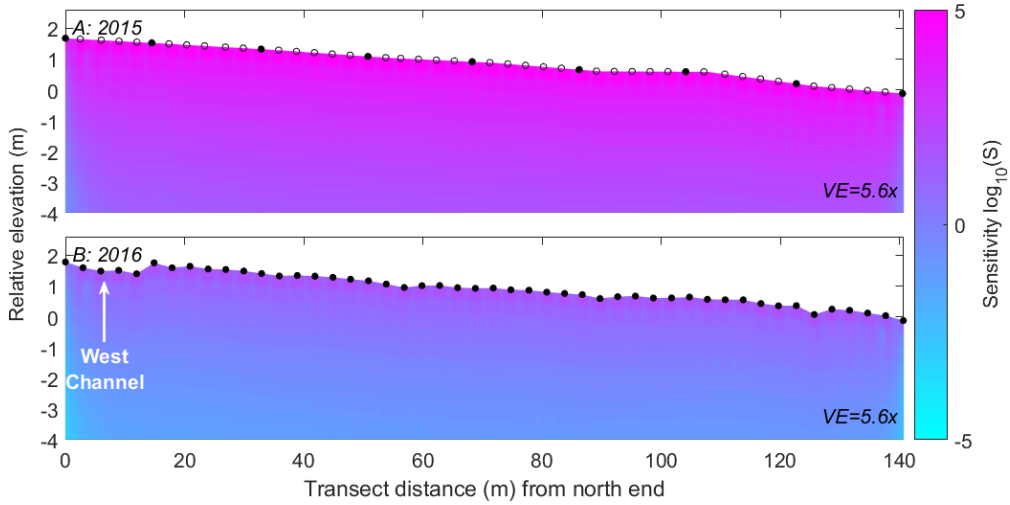

Figure J.42: Comparative electrical resistivity sensitivity matrix tomogram, entire length of transect XSLW. Panel a was measured in 2015, prior to channel realignment. Panel b was measured in 2016, following channel realignment. Circles represent electrode locations; solid circles represent surveyed electrode locations and open circles represent interpolated electrode locations. The 2015 transect was more sensitive to lower depths than the 2016 transect.